UNIVERSITY OF BIRMINGHAM

Matched Load for WR03 Waveguides

Thesis by:

Sanaz Roshanmanesh

A thesis submitted to the University of Birmingham

for the degree of M.Sc by Research

School of Electronic, Electrical and Systems Engineering

College of Engineering and Physical Sciences

University of Birmingham

March 2015

Synopsis

In this research, a design and simulation of a waveguide termination for WR03 band, using SU8 based micromachined waveguides is reported. To achieve low level reflection for the termination, two basic ideas are considered. Firstly, an open-ended waveguide port inside the lossy material of SU8 has been investigated. Secondly, thin film conductor layers (silver and platinum) are considered for waveguide walls. Additionally, for the improvement of the final result, different kinds of tapering of the SU8 open-ended waveguide have been analysed. Horn shaping of the waveguide structure in combination with tapering of SU8 has also been evaluated. The best structure was WR03 Platinum termination with height tapering with a predicted return loss of better than -30 dB over the WR03 band.

Acknowledgments

I am deeply indebted to my supervisor, Professor Mike Lancaster, for giving the opportunity to study and work on the project of WR03 band micromachined termination, and for kindly providing guidance throughout the development of this project. I could frequently profit from his experience and advice. Also, I wish to thank Dr Paul Smith, Dr Tim Jackson, and Dr Xiaobang Shang for all their support and help. My appreciation also goes to my colleagues in the Emerging Device Technology Research Group at the University of Birmingham for their support and friendship. Many special thanks to Mr Alan Yates for all his support during this project. Last but certainly not least, I want to express my great gratitude to all of my friends for their invaluable support and encouragement. I would also like to express my sincere thanks to my parents for their attentions to my situation. They helped me in progress of this project same as all my life.

List of Abbreviations

MEMS- Micro Electro Mechanical Systems

EDT- Emerging Device Technology

TE- Transverse Electric field

TM- Transverse Magnetic field

VSWR- Voltage Standing Wave Ratio

PEC- Perfect Electric Conductor

CONTENTS

LIST OF FIGURES

List of Tables

Chapter 1 INTRODUCTION

This thesis presents a fundamental study for the design of a waveguide termination in millimetre wave frequency band. Several possible ways for the improvement of the termination structure, using thin metal film waveguide, tapering, and horn shaping, have been evaluated.

The field of sub-millimetre wave technology has recently been a subject of substantial scientific research due to the development of new potential applications. This part of the electromagnetic spectrum occupies the range from about 300 GHz to several thousands of GHz; being between the microwave and infrared regions. Nowadays, both microwave and optical regions are widely developed and have found many different industrial applications. In the past the sub-millimetre frequencies were used mainly in radio-astronomy. The current state of technology and science permits more utilisation of these widely unused band of frequencies [1].

The engineering techniques at millimetre-wave frequencies bands are similar to the microwave technology on one side, and with the optics on the other. The same solutions for waveguides and resonators can of course be used in the millimetre frequency range. However, there are many distinctive features specific to the millimetre-wave structures that require further research and development, and implementation of the new technology [2]. Waveguides are a suitable choice for millimetre-wave devices. The difficulty in the fabrication of small waveguides in sub-millimetre wave region can be solved by using MEMS (MicroElectroMechanical Systems) technology[3].

One of the important waveguide components is the waveguide termination. A termination is a one-port device with an impedance that matches the characteristic impedance

of a given transmission line or waveguide. It is placed at a specific termination or port of a device to absorb the power transmitted to that terminal. Important properties of a termination are its low reflection coefficient and good power handling capability. Terminations have many applications such as the isolated port in a directional coupler, realisation of an isolator by a circulator, the unused port of a power divider and calibration kits of measurement instruments [1]. Terminations designed to accommodate high power are generally termed dummy loads. Absorber, matched load and terminating load are other terms which are used for termination.

The aim of this project is to study, design, and simulate a WR03 band waveguide termination. WR03 is a standard waveguide for the standard frequency range of 220-325 GHz and has a cut-off frequency of 173.58 GHz; its dimensions are described in Table 1-1.

Table 1-1 Dimensions of WR03 rectangular waveguide [3]

a(mm)	b(mm)	Cut-off frequency (GHz)
0.8643	0.4318	173.58

Some of the recent projects carried out by the Emerging Device Technology (EDT) research group at the University of Birmingham, have been focused on the design and fabrication of different waveguide structures in the frequency band of 220-325 GHz such as a diplexer [5], a slotted antenna [6], and waveguide filters [7]. The termination is useful for future development of integrated waveguide structures like directional couplers, circulators and non-reflecting filters. The measurement approaches at this frequency band have been described in [8] and [9].

Consider a WR03 waveguide supported by the SU8 which the waveguide walls are realised with evaporation of a good conductor like Silver or Platinum. Electrical conductivity

of Silver and Platinum are 6.3×10^7 (S/m) and 9.43×10^6 (S/m) respectively. SU8 is an epoxy based, negative, near ultraviolent (UV) photoresist used for MEMS and other microelectronic applications and was developed by IBM-Watson Research Centre in 1989. SU8 is highly transparent in the UV range. This allows the fabrication of relatively thick structures (with thicknesses being up to several hundreds of micrometres), with nearly vertical side walls [10]. SU8 is the desired type of material for this work due to its good sensitivity to UV light and the low cost instrumentation. SU8 has permittivity of 4.1 and loss tangent of 0.08 at 100GHz [3]. For the implementation of a termination there are different structures. These specific characteristics of SU8 lead to use it as a suitable material for micromachining a termination.

In this thesis the analysis and simulation of various terminating structures are performed to find the best methods for realization of a good termination with the SU8 fabrication available. In this project the figure of merit for termination is its' S_{11} (the corresponding reflection coefficient) which should be as small as possible. The small thickness of the metallic wall increases absorption of the propagating signal and energy leaks in to the SU8 resulting in better S_{11} for the termination. Additionally different methods of tapering such as wedge and pyramidal tapering, for matching between open-ended waveguide and SU8, have been used. Horn shaping at the open-ended port of waveguide has been investigated. CST Microwave Studio has been used for full-wave simulation of the designed structures. At the final stages of this project, the best structure has been chosen and an accurate analysis has been carried out.

1-2 Thesis Overview

This thesis consists of eight chapters. The first chapter includes an overall definition of the project and an overview of the thesis.

Chapter 2 contains a review of fundamental theory of waveguides and waveguide terminations and discussion of other important literature. In this chapter a few waveguide terminations which are published in the available literature are discussed.

Chapter 3 provides fundamental theory of loss in SU8 rectangular waveguide for thick conductor and thin film conductor walls. The proposed approach, for reducing the reflection, is discussed in this chapter. This approach contains two separate categories of path loss and radiation from the open end into SU8, each one of which are thoroughly discussed. The path loss consists of conductor loss, dielectric loss and radiation loss.

In chapter 4, the simple termination with different kinds of conductors is simulated and analyzed. This simple termination contains an open ended rectangular waveguide which is supported by SU8.

Chapter 5 presents different types of tapering on the previous simple termination described in chapter 4 for the improvement of the return loss. These tapered structures consist of three kinds of triangular tapering and a pyramidal tapering.

Chapter 6 describes a horn shaping approach for the improvement of the performance of the termination.

Chapter 7 discusses the complete design of SU8 micromachined WR03 termination waveguide circuit which has been simulated with H-plane bend. The H-plane 90 degree bend has been design to help the measurement technique. Both of these two circuits, WR03

waveguide termination and H-plane bend were designed using the separate SU8 single layer technique.

Chapter 8 presents the key conclusion of the present study and discusses possible future directions of this work.

1-3 Structure of the thesis

The structure of the thesis has been summarised in Fig. 1-2 which illustrate the approach of this research and the information in of this thesis.

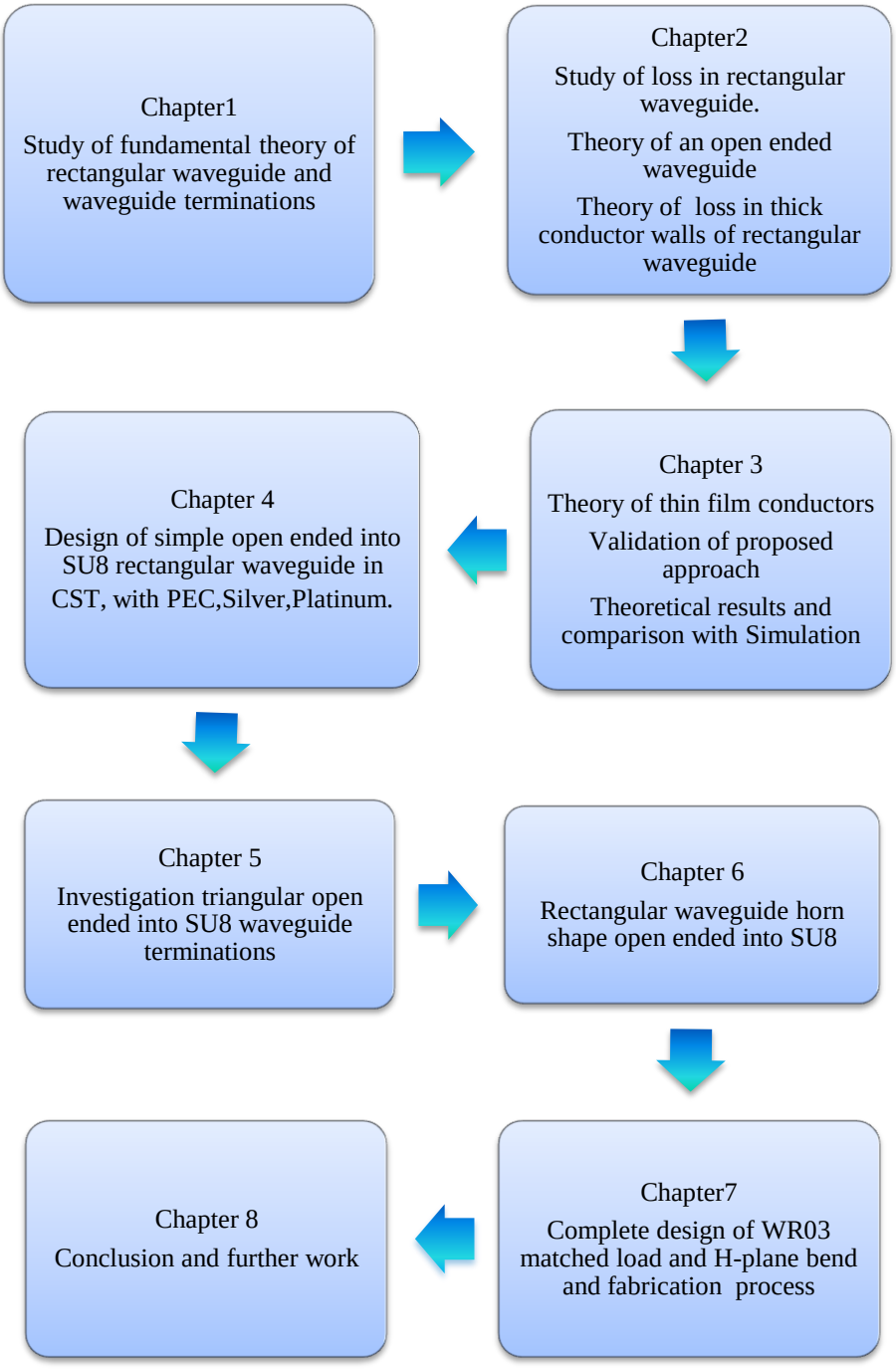

Fig. 1-1 Illustration of the structure of the thesis

Chapter 2 FUNDAMENTAL THEORY OF WAVEGUIDE AND TERMINATIONS

2-1 Introduction

This chapter contains two main sections; first, the basic theory of rectangular waveguide, propagation modes; second, the discussion of published papers on waveguide terminations. The theory used in this chapter can be found in [1] , [12] and [13]-[14].

In section 2-2 the general configuration of the rectangular waveguide is presented including the definition of transverse electric field (TE), transverse magnetic field (TM) and the cut-off frequency (f_{cmn}).

Section 2-2-1 introduces the TE mode in more depth followed by TE wave impedance formula (Z_{TE}), intrinsic impedance (η), propagation constant (β), wave number (k) , cut-off wave number (k_c) and cut-off frequency (f_{cmn}) equations.

In section 2-2-2 , the final section of Chapter 2, a published paper on waveguide terminations is reviewed.

2-2 Rectangular Waveguide

In microwave engineering, rectangular waveguides were one of the earliest types of transmission lines, they are used to transport microwave signals for many applications [1]. The geometry of the rectangular waveguide is shown in Fig. 2-1.

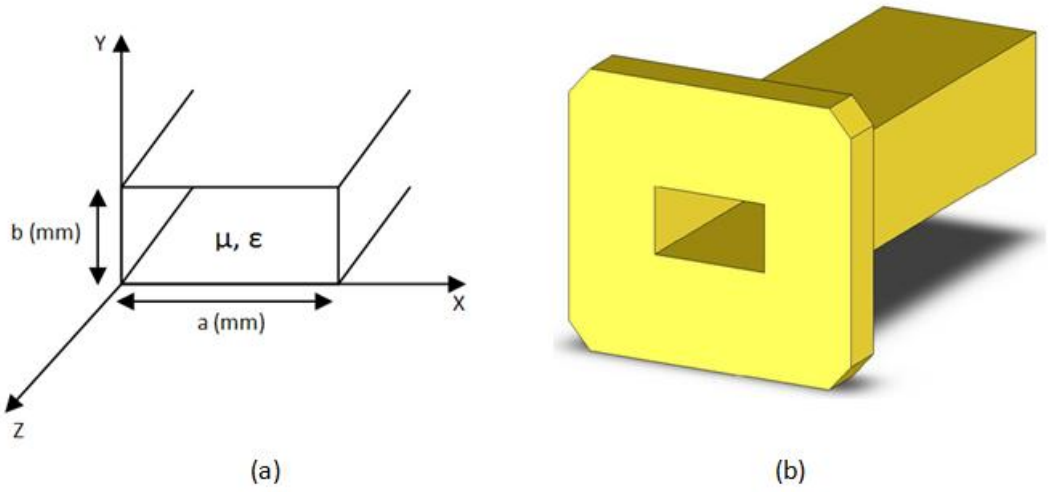

Fig. 2-1 General configuration of a rectangular waveguide (a) Structure (b) Rectangular waveguide with flange

Rectangular waveguides cannot support transverse electromagnetic (TEM) waves, because they consist of just one separated metal. Waves in rectangular waveguide propagate in transverse electric (TE) and transverse magnetic (TM) modes. There is a cut-off frequency (f_c), below which, the propagation is impossible [12]. Since it has been assumed that $a > b$, the lowest cut-off frequency (which is called dominant one) occurs for TE_{10}. The TE mode is discussed in the next section.

2-2-1 TE mode

The TE mode consists of a zero electric field and non-zero magnetic field in the direction of propagation. Thus the characteristic of TE mode is $E_Z=0$ and $H_Z\neq0$. The TE mode impedance is given by [12],

$$Z_{TE} = \frac{E_X}{H_Y} = -\frac{E_Y}{H_X} = \frac{\omega\mu}{\beta} = \frac{k\eta}{\beta} \tag{2-1}$$

where η is the intrinsic impedance of the material which fills the waveguide [12].

$$\eta = \sqrt{\frac{\mu}{\varepsilon}} \tag{2-2}$$

The propagation constant, β is defined as [12]:

$$\beta = \sqrt{k^2 - k_c^{\,2}} \tag{2-3}$$

k, is the free space wave number, defined as [12]:

$$k = \omega\sqrt{\mu\varepsilon} \tag{2-4}$$

and, k_c is the cut-off wave number [12]:

$$k_c = \sqrt{(\frac{m\pi}{a})^2 + (\frac{n\pi}{b})^2} \tag{2-5}$$

Each mode has a cut-off frequency given by (2-6), for frequencies below this propagation is not possible [12]:

$$f_{cmn} = \frac{1}{2\pi\sqrt{\mu\varepsilon}}\sqrt{\left(\frac{m\pi}{a}\right)^2 + \left(\frac{n\pi}{b}\right)^2} \tag{2-6}$$

The propagation mode with lowest frequency is called the dominant mode. TE_{10} is the dominant mode for TE modes. The distance between two equal phase planes along the waveguide is called the guided wavelength given by [12]:

$$\lambda_g = \frac{2\pi}{\beta} \tag{2-7}$$

2-2-2 Waveguide Terminations

Matched loads for waveguides are reported frequently in literature but most of them are for microwave frequencies. In the millimetre wave band, the implementation of a suitable termination is a new topic for researchers and engineers. The usual methods for realisation of termination at microwave frequencies are based on the use of a tapered wedge or slab of lossy materials, like graphite, inserted into waveguide as shown in Fig. 2-2. The dielectric loss of the material leads to absorption of the incident power. Tapering the shape of the lossy material causes a suitable low reflection coefficient. A length of one or more wavelengths is usually enough to have a termination with VSWR of better than 1.01:1 and return loss better than 46 dB [1]. An increase in length may be needed for high power terminations.

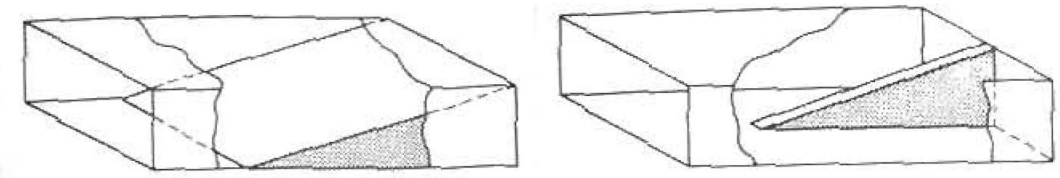

(a) (b)

Fig. 2-2 Terminations for a rectangular waveguide, a) wedge of a lossy material, b) tapered slab of a lossy material taken from [1]

The geometrical shape of the lossy material can be varied to achieve lower reflection and suitable high power capability. Fig. 2-3 shows two more structures for matched load of waveguide [13].

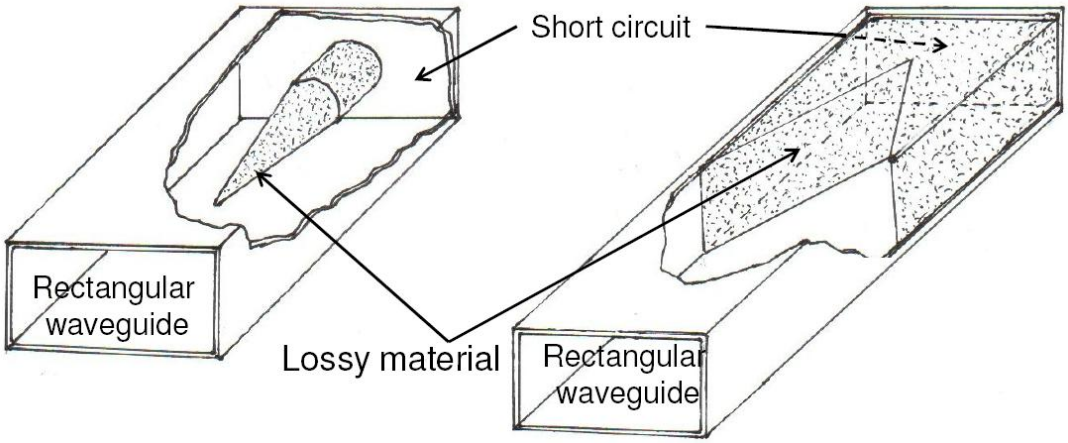

Fig. 2-3 two other structures for matched load of waveguide [13]

In [22] suitable termination structures are proposed for single-ridged waveguide and double-ridged waveguide with pyramid absorber which are shown in Fig. 2-4.

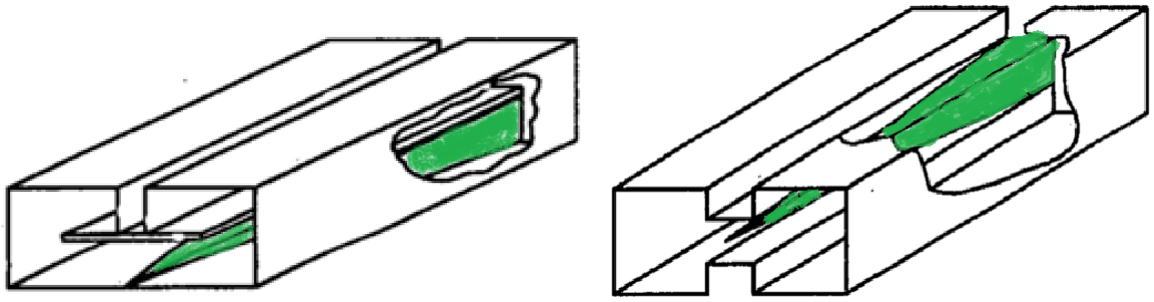

(a) (b)

Fig. 2-4 Termination structure for a) single-ridged waveguide, and b) double-ridged waveguide [22]. Green areas show lossy materials.

In [14] two novel methods are proposed, both of which use a single thin resistive sheet absorber supported by Styrofoam walls and total length of 50 mm for the waveguide dimensions of WR90, which a = 22.86 mm, b = 10.16 mm to achieve nominal absorption of-120 to -30 dB.

Fig. 2-5 (a) shows a standard tapered-wedge absorber. The wedge shape allows a gradual transition between waveguide and absorbing media. As the E-field is in Y-direction and the TE_{10} mode of the waveguide reaches a maximum at $x=a/2$, the best positioning of the

wedge is to place it vertically in the centre of the waveguide to achieve maximum absorption [14].

Fig. 2-5 (d) shows the structure of V-shaped wedge where in (e) it shows 40 mm taper with 10 mm deep rectangular base. In (f) the taper has been extended over the full length of 50 mm of absorber [14].

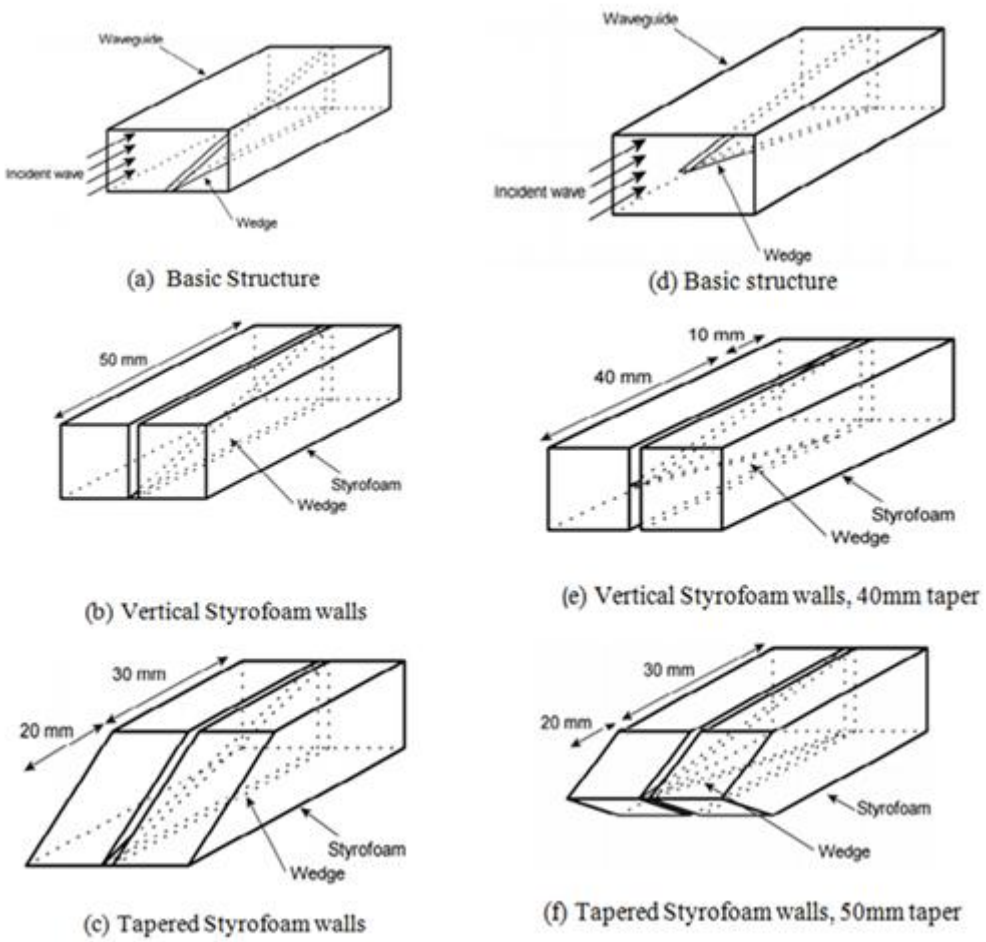

Fig. 2-5 Innovative structures for waveguide termination, (a) Basic Structure (b) Vertical Styrofoam Walls (c) Tapered Styrofoam Walls, (d) Basic Structure (e) Vertical Styrofoam walls with 40 mm taper (f) Tapered Styrofoam Walls with 50 mm taper [14].

At sub-millimetre wavelengths similar ways of power absorption can be used, but certainly more detailed considerations are required. Dimensions at millimetre wave frequencies are very small and therefore such devices need very accurate fabrication [10].

2-3 Conclusion

In this chapter a few fundamental concepts in waveguide theory have been discussed and the available literature on theory and fabrication of waveguide terminations has been investigated. At microwave frequencies there are many designs and products for dummy load, but at the millimetre waves there is a considerable lack for the suitable waveguide terminations. Microwave waveguide terminations are usually designed based on tapered absorbers inside the waveguide, but this concept has not been validated for mm-wave applications.

Chapter 3 LOSS IN SU8 RECTANGULAR WAVEGUIDE

3-1 Introduction

This chapter starts with a description of finding a suitable structure for the waveguide termination which provides the lowest reflection coefficient.

Fig. 3-1 presents the general configuration of the SU8 rectangular waveguide and SU8 rectangular waveguide termination. In this design the WR03 rectangular waveguide walls made by conductor and they are surrounded by dielectric which in this project it is SU8.

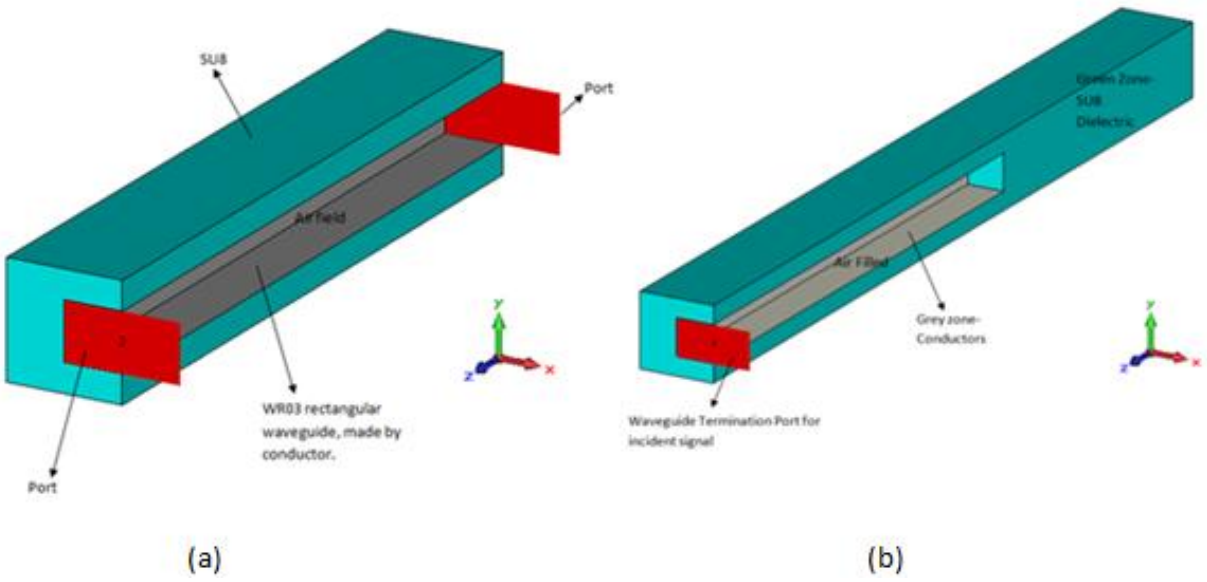

Fig. 3-1 General configuration of (a) WR03 rectangular SU8 waveguide (b) WR03 rectangular waveguide termination

Section 3-2 presents dissipations concept for increasing return loss. Section 3-3 contains a review of literature on open ended rectangular waveguide and the reflection coefficient from an ideal open ended waveguide. Additionally in this section, a comparison between the result

of the theory and the ones obtained by electromagnetic full-wave simulation using CST Microwave Studio will be discussed.

Section 3-4 describes the possible approaches in increasing the attenuation of the signal travel in to the rectangular waveguide. This section is divided into two sub-sections. Section 3-4-1 looks into the literature on attenuation of a signal in rectangular waveguide made by thick conductor walls. The graph of the attenuation for WR03 rectangular waveguide with different conductors versus frequency is shown in this section. The theory in this section can be found in [1] and [12]. This is followed by the theory of thin film conductors. Section 3-4-2 presents the equation of the attenuation of the signal in rectangular waveguide fabricated with thin film walls which is validated by the comparison with other works and simulations. The theory used in this section can be found in [12] and [15].

3-2 Dissipations Concept for Increasing Return Loss

The main focus of this project is to find a suitable terminating structure which provides the lowest reflection coefficient. Tapering structures such as triangular, pyramidal or cone are potentially suitable for this aim.

The low reflection coefficient means that the reflected power is essentially very low, which means that the power is dissipated in the termination. There are two general components of dissipation in the termination: First, from the open-ended side of waveguide, some amount of power will be radiated into the environment filled area (Fig. 3-1 (b) SU8, in this case). Second component is the path loss of power in the forward and backward directions in the waveguide. This path loss is due to two different sources: a) conductor loss of waveguide walls, b) leakage of wave into waveguide environment, part of which will be

dissipated due to dielectric loss of the dielectric environment and the remainder will be radiated. Fig. 3-2 depicts the above-mentioned procedure for increasing the return loss.

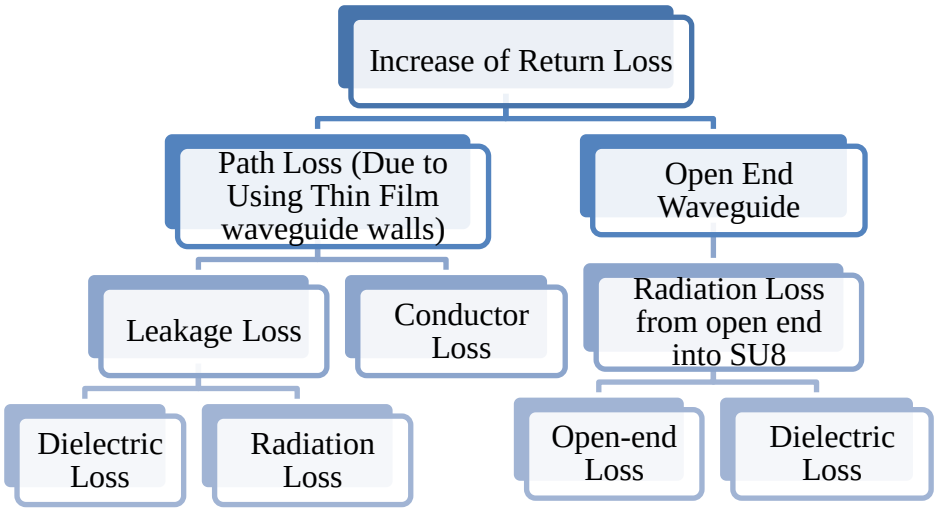

Fig. 3-2 Block diagram of dissipations concept for increasing return loss

One strategy to have higher losses is using very thin conductor walls (adequately thinner than the skin depth δ_s) to increase conductor loss and also allow radiation into the SU8. This approach is potentially feasible as the fabrication can include controlled evaporation of metal layer on SU8 waveguide walls.

Therefore, for analysis and design of a termination two separate cases are considered: 1- Open-ended waveguide to realise the reflection from an open ended waveguide in to the air, 2- Path loss (leakage waveguide and resistive loss). Finally the termination will be a combination of these two cases.

Additionally, to compare the level of matching between waveguide and SU8 environment at the open-end, various types of tapering on SU8 have been evaluated. Matching decreases the amount of reflected wave at open-end and therefore increases the radiation loss.

3-3 Open-Ended Waveguide

As mentioned previously an open-ended waveguide may be a suitable platform for realisation of a waveguide termination. There are closed form expressions for radiation from an ideal open-ended waveguide [16]-[17]. Fig. 3-3 shows the general configuration of a rectangular waveguide with a wall thickness *t*.

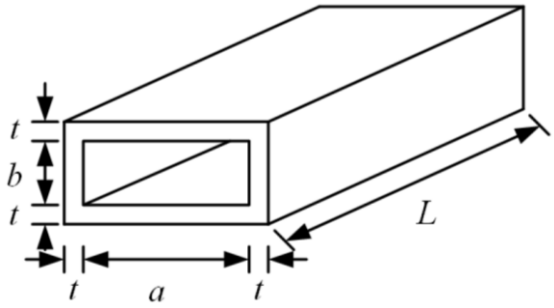

Fig. 3-3 The general configuration of a rectangular waveguide

An expression from [18] is used for reflection coefficient from an ideal open-end waveguide, which is given by:

$$|\Gamma| = \begin{cases} -8.023 + 24.083r - 27.624r^2 + 15.747r^3 - 4.484r^4 + 0.51r^5 + \dfrac{t}{3.3a} & , 0 < \dfrac{t}{a} < 0.11 \\ -4.31 + 0.496r + \dfrac{0.009r}{\ln(r)} + \dfrac{4.412(\ln(r))}{r} + \dfrac{3.849}{r} - \dfrac{t}{5.5ar^2} & , 0.11 \le \dfrac{t}{a} < 0.31 \end{cases} \quad (3\text{-}1)$$

where *r* is the normalized frequency given by:

$$r = \frac{f}{f_C} \quad (3\text{-}2)$$

Comparison of the results obtained from the aforementioned theory with ones obtained by electromagnetic full-wave simulation using CST Microwave Studio has been

performed. Fig. 3-4 shows the comparison between above-mentioned theory, with CST results for a WR03 open ended waveguide into the air with PEC[1] walls.

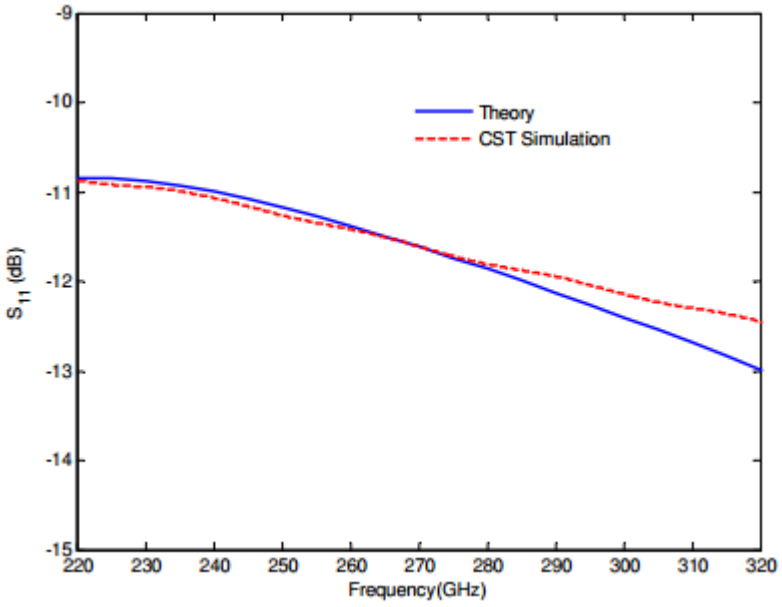

Fig. 3-4 The comparison between S_{11} evaluated theory from eq (3-1) and CST for an open-ended WR03 waveguide with PEC walls.

However in this project, the waveguide is not open-ended into the air as it is enclosed by SU8, as shown in Fig. 3-5.

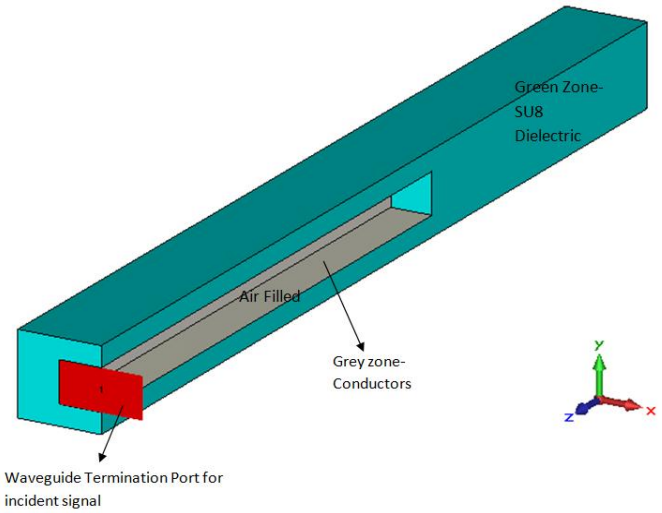

Fig. 3-5 Section view of the WR03 waveguide supported by the SU8 in CST enviroment. The green region is SU8, gray parts are metal and the red part is the port.

[1] Perfect Electric Conductor

Fig. 3-6 displays S_{11} for a WR03 waveguide open-ended into SU8 which simulated with open boundary condition, with its structure defined in Fig. 3-5. As expected, the mismatch between open-ended waveguide and waveguide environment which is filled with SU8 is increased (in comparison with waveguide and air environment). The reflection coefficient at the open end depends on the wave impedance outside the waveguide. As this has changed to a value close to 50 Ω ($\eta = \eta_0 / \sqrt{\varepsilon_r}$) hence the reflection has increased.

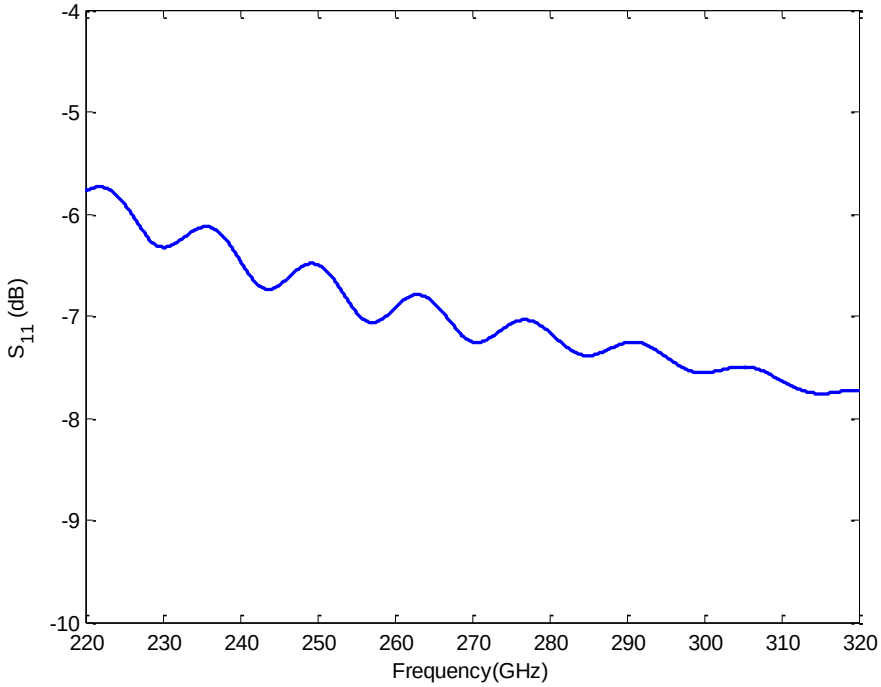

Fig. 3-6 S_{11} in dB for a WR03 waveguide open-ended by SU8 shown in Fig. 3-5

Comparison between Fig. 3-4, S_{11} versus frequency for open ended waveguide into air and Fig. 3-6, S_{11} versus frequency for open ended waveguide into SU8, it can be seen that SU8 increases reflection and hence degrades the termination performance, but SU8 is preferred for the physical realization of the structure of this project.

Improvement of the reflection by the second method, path loss, will be investigated in the next part.

3-4 Path Loss

To have a termination with minimum amount of reflection, the signal must be attenuated in the waveguide as much as possible. Therefore the path loss is going to be increased and it is consists of:

1) Conductor Loss: because of conductor loss of waveguide walls (thick and thin conductors are looked at)

2) Leakage Loss: because of leakage of wave into waveguide environment (SU8), the wave will be dissipated due to the dielectric loss of SU8, and the remaining power will be radiated.

Absorber's material is previously determined to be SU8 which has loss tangent of 0.08 at frequency of 100 GHz [3]. Hence only the optimization of the waveguide walls is required. If the waveguide walls become too thin, the energy escapes as the wave travels down the waveguide which increases the leakage loss and conductor loss and this effectively acts as an absorber. To calculate the values of conductor losses we begin by investigating the normal conductor case and then extend it for relatively thin conductors.

3-4-1 Thick Conductor Walls

There exist two sources for attenuation of the signal in waveguides, conductor loss and leakage loss. In this section it is assumed that within the body of the conductor the current density is zero. For a hollow rectangular waveguide with width a and height b, the attenuation due to conductor loss in Np/m (for dominant mode of TE_{10}) can be written as [12]:

$$\alpha_{CT} = \frac{P_L}{2P_{10}} \tag{3-3}$$

Where P_L is power loss and P_{10} is the propagated power in the rectangular waveguide [12]. Therefore, the attenuation due to conductor loss can be calculated by the following equation [12]:

$$\alpha_{CT} = \frac{P_L}{2P_{10}} = \frac{2\pi^2 R_S \left(\mathrm{b} + \frac{a}{2} + \frac{\beta^2 \mathrm{a}^3}{2\pi^2}\right)}{\omega\mu a^3 b\beta} = \frac{R_S}{a^3 b\beta k\eta}\left(2\mathrm{b}\pi^2 + \mathrm{a}^3\mathrm{k}^2\right) \quad (\mathrm{Np/m}) \tag{3-4}$$

In equation (3-4) β is the propagation constant, k is the wave-number and η is the inherent impedance of free space,

$$\eta = \sqrt{\frac{\mu_0}{\varepsilon_0}} = 377\ \Omega \tag{3-5}$$

and R_s is the surface resistance of waveguide conductor walls, which at an angular frequency of ω is equal to [12]:

$$R_S = \sqrt{\frac{\omega\mu}{2\sigma}} = \frac{1}{\sigma\delta_S} \tag{3-6}$$

In equation (3-6), σ is the conductivity of waveguide conductor walls and δ_S is the skin depth which is a function of the frequency and defined as the depth below the surface of the conductor where the current density has fallen to 1/e for any planar conductor. The current density is maximum near the surface and decrease with greater depths into the conductors [1]:

$$\delta_S = \sqrt{\frac{2}{\omega\mu\sigma}} \tag{3-7}$$

Fig. 3-7 shows the attenuation in dB/mm versus frequency which has been calculated from eq.(3-4) for six different conductors with different conductivity values. From Fig. 3-7, silver and platinum have been chosen to use in this project.

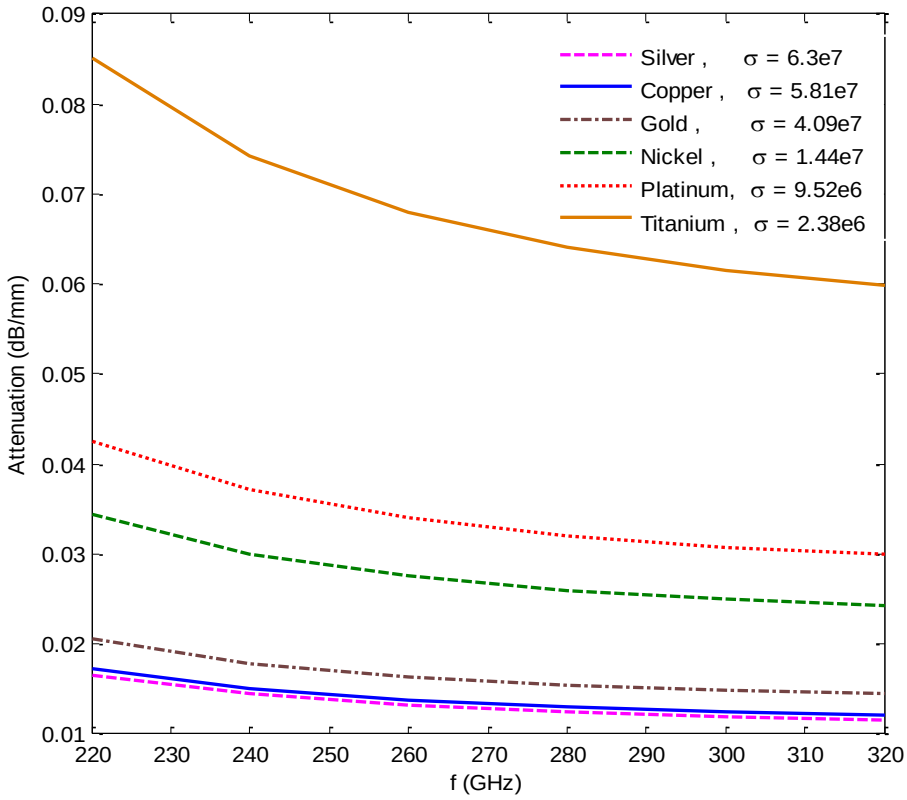

Fig. 3-7 The attenuation for WR03 rectangular waveguide with different conductors versus frequency based on proposed theory from [12] in eq. (3-4).

In the case of this design, for the silver conductor at frequency of 300 GHz, from (3-7) the skin depth is 115.768 nm, from (3-6) $R_S = X_S = 0.137\ \Omega/sq$ so, $Z_S = 0.137 + j0.137\ \Omega/sq$.

For Platinum, another candidate for the realization of this waveguide structure, the skin depth is found to be, $\delta_S = 297$ nm, $R_S = X_S = 0.354\ \Omega/sq$. So $Z_S = 0.354 + j0.354\ \Omega/sq$.

α is usually described by Np/m but it can be also useful if it is shown by dB/m. To change between these two units, the following equation can be used [12]:

$$\alpha\ (dB/m) = 8.686 \times \alpha\ (\ Np/m) \tag{3-8}$$

In equation (3-8), 8.686 is 20log(e). Fig. 3-7 shows the attenuation in dB/mm for WR03 waveguide with different conductors versus frequency.

Additionally the value of the attenuation in WR03 for different frequencies versus conductivity is displayed in Fig. 3-8.

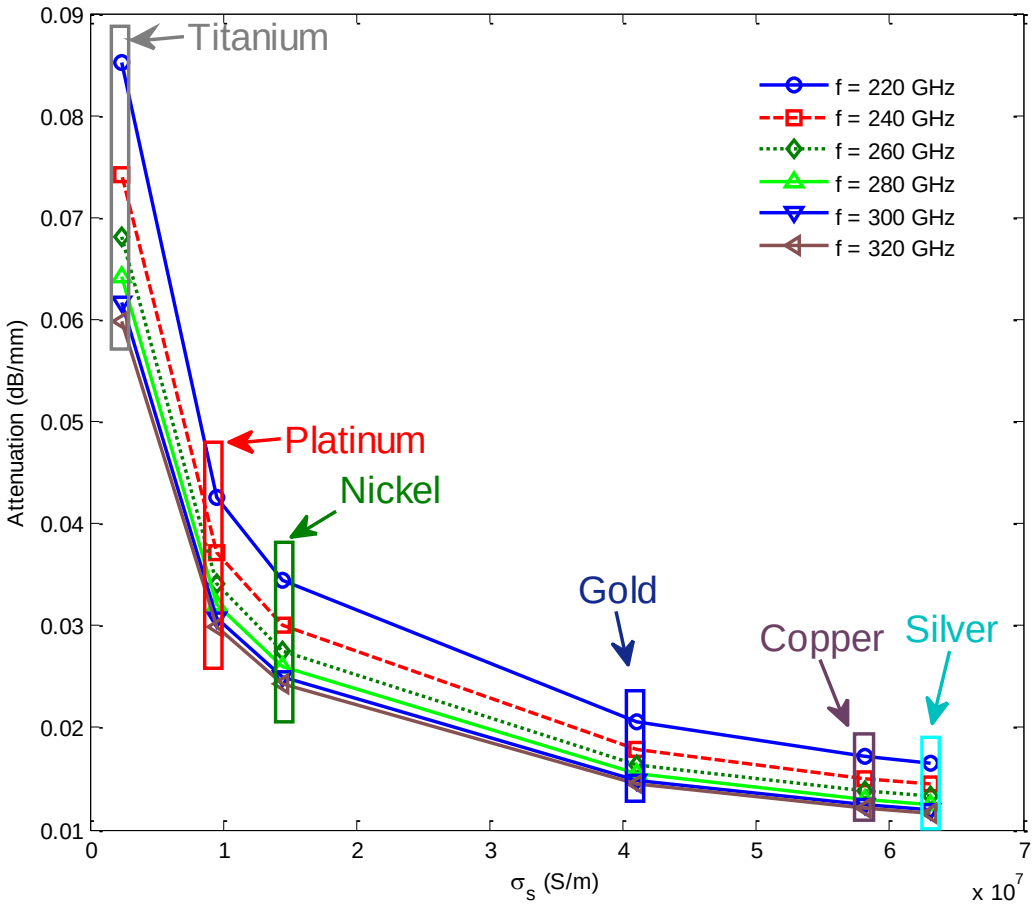

Fig. 3-8 Loss versus conductivity in WR03 rectangular waveguide for different frequencies

3-4-1-2 *Comparison with Simulation*

In this stage, for the validation of the presented approach, the calculated results from the proposed theory from [12] are compared with simulation results which are obtained from CST Microwave Studio. Fig. 3-9 compares the calculated amount of the attenuation with the CST simulation results. There is good agreement between the two results.

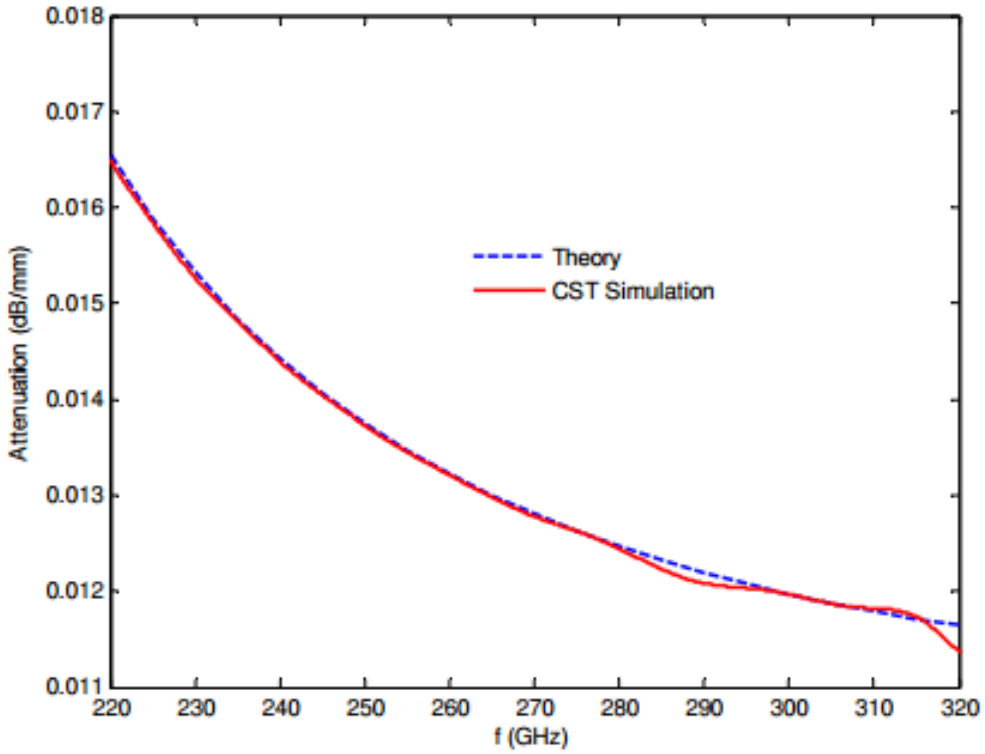

Fig. 3-9 Attenuation in dB/mm versus frequency for WR03 Silver rectangular waveguide, comparing theory from eq. (3-4) and simulation from CST.

The values of attenuation for a normal thickness conductor are not sufficient for this case to adequately improve the reflection coefficient. For example for a return loss of -20 dB a l = 1667 mm long waveguide is needed. Therefore to increase the attenuation thin film conductors are to be used as waveguide walls. To achieve this goal the concept of finite thickness thin films should be analysed [15].

3-4-2 Thin Film Conductors

It has been mentioned that in order to increase the attenuation level, thin film conductors shall be used as waveguide walls. Fig. 3-10 shows a plane wave incident onto a thin film of conducting material. The thickness of the substrate is assumed to be infinite.

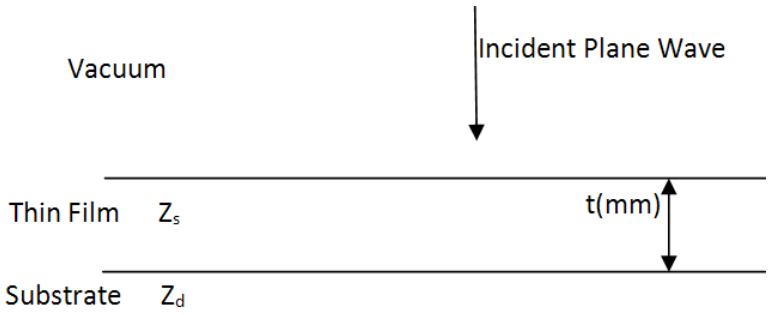

Fig. 3-10 Film of conducting material with thickness of *t* on the surface of a substrate showing an incident plane wave [15].

As shown in Fig. 3-10, if a film of conducting material with surface impedance Z_s and complex propagation constant γ_s is grown on a substrate with surface impedance Z_d, then the impedance, looking from the upper surface of the film towards the substrate as shown in Fig. 3-10, is fundamentally similar to the input impedance of a transmission line with impedance of Z_s and length of *t* which is loaded by load impedance of Z_d and therefore can be given by [15]:

$$Z_f = Z_s \frac{Z_d + Z_s \tanh(\gamma_s t)}{Z_s + Z_d \tanh(\gamma_s t)} \tag{3-9}$$

Where 't' is the thickness of the thin film. This is a well-known expression for calculating the impedance of a block of material. Z_S is the normal conductor impedance [12] given by:

$$Z_S = R_S + jX_S = (1+j)\sqrt{\frac{\omega\mu}{2\sigma}} \tag{3-10}$$

Therefore it can be inferred that:

$$X_S = R_S = \sqrt{\frac{\omega\mu}{2\sigma}} = \frac{1}{\sigma\delta_S} \tag{3-11}$$

Assuming the dielectric is not lossy, in eq. (3-9) the impedance of Z_d can be written as, [15],

$$Z_d = R_d + jX_d \approx \sqrt{(\frac{\mu}{\varepsilon})}\,(1+j\frac{\sigma}{2\omega\varepsilon}-\frac{3\sigma^2}{2\omega^2\varepsilon^2}) \tag{3-12}$$

Hence from eq (3-12) it can be concluded that:

$$R_d = \sqrt{(\frac{\mu}{\varepsilon})}\;(1-\frac{3\sigma^2}{2\omega^2\varepsilon^2}) \tag{3-13}$$

and

$$X_d = \sqrt{(\frac{\mu}{\varepsilon})}\,(\frac{\sigma}{2\omega\varepsilon}) \tag{3-14}$$

In addition it is known that:

$$\sigma = \omega\varepsilon\tan\delta \tag{3-15}$$

In this case where the dielectric is SU8 with $\varepsilon_r = 4.1,\ \tan\delta = 0.08$ we have $\sigma = 5.474122$.

Therefore, for the SU8, from (3-13), R_d = 184.26 Ω, from (3-14), X_d = 7.44 Ω, hence Z_d = 184.26 + j7.44 Ω.

The complex propagation constant of a conductor is [12]:

$$\gamma_s = (1+j)\sqrt{\frac{\omega\mu\sigma}{2}} \tag{3-16}$$

Based on the aforementioned equations the amount of conductor loss of the waveguide with thin film walls can be calculated. For this purpose, R_s in eq. (3-4) must be calculated by real part of Z_f in eq. (3-9). This means that considering $Z_f = R_f + jX_f$, then according to eq. (3-4) the attenuation constant for a thin film conductor can be calculated by the following equation.

$$\alpha_{CT} = \frac{R_f}{a^3 b\beta k\eta}(2b\pi^2 + a^3k^2) \tag{3-17}$$

3-4-2-1 *Validation of the proposed approach*

In order to validate this approach a comparison between this method and another formulation has been performed for the attenuation constant derived from Lucyszyn, et. al., [25]. They proposed a formulation for the complex propagation constant that is dependent on surface impedance, the attenuation constant will be the real part of the propagation constant. For the surface impedance the expression of eq. (3-9) must be used. According to [25], the propagation constant of a metal dielectric-filled rectangular waveguide in TE_{m0} mode can be expressed as follows [25]:

$$\gamma^2 = \Gamma_d{}^2 - j\frac{2Z_S}{\omega\mu b}[(\frac{\Gamma_d}{k_C}\frac{m\pi}{a})^2 - k_C{}^2(1+\frac{2b}{a})] \tag{3-18}$$

Where; Γ_d is [25]:

$$\Gamma_d{}^2 = k_C{}^2 - k_{od}{}^2 \tag{3-19}$$

In which, k_C cut off wave number is [25]

$$k_C = \omega_C\sqrt{\mu\varepsilon} \tag{3-20}$$

And, k_{od} wave number in TE_{0d} mode is [25]

$$k_{od} = \omega\sqrt{\mu\varepsilon(1 - j\tan\delta)} \tag{3-21}$$

where tan δ is the loss tangent of dielectric inside the waveguide which is equal to zero in the case of air-filled waveguide. Now in the case of thin films Z_f of eq. (3-9) has been used instead of Z_s, and therefore attenuation constant for TE_{10} mode can be written as [25]:

$$\alpha_{CT} = \mathrm{Re}\left\{\sqrt{\Gamma_d{}^2 - j\frac{2Z_f}{\omega\mu b}[(\frac{\Gamma_d}{K_C}\frac{\pi}{a})^2 - K_C{}^2(1+\frac{2b}{a})]}\right\} \tag{3-22}$$

The attenuation curves for different values of waveguide height, b, for a rectangular waveguide with a=1.5 mm (the cut-off frequency in TE_{10} of f_C =100 GHz) versus normalized frequency (normalized to f_C) have been calculated and then compared with the reported results in [25]. These are shown in Fig. 3-11. There is good agreement between two approaches.

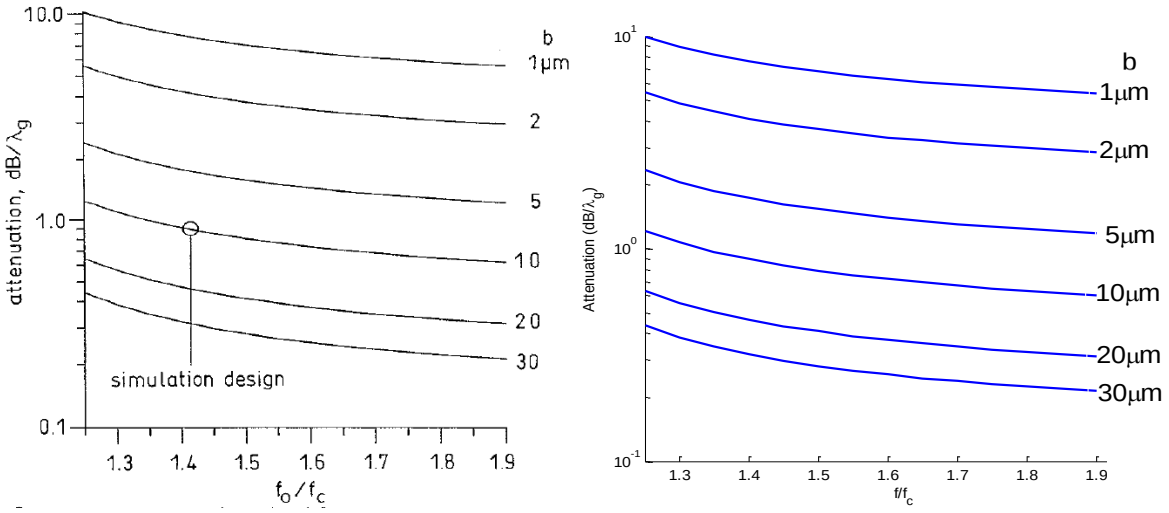

(a) (b)

Fig. 3-11 The attenuation curves (in dB per guided wavelength) for the different values of 'b', for an air-filled rectangular waveguide with a=1.5 mm (f_C =100GHz) versus the normalized frequency (f/f_C), a) reported in [25] from eq. (3-18), and b) Results obtained from eq (3-17) for $t = a/100$.

Fig. 3-12 displays a comparison of these two methods for loss of $0.01\delta_S$ thickness of Silver WR03 waveguide. Hence the validity of the proposed approach based on eq. (3-17) has been confirmed.

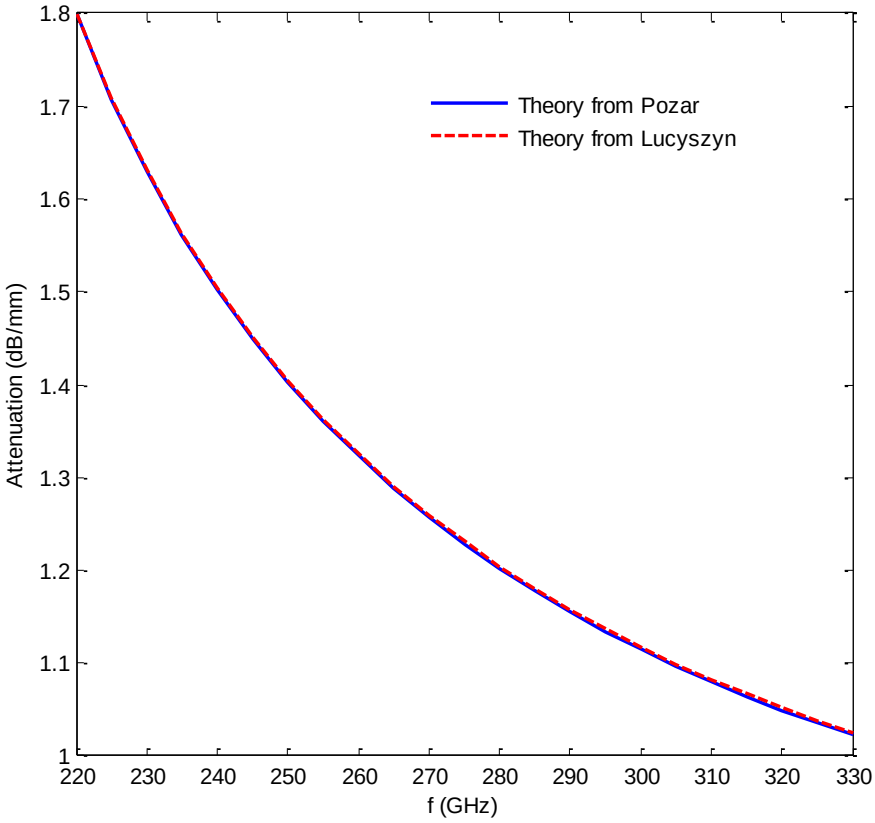

Fig. 3-12 Comparison of two different theory methods based on Pozar [12] from eq(3-17)and Lucyszyn, et. al., [25] from eq (3-22) for loss of $0.01\delta_S$ thickness of Silver WR03 waveguide

3-4-2-2 *Theoretical Results*

It has been inferred that the formulations of eq. (3-17) and eq. (3-22) have same results and therefore either of them may be used. Fig. 3-13 displays the calculated loss versus relative thickness (ratio to skin depth) of Silver thin film using eq. (3-17).

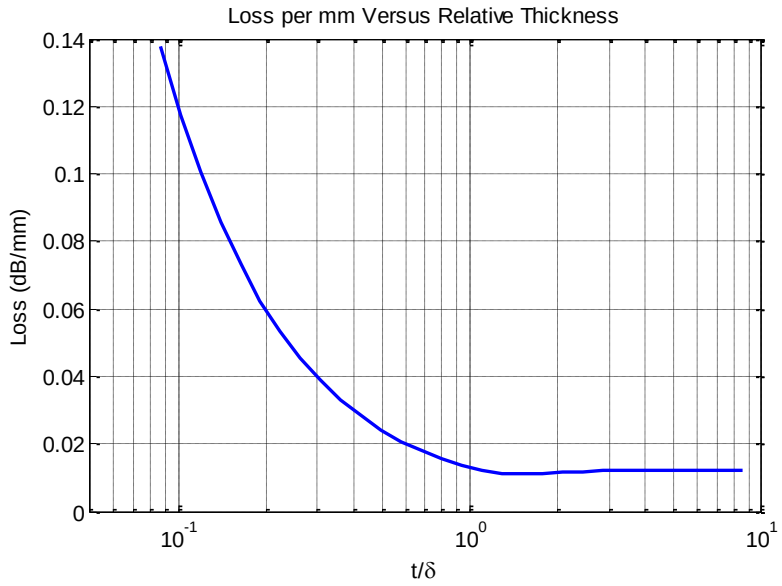

Fig. 3-13 The amount of the conductor loss in dB/mm for Silver.

Fig. 3-14 displays the loss versus frequency for the different thicknesses of Silver relative to skin depth at 300 GHz (which is equal to: $\delta_S = 115.7$ nm) for WR03 waveguide.

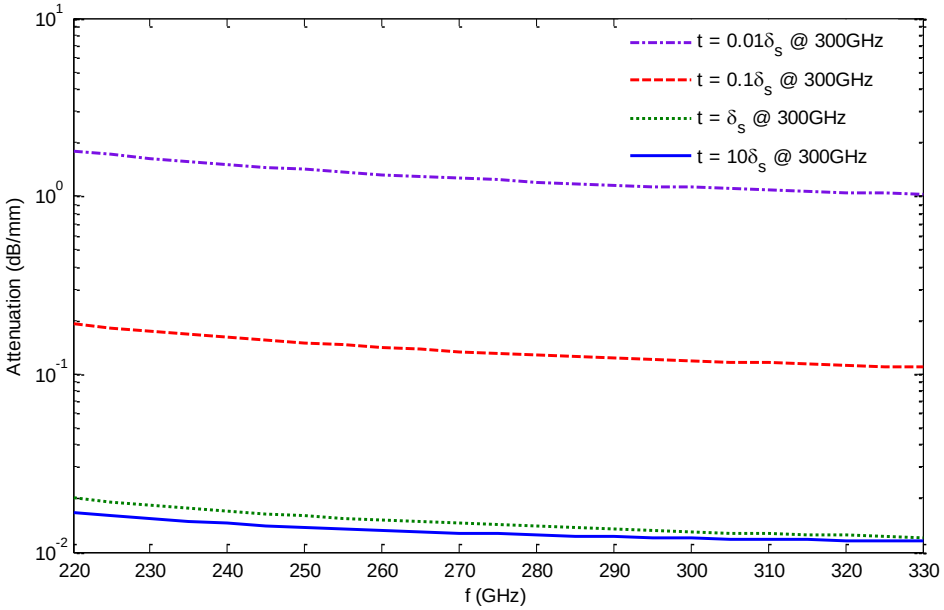

Fig. 3-14 Conductor loss versus frequency for different relative thicknesses in WR03 Silver rectangular waveguide (relative to skin depth of Silver at 300GHz) from eq. (3-17)

As expected, it can be seen that for the thinner conductors, the values of losses are considerably increased. Also the loss versus frequency has been plotted for the different

thicknesses of Platinum relative to its skin depth at 300 GHz (here δ_S = 297 nm) for WR03 waveguide the results are shown in Fig. 3-15.

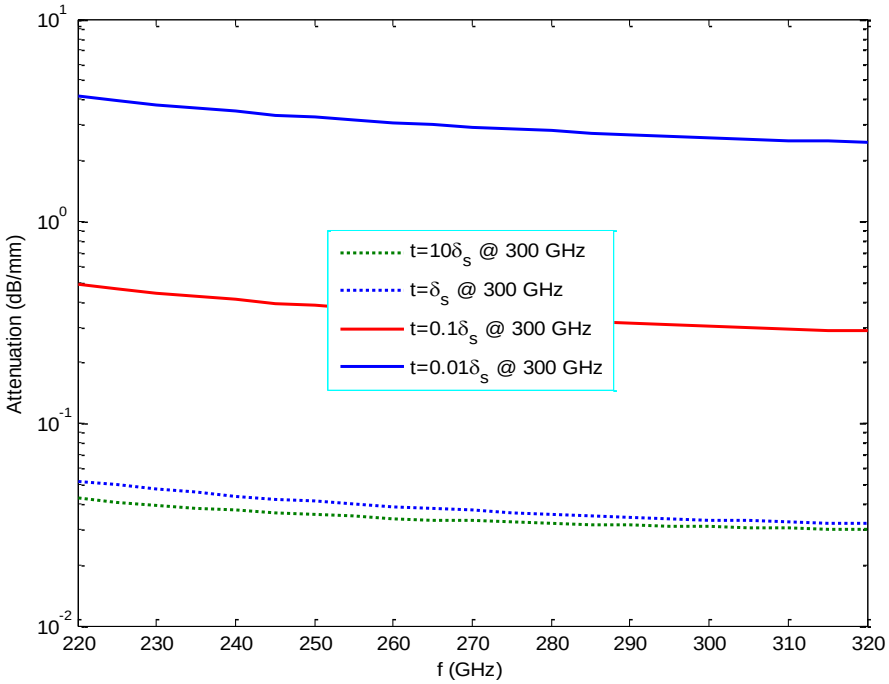

Fig. 3-15 Conductor loss versus frequency for different relative thicknesses in WR03 Platinum rectangular waveguide (relative to skin depth of Platinum at 300GHz) from eq. (3-17)

It can be concluded that the value of losses for Platinum is considerably greater than Silver. Therefore Platinum is better than Silver as a possible attenuator or a termination.

3-4-2-3 *Comparison with Simulation*

In this section the results of the thin film theory will be compared with the results of simulations carried out in CST Microwave Studio to confirm the accuracy of the proposed method and to validate the calculations. For this purpose a WR03 waveguide with thin film walls supported by SU8, as shown in Fig. 3-16, is considered.

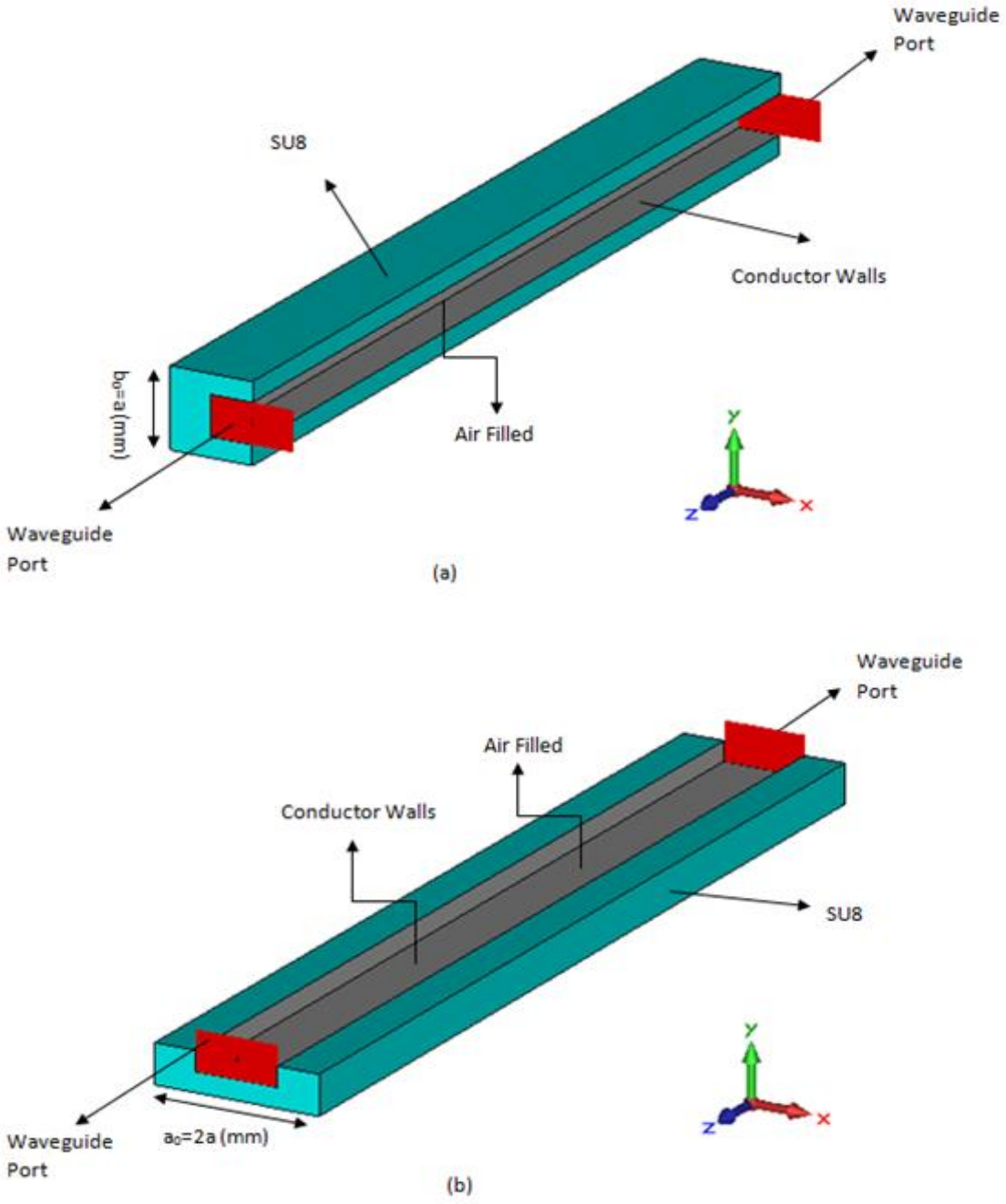

Fig. 3-16 A thin film WR03 rectangular waveguide supported by SU8 in CST. (a) Side View- (b) Top View. Grey zone show the thin film walls, green zone shows SU8, and two red sections show waveguide ports.

For good simulation of a thin film waveguide in CST, at first the usual waveguide structure was used and thin film walls were modelled with a very thin built-in lossy metal material. But with this approach CST cannot simulate thin film walls properly and results

were independent of wall thicknesses, as the built-in lossy metal material model in CST supposes that the metal thickness is much greater than the skin depth. Therefore modelling thin walls with thin metal bulks is not suitable and another solution should be found. It was seen that the best solution for modelling of thin film lossy metals in CST is by using tabulated surface impedance materials which are dedicated for thin layer of lossy metals. For these materials, there are tables which contain the values of the normalized surface resistances (R_{SN}) and reactances (X_{SN}) for different frequencies which can be calculated by:

$$R_{SN} = \mathrm{Re}\left(Z_s \frac{Z_d + Z_s \mathrm{tgh}(\gamma_s t)}{Z_s + Z_d \mathrm{tgh}(\gamma_s t)}\right) \tag{3-23}$$

$$X_{SN} = \mathrm{Im}\left(Z_s \frac{Z_d + Z_s \mathrm{tgh}(\gamma_s t)}{Z_s + Z_d \mathrm{tgh}(\gamma_s t)}\right) \tag{3-24}$$

Therefore by using this approach thin layer of lossy metals can be modelled in CST. Fig. 3-17 shows the values of the attenuation versus frequency for WR03 air-filled Silver rectangular waveguide supported by SU8 for different thicknesses relative to its skin depth at 300 GHz (which is equal to: $\delta_S = 115.7$ nm).

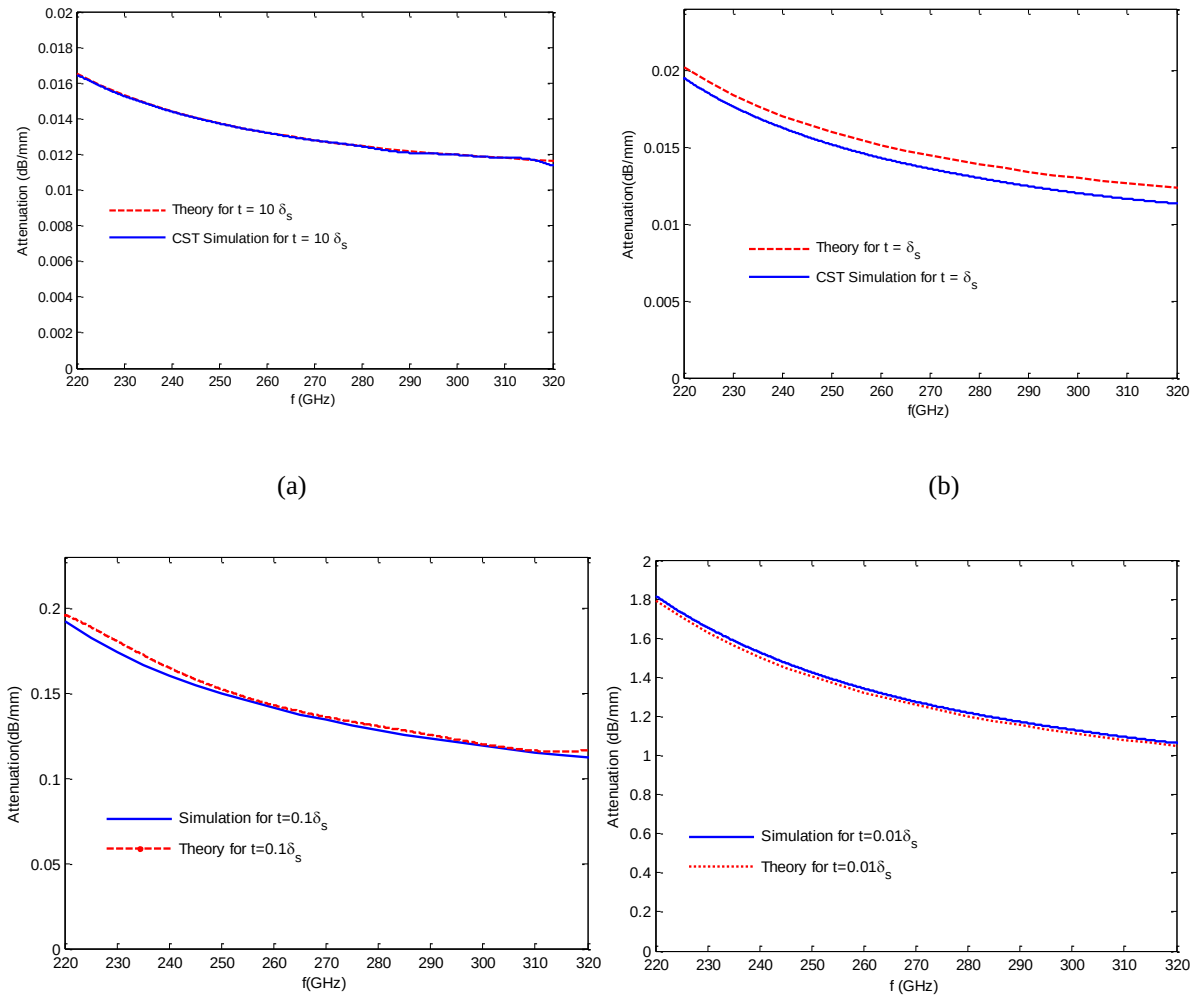

Fig. 3-17 Comparison of theory and simulation for the values of the losses versus frequency for WR03 air filled Silver rectangular waveguide supported by SU8 for a) $t = 10\delta_S$, b) $t = \delta_S$, c) $t = 0.1\delta_S$ and d) $t = 0.01\delta_S$. Theory is based on proposed formulation of eq. (3-17).

It can be seen that the simulation results obtained with CST have good agreement with the theoretical results. At first glance, more losses at higher frequencies may be expected, but it must be noted that *t* is assumed constant (is equal to skin depth of Silver at 300 GHz = 115.7 nm) and therefore the relative thickness of waveguide walls (*t* ratio to skin depth at each frequency) at lower frequencies is lower than the relative thickness at higher frequencies

and therefore the amount of attenuation at lower frequencies will be greater than those at high frequencies.

Additionally, Fig. 3-18 displays the values of the attenuation versus frequency for WR03 air-filled Platinum rectangular waveguide supported by SU8 for different thicknesses relative to its skin depth at 300 GHz (which is equal to: δ_S = 297 nm).

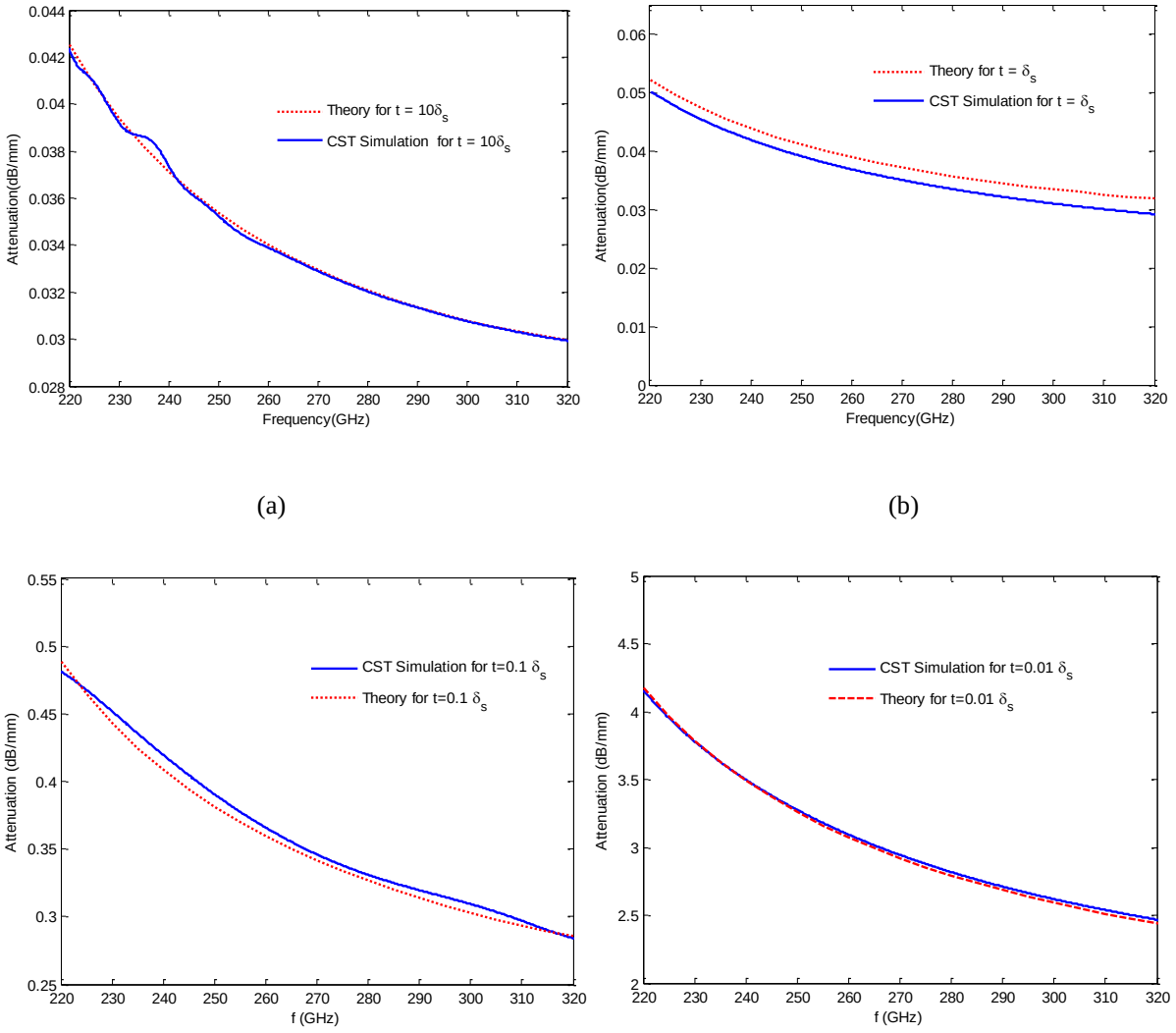

Fig. 3-18 The values of the losses versus frequency for WR03 air filled Platinum rectangular waveguide supported by SU8, for: a) $t = 10\delta_S$, b) $t = \delta_S$, c) $t = 0.1\delta_S$ and d) $t = 0.01\delta_S$. Theory is based on proposed formulation of eq. (3-17)

In the case of Platinum also, the theory and CST agreed.

Another method described in the CST literature is by using the formula of sheet resistance, this is the resistance of thin film that are uniform in the thickness. It is applicable to two dimensional systems in which thin films are considered as two dimensional objects. In the three dimensional case, as shown in, Fig. 3-19 the resistance can be written as [33]:

$$R = \rho \frac{L}{A} = \rho \frac{L}{Wt} \tag{3-25}$$

In equation (3-25) ρ is the resistivity, A is the cross-sectional area and L is the length. The cross sectional area is split into the width and the sheet thickness.

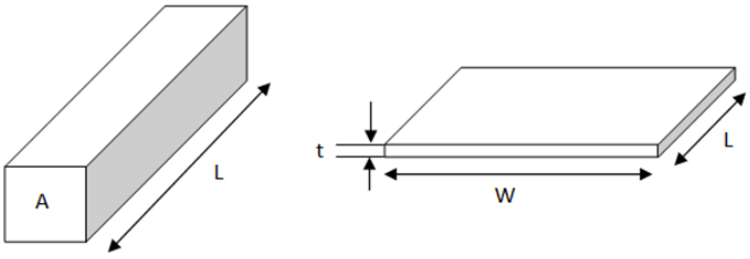

(a) (b)

Fig. 3-19 a) Resistivity of a bulk conductor b) resistivity in a thin conductor. In both cases, the current is parallel to the double arrow near the letter L [35]

By dividing the resistivity by thickness, the resistance can be written as [33]:

$$R = \frac{\rho}{t}\frac{L}{W} = R_S \frac{L}{W} \tag{3-26}$$

Where, R_s is the sheet resistance. So if the thickness of the film is known the sheet resistance can be calculated from:

$$R_S = \frac{\rho}{t} \tag{3-27}$$

Moreover, the mentioned formula can also be concluded based on eq.(3-9). Assuming a good level of conduction ($Z_d \tanh(\gamma_s t) >> Z_S$), then regarding to small amount of *t*, we will also have $\tanh(\gamma_s t) << 1$, therefore the eq. (3-9) can be approximated by:

$$Z_f = Z_s \frac{Z_d + Z_s \tanh(\gamma_s t)}{Z_s + Z_d \tanh(\gamma_s t)} = Z_s \frac{Z_d}{Z_d \tanh(\gamma_s t)} = \frac{Z_s}{\tanh(\gamma_s t)} \tag{3-28}$$

By assuming the film is adequately thin ($\gamma_s t << 1$), then it is clear that:

$$Z_f = \frac{Z_s}{\gamma_s t} \tag{3-29}$$

Using eq. (3-10) for Z_s and eq. (3-16) for γ_s, it can easily be concluded that

$$Z_f = \frac{(1+j)\sqrt{\frac{\omega\mu}{2\sigma}}}{(1+j)\sqrt{\frac{\omega\mu\sigma}{2}}t} = \frac{1}{\sigma t} = \frac{\rho}{t}; \qquad \text{Therefore:} \quad R_f = \frac{\rho}{t}, \quad X_f = 0 \tag{3-30}$$

3-5 Conclusion

In this chapter, the dissipation strategies for increasing return loss have been discussed and then each loss component has been analyzed separately. These strategies are increasing path losses due to using thin film conductor wall waveguide and having open-ended into dielectric environment. The conductor loss of different materials has been discussed and finally an analytical formulation for calculating of thin film conductor has been proposed. Its validation has been confirmed by comparison with other works and simulation results.

Chapter 4 WAVEGUIDE TERMINATIONS

4-1 Introduction

The reflection from an open-ended waveguide is discussed in Chapter 3. The main objective of this chapter is to propose a design of simple WR03 rectangular waveguide termination using the theory of open ended waveguide which is discussed in Chapter 3, section 3-3 and using thin film conductors for waveguide walls, by electromagnetic full-wave simulation using CST Microwave Studio.

In section 4-2 the general configuration and dimensions of the termination will be followed by sections 4-3 , 4-4 and 4-5 which PEC, Silver and Platinum has been used for the design and simulation.

4-2 General Configuration

The reflection from an open-ended waveguide and path loss of thin film waveguides has been discussed previously. Now the combination of these two concepts will be considered. The general configuration of a simple termination is shown in Fig. 4-1. For SU8 reasonable values of width, $a_0=2a$ and height, $b_0=a$ are assumed. Therefore, the final size of termination to be studied will be $(L+d)\times 2a\times a$.

Waveguide with thin Silver and Platinum to help form terminations will be discussed in the separate sections. For the case of Silver and Platinum, relative thicknesses of skin depth fraction of 0.1 δ_s and 0.01δ_s at 300 GHz will be investigated.

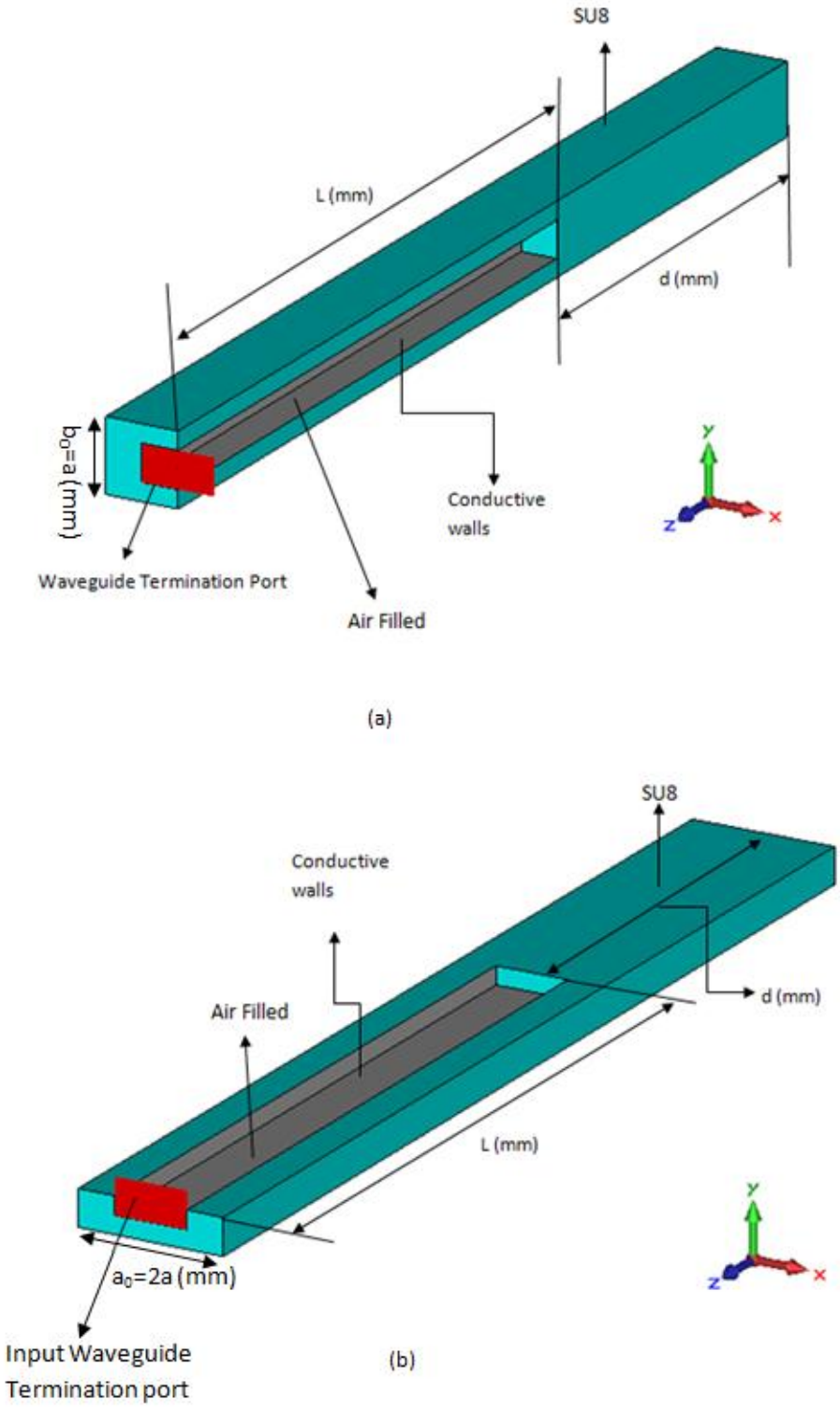

Fig. 4-1 General configuration of a half section, of simple open ended into SU8 termination. Grey zone show the thin film conductor walls, green zone shows SU8. (a) ZY sectioned view, (b) XZ sectioned view

4-3 Simple Termination with PEC

First a simple termination with PEC, shown in Fig. 4-1 has been designed and simulated for different amounts of *d*. The boundary conditions are considered as open to see the radiation. By comparing the results of the simulation from Fig. 4-2, it can be seen that for *d*, 5 mm S_{11} has optimum result as it has uniform ripples in the whole frequency band with less changes and as it moves toward the higher frequency the ripples decreased considerably. Fig. 4-3 displays the magnitude of S_{11} of a WR03 termination with PEC for *L*=10 mm and *d*= 5 mm. Also the loss tangent of SU8 in this simulation has been considered as 0.08 at 100 GHz, which quantifies the dielectric material's inherent dissipation of the electromagnetic energy into heat.

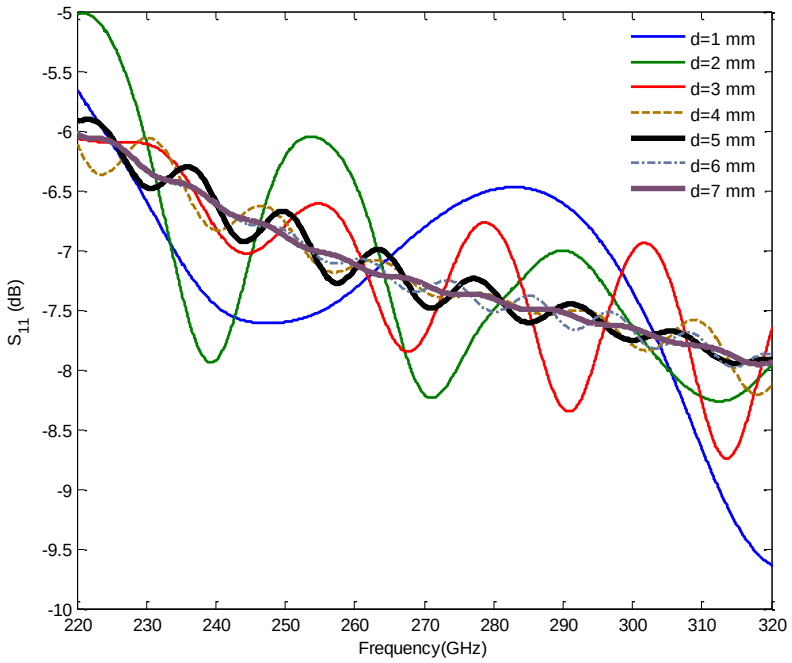

Fig. 4-2 The S_{11} of a WR03 simple open ended into SU8 termination with PEC for *L*=10 mm and different values of '*d*'.

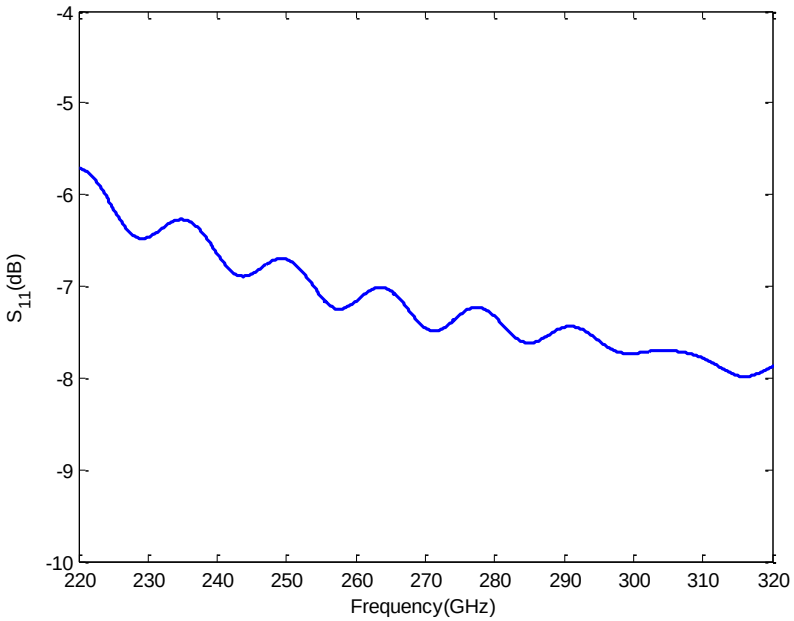

Fig. 4-3 The S_{11} of a WR03 simple open ended into SU8 termination with PEC for L=10mm and d=5 mm.

As it can be seen from the Fig. 4-3 the WR03 simple termination with PEC is a poor termination due to the high amount of reflection it.

4-4 Simple Termination with Silver

First a WR03 waveguide termination as shown in Fig. 4-1 with Silver thin layer walls has been simulated. Fig. 4-4 shows the magnitude of S_{11} for the WR03 Silver termination with metal thickness of $t = 0.1\delta_S$ (skin depth of Silver at 300GHz which it is equal to: δ_S = 115.7 nm) for L=10mm and d=5mm. A tabular surface impedance model for thin films was used [34]. According to eq. (3-9) discussed in section 3-4-2, thin film conductors, the impedance, looking from the upper surface of the thin film towards the SU8, has been calculated. The calculated resistance and reactance for silver thin film sheet at 3 different frequencies is been given in Table 4-1.

Table 4-1 Tabular surface impedance model, used for Silver in CST for $t = 0.1\ \delta_s$ where $\delta_s = 115.7$ nm

Frequency (GHz)	Resistance (Ω)	Reactance (Ω)
220	$R_{SN} = 1.3617$	$X_{SN} = 0.0073$
270	$R_{SN} = 1.3618$	$X_{SN} = 0.0087$
300	$R_{SN} = 1.3618$	$X_{SN} = 0.0096$

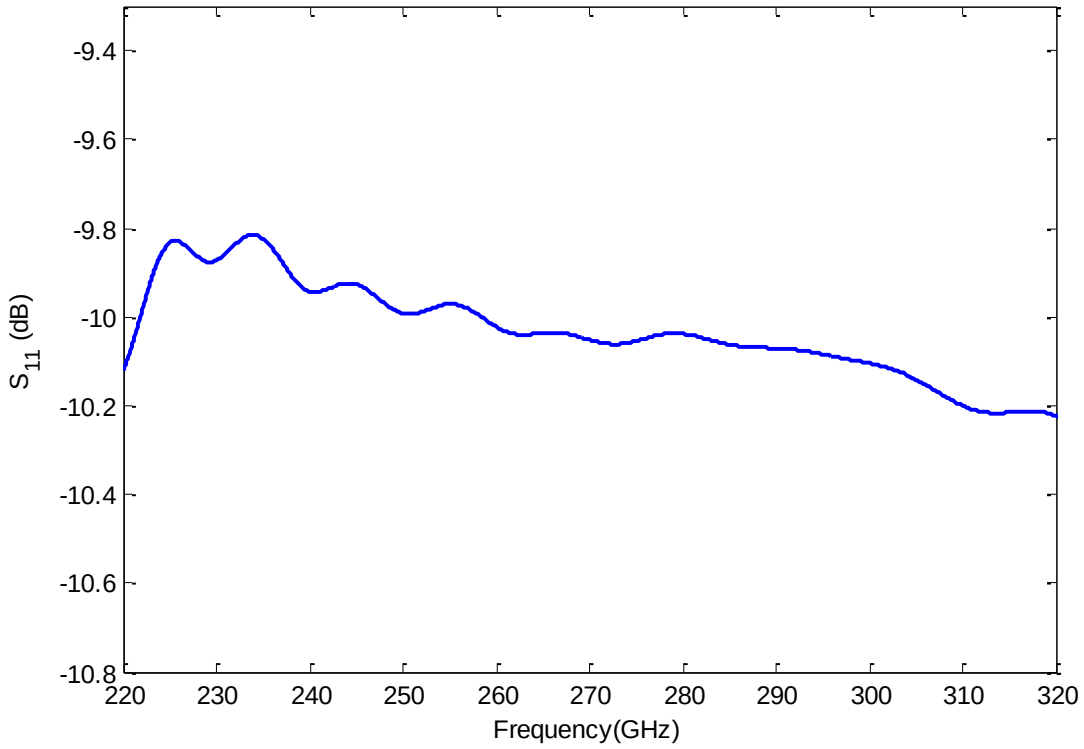

Fig. 4-4 The S_{11} of a WR03 Silver termination with thickness of $t = 0.1\ \delta_s$ where δ_s=115.7 nm at 300 GHz for L=10 mm

The effect of the length of SU8 in the front of the open-end (parameter of d), for three different values of d have been compared and displayed in Fig. 4-6.

For constant amount of thickness it is clear that the ratio of t/δ is increased at higher frequencies (because the skin depth (δ) is decreased at higher frequencies) therefore the effect of using thin film for improvement of reflection will be decreased at higher frequencies.

Additionally from open ended equations (which it is shown for PEC waveguide in Fig. 3-4) we expect that S_{11} will be decreased at higher frequencies.

These two mentioned independent trends make frequency behaviour of total reflection.

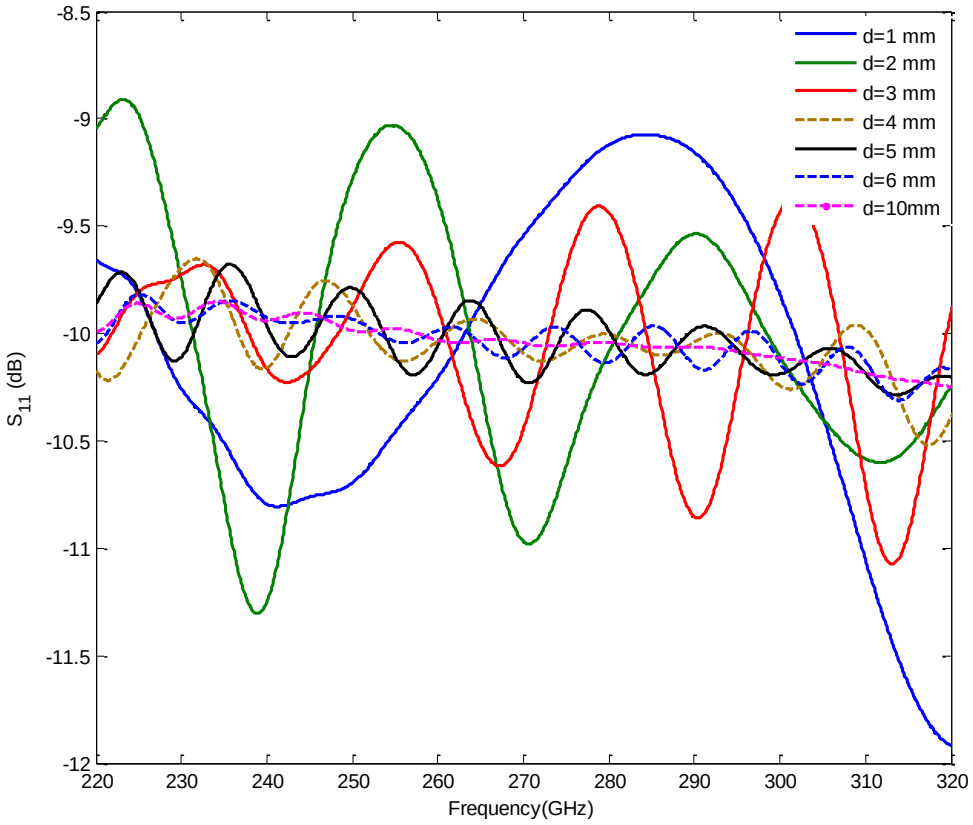

Fig. 4-5 Comparison of the S_{11} of a WR03 Silver termination with thickness of $t = 0.1\ \delta_S$ where δ_s= 115.7 nm at 300GHz for different values of *d* and *L*=10 mm.

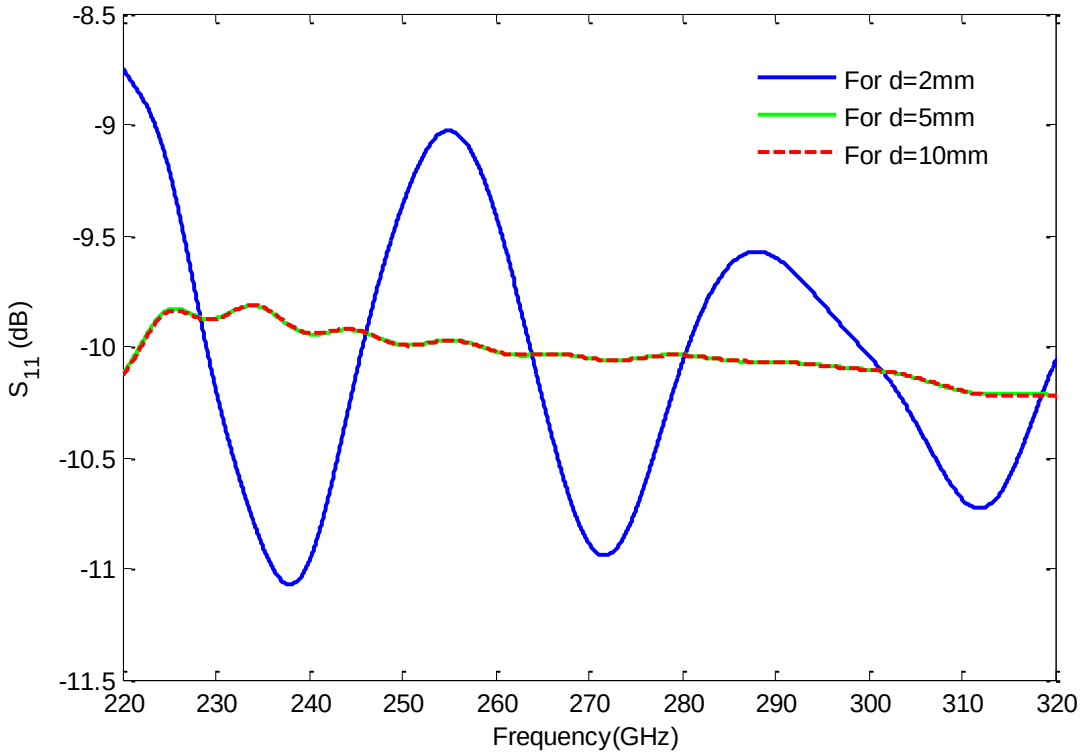

Fig. 4-6 Comparison of the S_{11} of a WR03 Silver termination with thickness of $t = 0.1\ \delta_S = 11.57\text{nm}$ for different values of d and L=10 mm.

It can be seen that the small values of d degrade the termination a little and higher values do not improve the result considerably. Therefore, it can be deduced that d=5 mm will be a good value for this termination structure with a film thickness of $t = 0.1 \times \delta_S$.

Additionally, to evaluate the effect of the thickness of thin film conductor walls on reflection coefficient of the desired termination Fig. 4-7 shows the value of the S_{11} for a WR03 Silver termination with metal thickness of $t = 0.01\delta_S$ for L=10 mm and d=5 mm. The values of resistance and reactance have been calculated and are shown in Table 4-2.

Table 4-2 Tabular surface impedance model, data for Silver in CST for $t = 0.01\ \delta_s$ where $\delta_s = 115.7$ nm

Frequency (GHz)	Resistance (Ω)	Reactance (Ω)
220	$R_{SN} = 12.7636$	$X_{SN} = 0.0501$
270	$R_{SN} = 12.7681$	$X_{SN} = 0.0407$
300	$R_{SN} = 12.7698$	$X_{SN} = 0.0367$

The reflection in this case is acceptable for a termination and it is considerably better than a normal Silver thick waveguide, but it must be noted that the thickness of Silver is very small (1.157 nm which approximately is equal to height of 4 atoms of Silver).

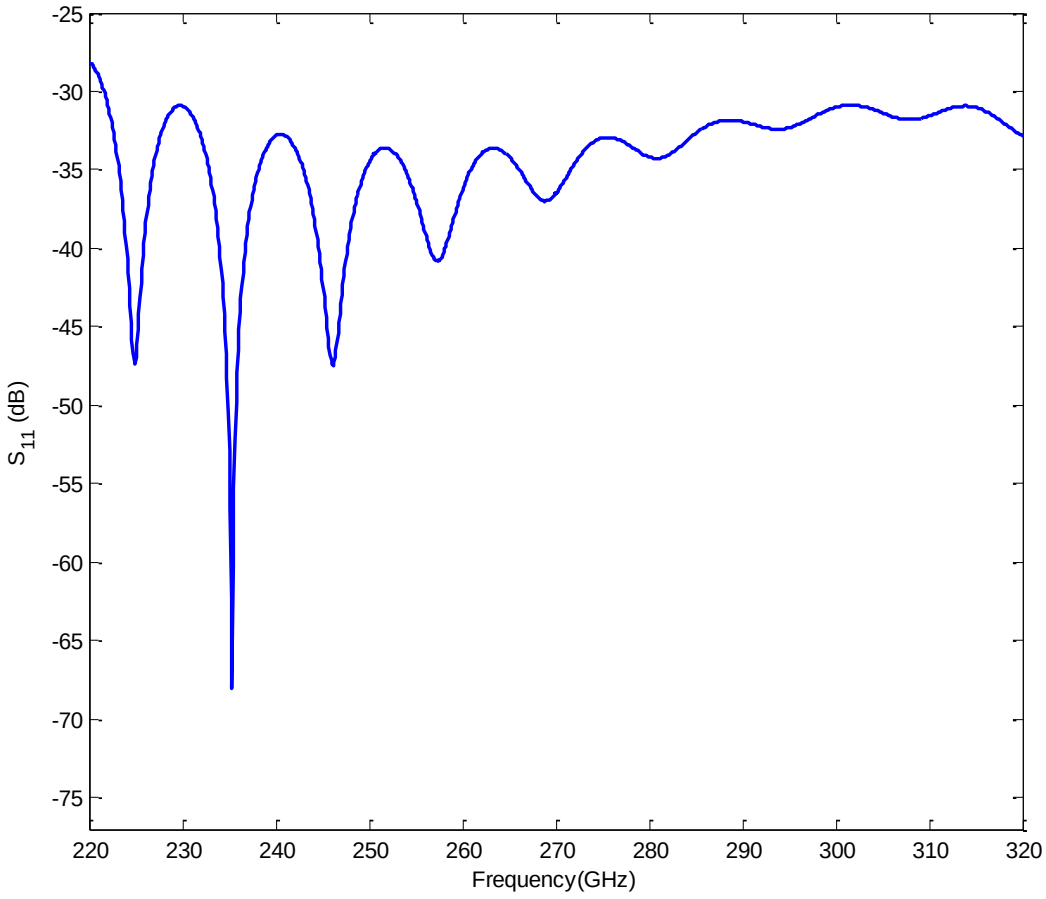

Fig. 4-7 The S_{11} of a WR03 Silver termination with thickness of $t = 0.01\delta_s = 1.157\text{nm}$ for L=10 mm and d=5 mm.

In this case the value of the reflection coefficient is compared for different values of *d* and *L=10* mm which it is shown in Fig. 4-8.

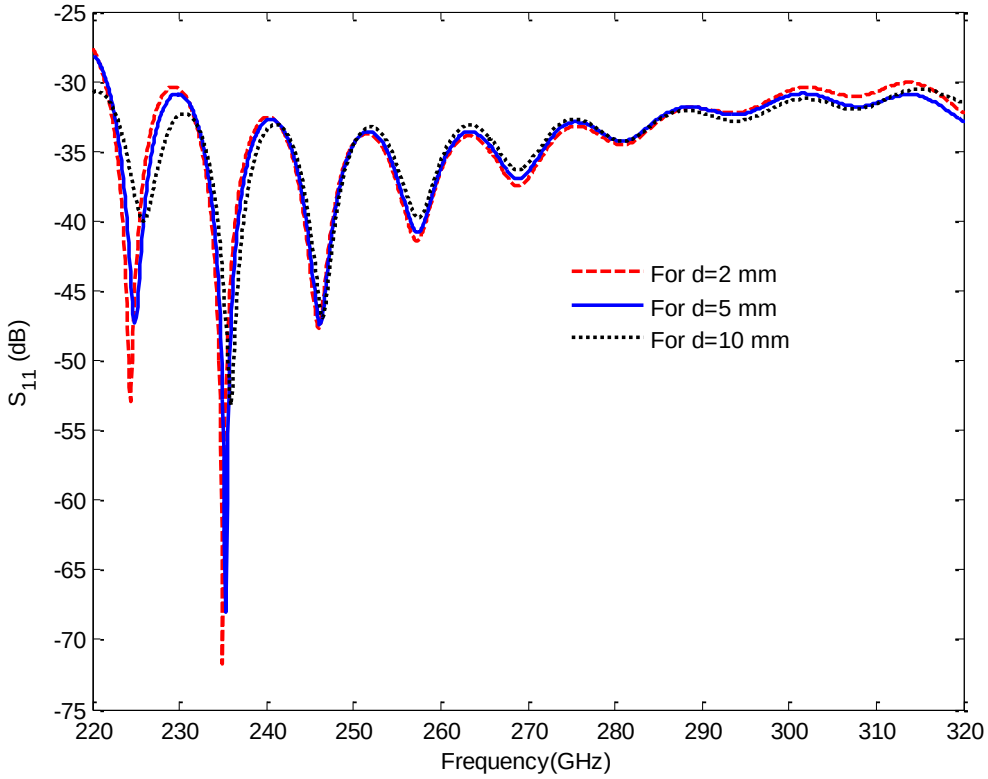

Fig. 4-8 Comparison of the S_{11} of a WR03 Silver termination with thickness of $t = 0.01\delta_S = 1.157\text{nm}$ for different values of *d* and *L*=10 mm.

In the case of $t = 0.01\delta_S$ also the value of *d= 5 mm* seems to be a proper value.

4-5 Simple Termination with Platinum

Here Platinum is used for carrying out a comparison with Silver. Platinum is a metal with lower conductivity. Fig. 4-9 shows the S_{11} of a WR03 Platinum termination with metal thickness of $t = 0.1\delta_S$ (skin depth of Platinum at 300 GHz which it is equal to: δ_S=297 nm) for *L=10*mm and *d=5*mm. Data for the tabular surface impedance model, according to eq.(3-9), is given in the following table:

Table 4-3 Tabular surface impedance model data for Platinum in CST for $t = 0.1\ \delta_S$ where $\delta_S = 29.7$ nm

Frequency (GHz)	Resistance (Ω)	Reactance (Ω)
220	R_{SN} =3.4698	X_{SN}=0.0212
270	R_{SN}=3.4702	X_{SN}=0.0244
300	R_{SN}=3.4703	X_{SN}=0.0265

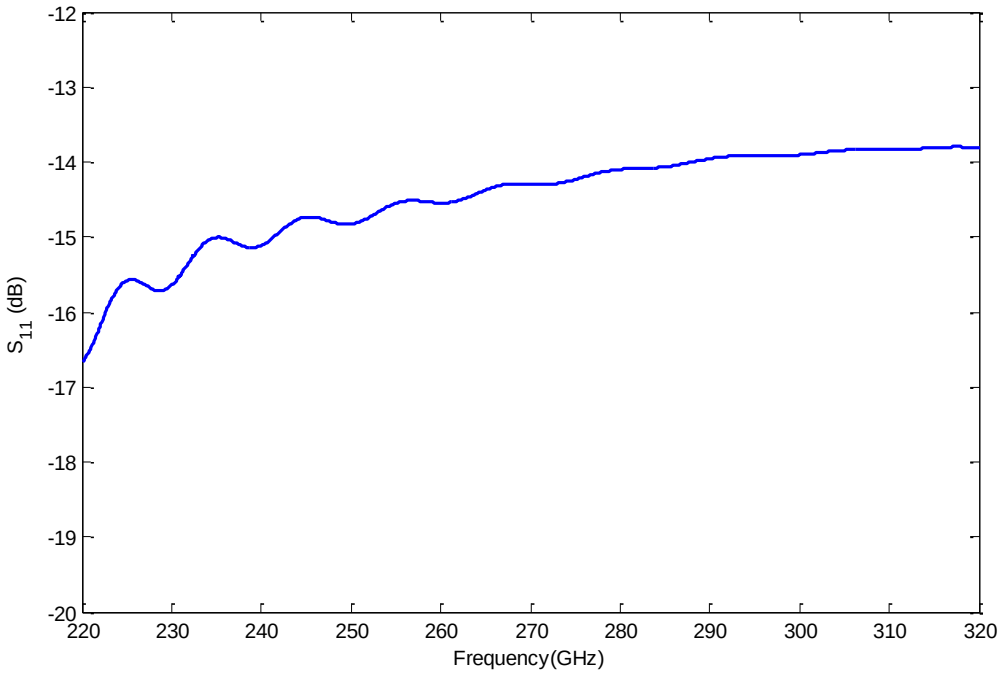

Fig. 4-9 The S_{11} of a WR03 Platinum waveguide termination with thickness of $t = 0.1\delta_S$ for L=10 mm and d=5 mm.

In this case also the value of reflection is compared for different values of d and L=10 mm which it is shown in Fig. 4-10. Therefore from Fig. 4-10 for Platinum d=5 mm is an optimal value as it has less ripples and changes in the whole frequency band comparing with d=2 mm. As the total size of the device at the end will be important and it would be great to be able to make it as small as possible, between d = 5 mm and d = 10 mm, d = 5 mm will be chosen.

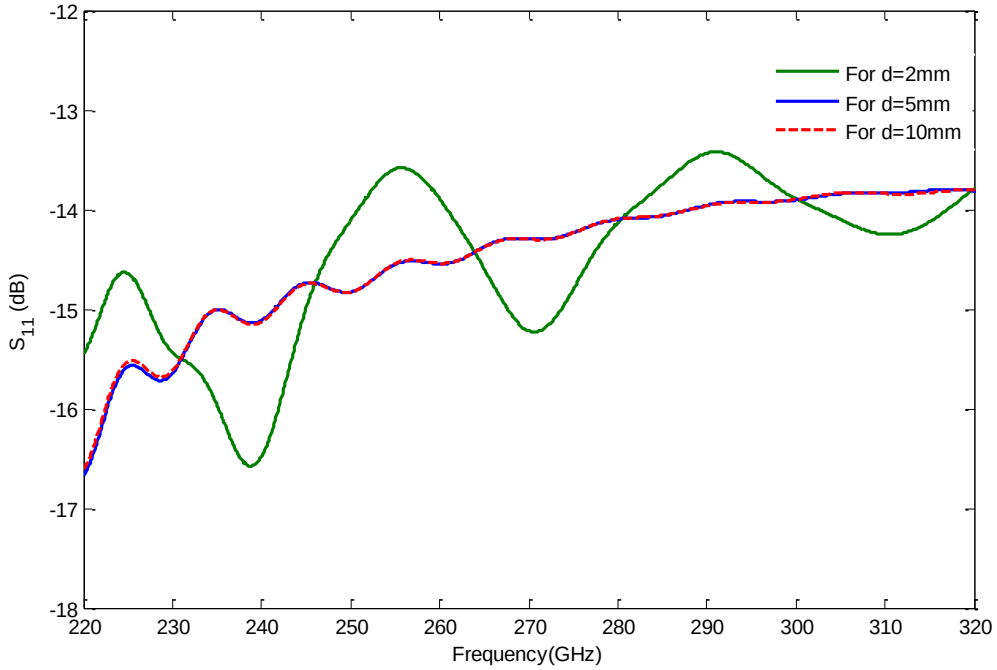

Fig. 4-10 Comparison of the S_{11} of a WR03 Platinum termination with thickness of $t = 0.1\delta_S$ for different values of d and L=10 mm.

Moreover Fig. 4-11 shows the value of the S_{11} for a WR03 Platinum termination with metal thickness of $t = 0.01\delta_S$ for L=10 mm and d=5 mm. For defining this thickness of Platinum in CST as a tabular surface impedance model, eq. (3-9) has been used to define the values which are given in the following table.

Table 4-4 Tabular surface impedance model, data for Platinum in CST for $t = 0.01\delta_S$

Frequency (GHz)	Resistance (Ω)	Reactance (Ω)
220	R_{SN}=29.6448	X_{SN}=0.2683
270	R_{SN}=29.6697	X_{SN}=0.2174
300	R_{SN}=29.6790	X_{SN}=0.1955

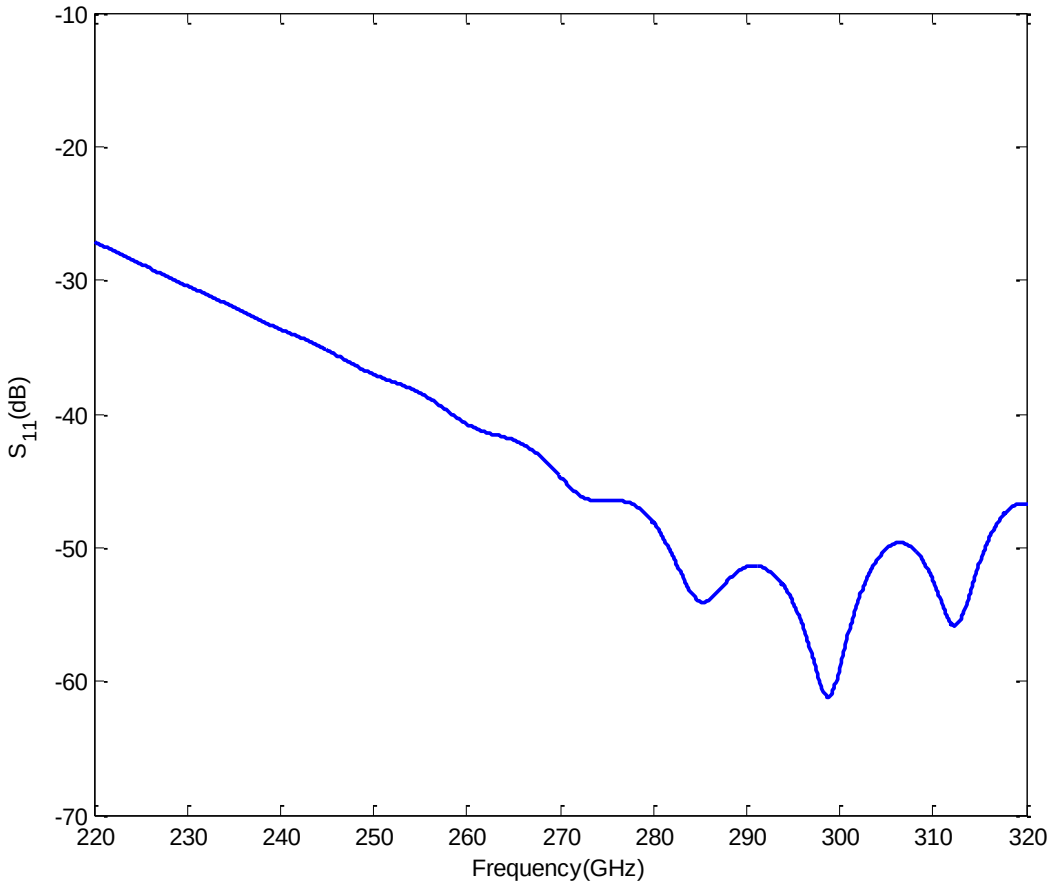

Fig. 4-11 The S_{11} of a WR03 Platinum termination with thickness of $t = 0.01\delta_S = 2.97\text{nm}$ for *L=10* mm and *d=5* mm.

In this case as can be seen from the Table 4-4 , the values of R_{SN} and X_{SN} are high so the S_{11} result is completely different from all previous plots and it does not look reasonable result this is because CST cannot simulate very thin conductor films.

4-6 Conclusion

Simple terminations for PEC, Silver and Platinum waveguide have been simulated in this chapter. To model thin film conductor in CST, tabular surface impedance model has been used. It can be concluded that Platinum is better than Silver, but both of them in this simple form have not enough return loss to use as a good waveguide termination and the

modification of the structure may be needed. One of the good approaches for this purpose is the tapering of dielectric material, in this case SU8, in open-ended terminal.

The open ended waveguide is not a good choice for termination. Despite its lower conductivity, Platinum termination has less return loss in comparison with Silver termination but due to its very small thickness, physical realization of the Platinum termination is too difficult. For this reason the following chapter will look at the new design techniques.

Chapter 5 TAPERED TERMINATIONS

In chapter 4 simple waveguide, open ended terminations with silver and platinum for different conductor thicknesses has been proposed and simulated. To improve the performance of the termination, a suitable technique is to taper the SU8 at the open-end of the waveguide. To see the effect of the tapering, different kinds of SU8 tapering will be proposed in the following subsections.

5-1 Triangular Tapering open ended into **SU8**

5-1-1 Height Tapering

First kind of tapering which is considered is height tapering, as shown in Fig. 5-1. The length of the taper is named L_{tap}.

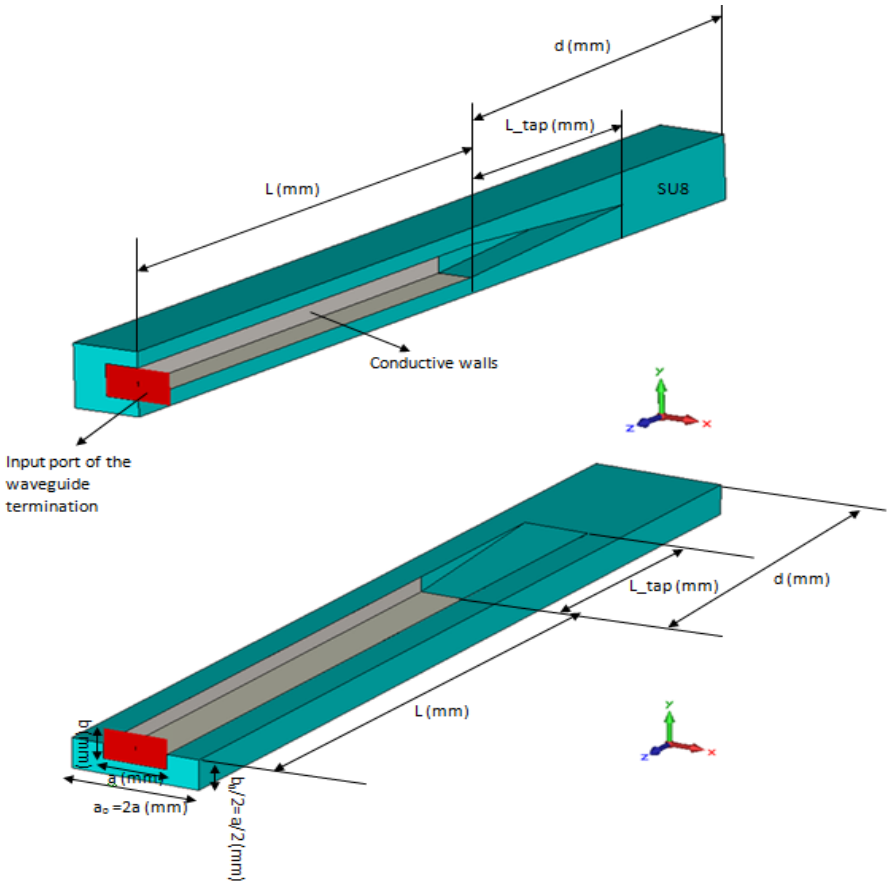

Fig. 5-1 General configuration of a waveguide termination with height tapering inside the SU8.

Fig. 5-2 (a) Side view (b) Top View

The height tapered terminations will be discussed for PEC, Silver and Platinum.

5-1-1-1 *Height Tapering with PEC*

According to Fig. 5-1 a waveguide termination where the waveguide walls are PEC and with height tapering inside the SU8 has been considered. To demonstrate the effects of height tapering and produce the optimum length for taper, Fig. 5-3 displays S_{11} of a WR03 height tapered termination with PEC for different values of L_{tap} with L=10 mm and d=5 mm.

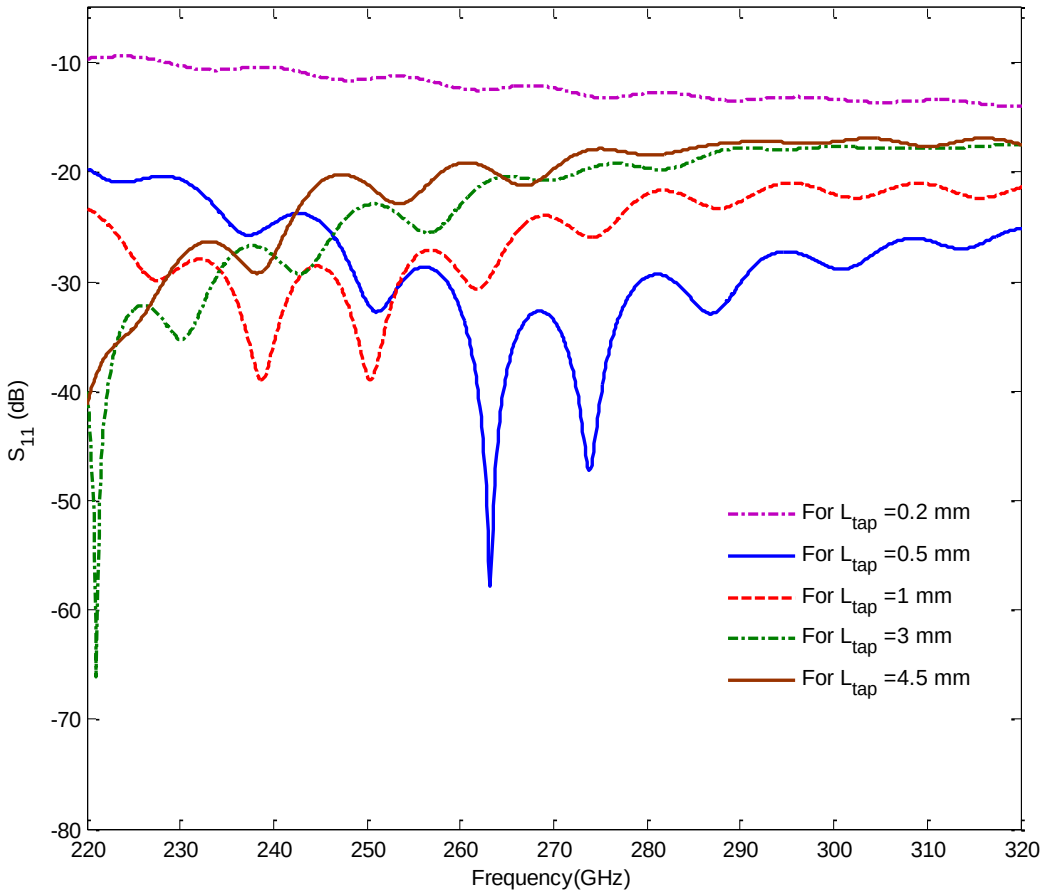

Fig. 5-3 The S_{11} of a WR03 height tapered termination with PEC for different values of L_{tap} and L=10mm and d=5 mm.

From Fig. 5-3, comparing the results of the CST simulation it can be concluded that L_{tap}=0.2 mm is very small value for tapering and it is almost the same result as having no taper.

It can be seen that as L_{tap} increases, the reflection decreases for the structure of the termination. With L_{tap}=0.5 mm the reflection is less than -25 dB. So L_{tap}=0.5 mm can be good value to start the design of height tapered termination with PEC.

5-1-1-2 *Height Tapering with Silver*

Fig. 5-1 is the configuration of the WR03 height tapering waveguide termination, here it is modified to demonstrate the effect of different conductors and their thickness. PEC has been replaced by thin film silver and the simulation has been repeated. Fig. 5-4 shows S_{11} for a WR03 silver termination with metal thickness of $t = 0.1\delta_S$, for different amount of tapering length (L_{tap}) and L=10 mm and d=5 mm.

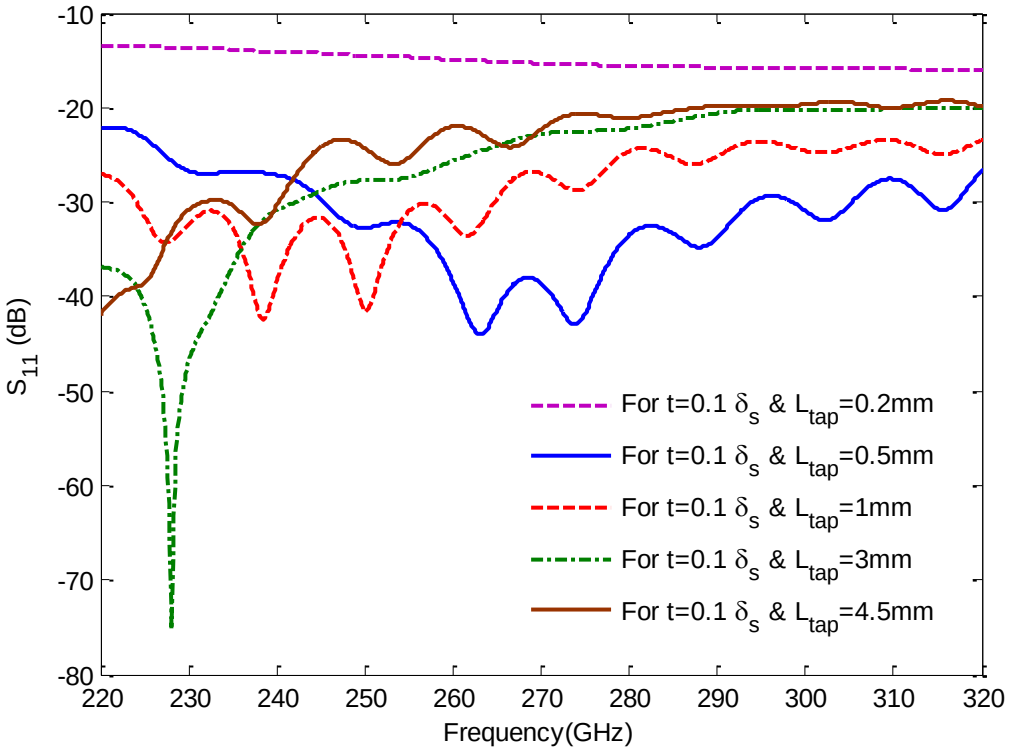

Fig. 5-4 The S_{11} of a WR03 Silver height tapered termination with thickness of t = 0.1 δ_s for different values of L_{tap} .L=10 mm and d=5 mm.

It can be seen that for configuration of WR03 Silver waveguide termination with L_{tap}=0.5 mm the mean of S_{11} is better than 30 dB and it is a good choice as in the frequency range of 250 GHz to 310GHz the reflection is less than -30 (dB).

Now, to see the effect of the thickness of WR03 Silver in a height tapered termination with conductive walls, a WR03 Silver waveguide termination with $t = 0.01\delta_S$, height tapering has been simulated. Fig. 5-5 shows the S_{11} of a WR03 Silver termination with metal thickness of $t = 0.01\delta_S$, for different amount of tapering length and with *L=10* mm and *d=5* mm. To define the thickness for Silver in CST, tabular surface impedance model discussed in Chapter 4 and Table 4-2 has been used.

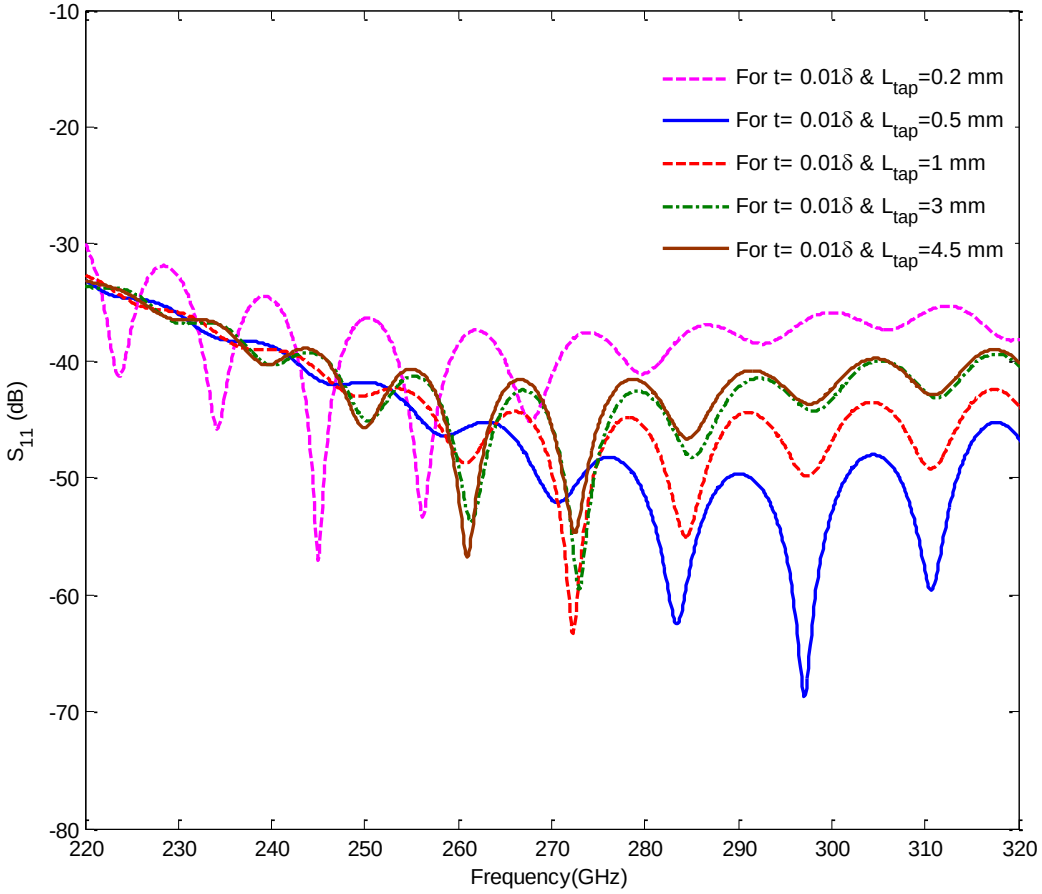

Fig. 5-5 The S_{11} of a WR03 Silver height tapered termination with thickness of $t = 0.01\delta_s$ for different values of L_{tap} . *L*=10 mm and *d*=5 mm.

From Fig. 5-5 it can be seen that for WR03 Silver height tapered termination with thickness of t=0.01δ_s = 1.157 nm, in the whole frequency band, 220 GHz to 320 GHz the S_{11} is better than -32 dB. In this case also L_{tap}=0.5 mm seems to be the best value for tapering length inside the SU8 as the S_{11} in better than 46 dB for L_{tap}=0.5 mm.

L_{tap}=0.5 mm has been chosen but because Silver material with t=0.01 δ_s= 1.157 nm is very thin and it is hard to make, the simulation has been repeated by replacing Silver with Platinum for t=0.1δ_s=27.9 nm. This is discussed in the next section.

5-1-1-1 Height Tapering with Platinum

In Chapter 3, Fig. 3-7, the attenuation for WR03 rectangular waveguide with different conductors has been shown. Also it has been discussed that the value of attenuation (dB/mm) for WR03 rectangular waveguide made by platinum is about 8 times more than the WR03 rectangular waveguide made by Silver.

This time to see the effect of using thin film platinum and to compare the results with thin film Silver, as in the Fig. 5-1, the WR03 height tapering waveguide termination, the thin film Silver has been replaced by thin film Platinum and the WR03 Platinum waveguide termination with height tapering has been simulated. Fig. 5-6 displays the S_{11} of a WR03 Platinum termination with metal thickness of Platinum $t = 0.1\delta_s$ for different amount of tapering length (L_{tap}) and with L=10 mm and d=5 mm.

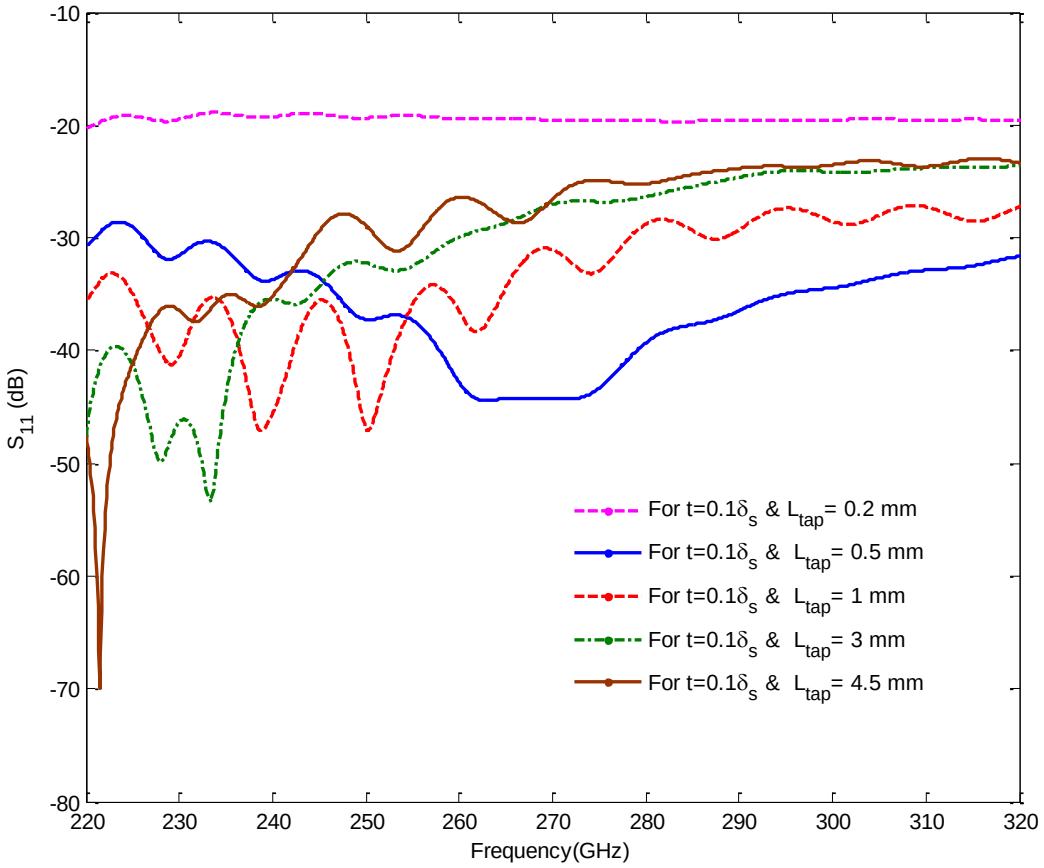

Fig. 5-6 The S_{11} of a WR03 Platinum height tapered termination with thickness of $t = 0.1\delta_S$ for different values of L_{tap} . L=10 mm and d=5 mm.

It shows that in the case of platinum with t=0.1 δ_s=29.7 nm, L_{tap}=0.5 mm, the S_{11} is better than -36 dB.

Also by comparing Fig. 5-4 and Fig. 5-6 it can be concluded that between Silver and Platinum, Platinum gives better results for the WR03 waveguide termination.

In this section, different lengths of tapering have been tested and simulated. The CST simulation results, show that L_{tap}= 0.5 mm is the proper value for the length of tapering. Also CST simulation has been done for both Silver and Platinum with different thickness which can be inferred that Platinum has the best result because in comparison with Silver it leads to less reflection.

The effect of the direction of the tapering which means inner or outer height tapering will be discussed in section 5-1-2 for PEC and platinum with L_{tap}= 0.5 mm.

5-1-2 Inner Height Tapering

A second kind of tapering is the inner height tapering which is similar to height tapering with tapering inside the waveguide as shown in Fig. 5-7. This kind of tapering is common for implementation of microwave waveguide terminations, which use a triangular absorber inside a short circuited waveguide.

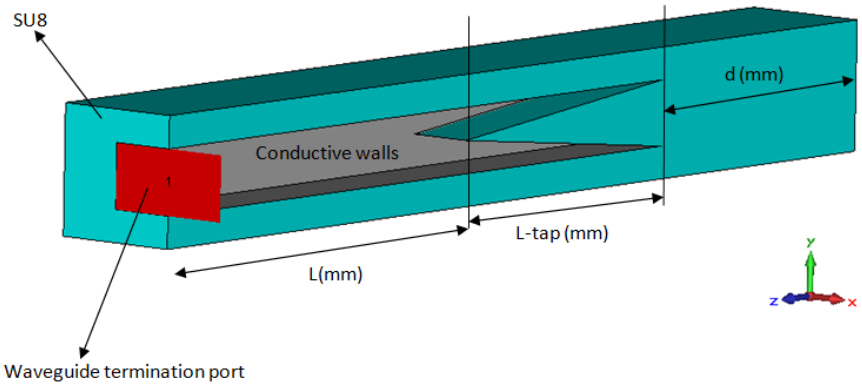

Fig. 5-7 General configuration of a waveguide termination with inner height tapering inside the Waveguide

To compare the inner height tapering model with height tapering termination, PEC has been used to model the WR03 PEC termination.

As discussed in the previous section that L_{tap} = 0.5 mm gives the best results comparing with the other tapering length. Fig. 5-8 presents the S_{11} for the WR03 PEC termination with inner height tapering for L_{tap}=0.5 mm with L=10 mm and d=5 mm. It can be seen that in the whole frequency band S_{11} is better than - 20 dB.

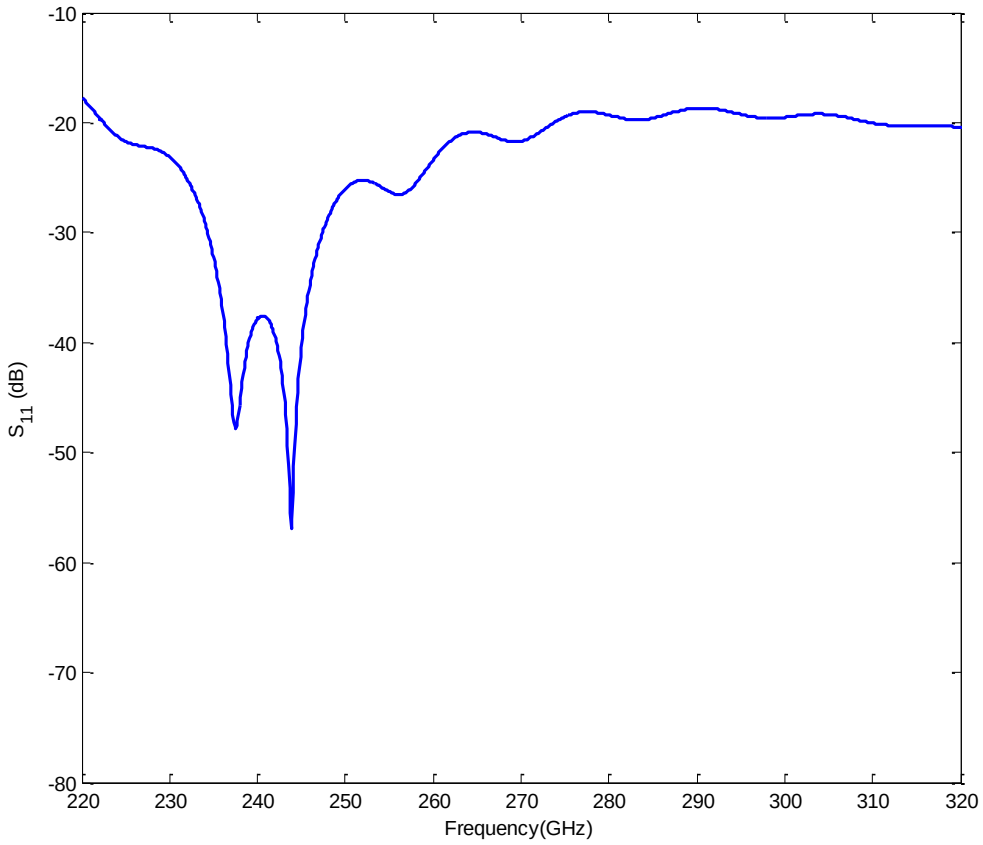

Fig. 5-8 The S_{11} of a WR03 PEC termination with inner height tapering for L_{tap}=0.5 mm, L=10 mm and d=5 mm.

Different length of tapering for WR03 PEC inner height tapering has been simulated by Microwave CST Studio design and then the S_{11} (dB) has been compared. From Fig. 5-8 it can be seen that the average value of S_{11} for L_{tap}=0.5 mm the S_{11} is better than -24 dB.

Comparing the average value of S_{11} versus L_{tap} for height tapering PEC termination and inner height tapering termination, it can be concluded that between the height tapering and inner height tapering, the height tapering method for L_{tap}=0.5 mm with S_{11} better than 30 dB gives less return loss and it is a more convenient design.

As it is shown in section5-1-1 , a WR03 waveguide termination with Platinum, L_{tap} = 0.5 mm, L=10 mm has a good result in comparison with Silver. In this section CST simulation have been done for WR03 Platinum termination with waveguide wall thickness of $t = 0.1\delta_S$ =29.7 nm, for L_{tap}=0.5 mm, L=10 mm and d=5 mm.

Fig. 5-9 displays the S_{11} of the WR03 platinum termination with inner height tapering and metal thickness of $t = 0.1\delta_S$ for L_{tap} = 0.5 mm, L=10 mm and d =5 mm.

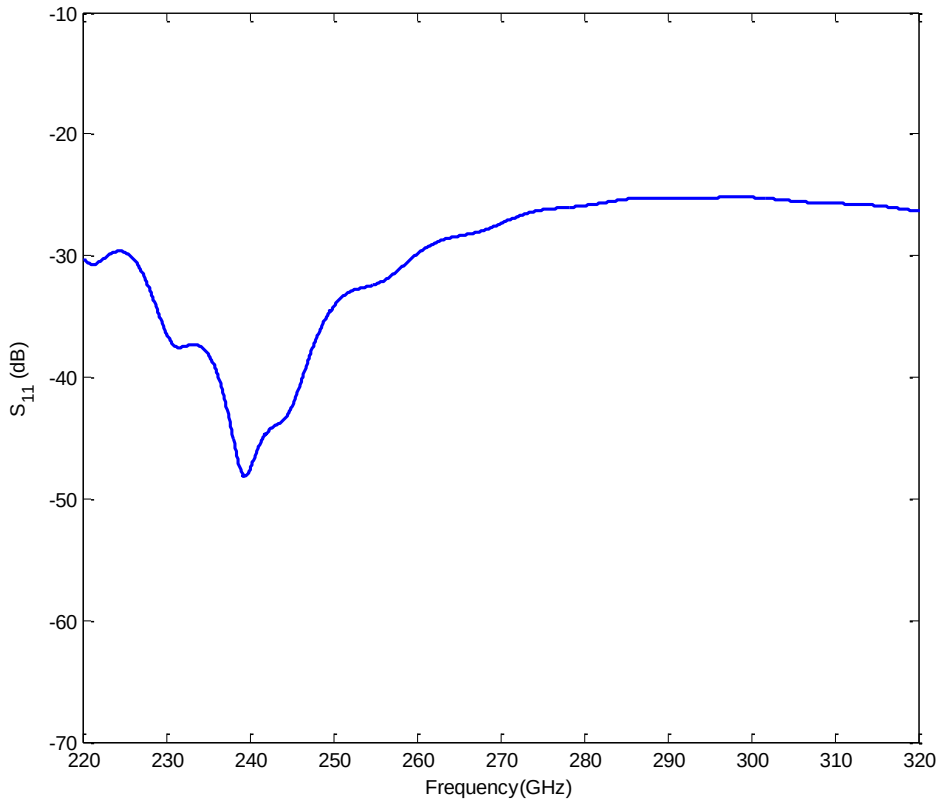

Fig. 5-9 The S_{11} of a WR03 Platinum termination with inner height tapering and metal thickness of $t = 0.1\delta_S$ = 29.7 nm for L_{tap}=0.5 mm, L=10 mm and d=5 mm.

The value of S_{11} for WR03 Platinum inner height tapering with t =$0.1\delta_s$ can be seen from Fig. 5-9. It can be seen that L_{tap} = 0.5 mm gives the S_{11} about -31 dB. In this case the return loss will be more than the return loss from WR03 platinum height tapering t =0.1 δ_s.

Comparison between this case and height tapering technique, which has been discussed in section 5-1-1, shows that the inner height tapering technique is not as good as the height tapering one.

Other tapering methods which can be investigated are tapering in width direction. This method is discussed in the next section.

5-1-3 Width Tapering

A third type of tapering is width tapering. This is shown in Fig. 5-10.

In this section PEC and Platinum have been used for Microwave CST Studio design simulations.

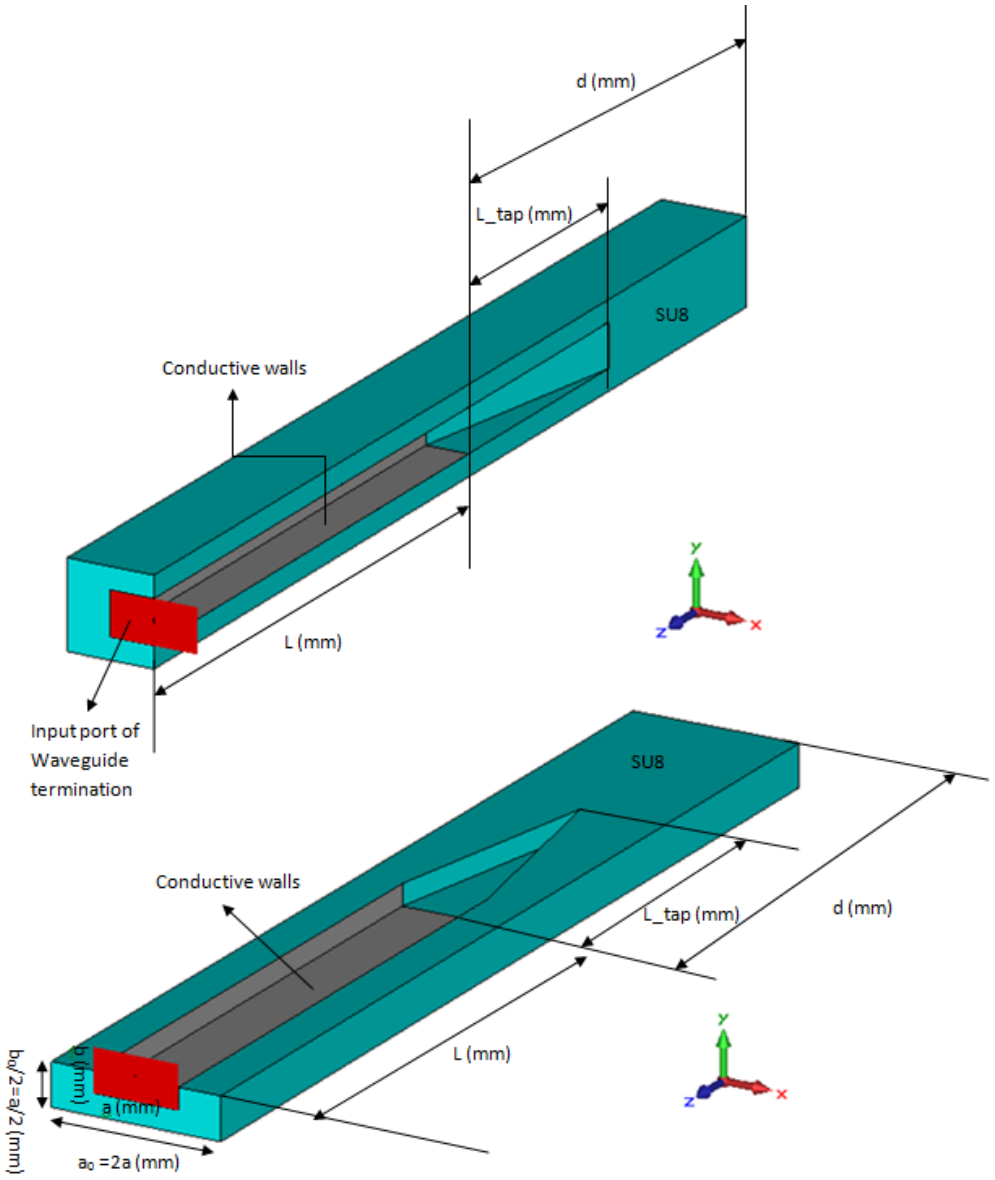

Fig. 5-10 General configuration of a waveguide termination with width tapering inside the SU8

From Fig. 5-11 and comparing different values of L_{tap} it can be seen that L_{tap} = 0.5 mm is good enough for width tapering method as it has less ripples and smooth manner in the whole frequency range in compare with other values of L_{tap}.

To compare the width tapering and height tapering design, WR03 termination with PEC has been modelled and tapered in width direction. Fig. 5-11 shows that the WR03 PEC termination with width tapering for different length of tapering. It can be seen that the average value of S_{11} in width tapering design is about -20 dB while from Fig. 5-3 in section 5-1-1-1 the average value of S_{11} for height tapering design is about -35 dB.

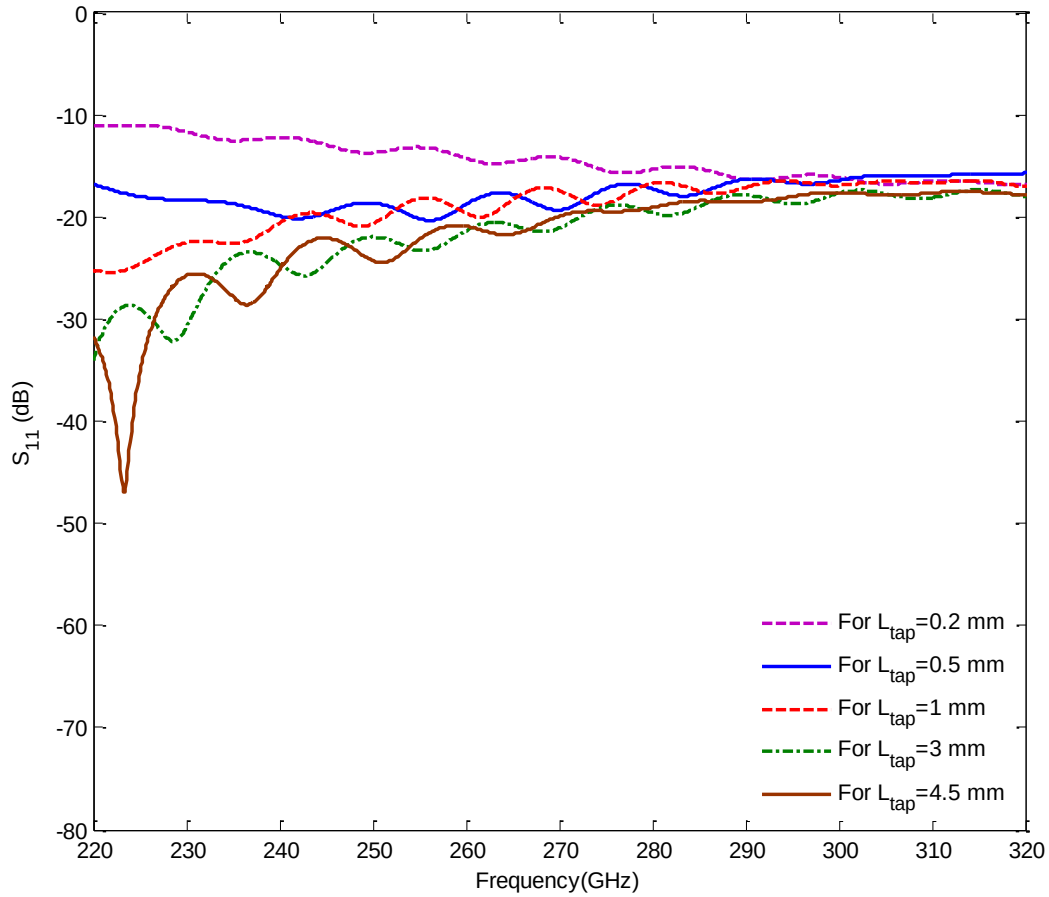

Fig. 5-11 The S_{11} of a WR03 PEC termination with width tapering for different L_{tap}, L=10 mm and d=5 mm.

The CST simulation has been repeated for WR03 width tapering. PEC has been replaced by Platinum with thickness of $t = 0.1\delta_S$ for L_{tap}=0.5 mm, L=10 mm and d=5 mm.

In Fig. 5-12, the comparison between WR03 Platinum, height tapered termination and width tapered termination for t=0.1δ_s design has been done.

It can be seen that for the frequency range of 220 GHz to 260 GHz, the magnitude of S_{11} for width tapered design is almost better than -24 dB but for the range of 260 GHz to 320 GHz the reflection has been increased and S_{11} varies between -20 dB to -25 dB. For height tapered termination in the whole frequency range the S_{11} is better than -30 dB.

This is not as good as the S_{11} of height tapering method.

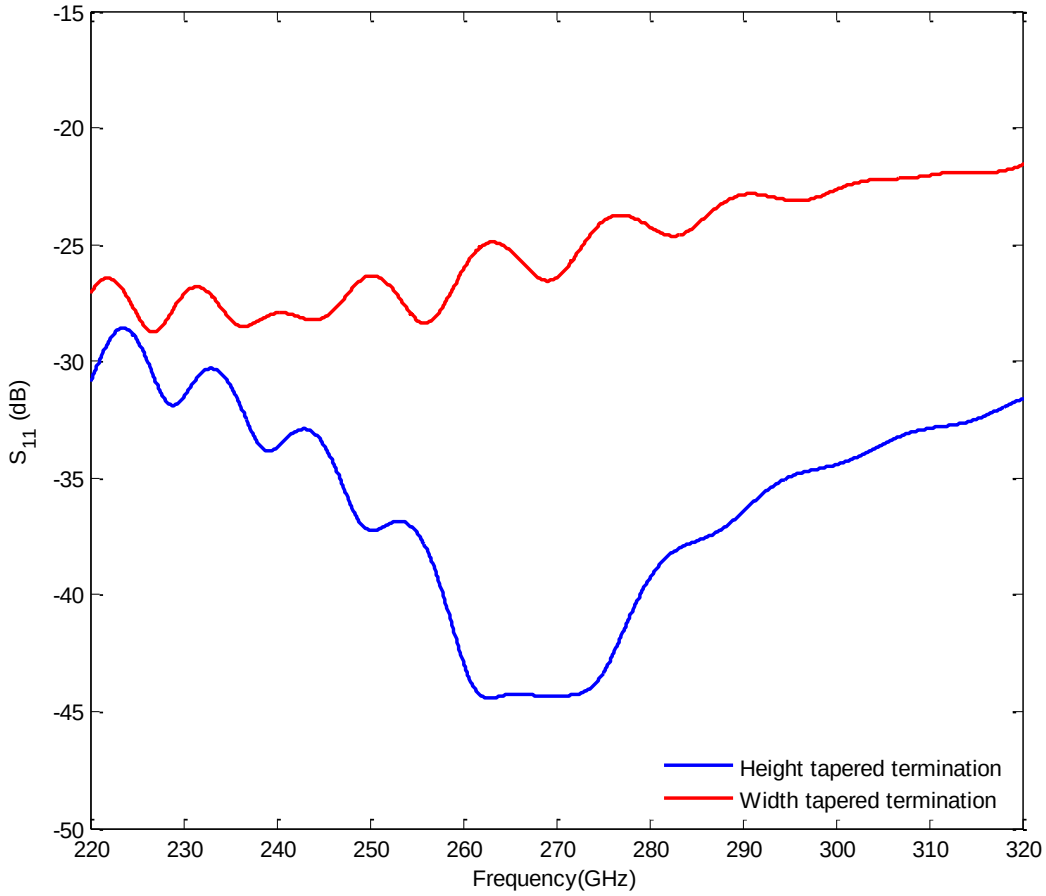

Fig. 5-12 The S_{11} of a WR03 Platinum termination with height tapering and width tapering. Metal thickness of $t = 0.1\delta_S$ = 29.7 nm for L_{tap}=0.5 mm, L=10 mm and d=5 mm.

5-1-4 Comparison Triangular Tapers

Here the optimum results of three kinds of triangular tapering, Height tapering, Inner height tapering and width tapering from sections 5-1-1, 5-1-2, 5-1-3 are compared in the similar conditions, L=10 mm, d= 5 mm, L_{tap} = 0.5 mm for PEC. The comparison result is shown in Fig. 5-13. From the CST simulations results it can be concluded that between the three kinds of tapering, height tapering (dotted blue line) shows best result as in the whole frequency band, from 250 GHz to 320 GHz the S_{11} is better than -25 dB.

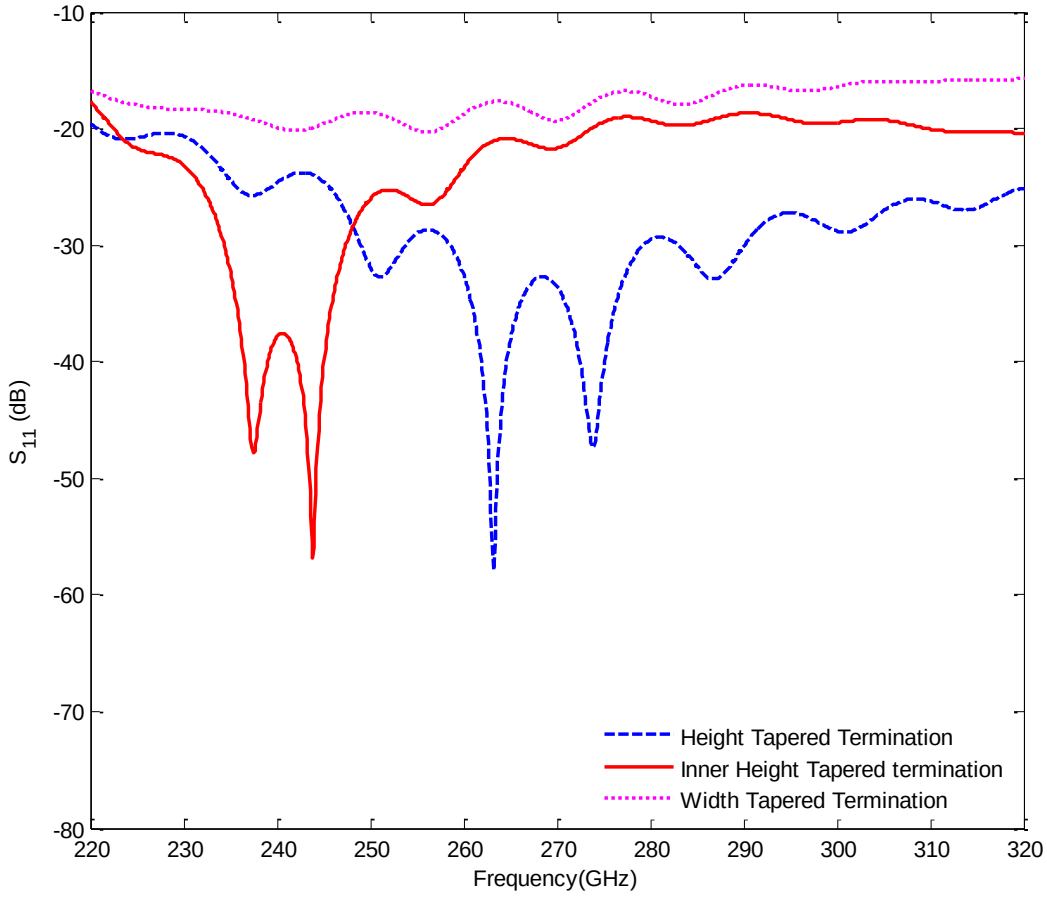

Fig. 5-13 Comparison of the S_{11} of a WR03 PEC termination with different kinds of triangular tapering.

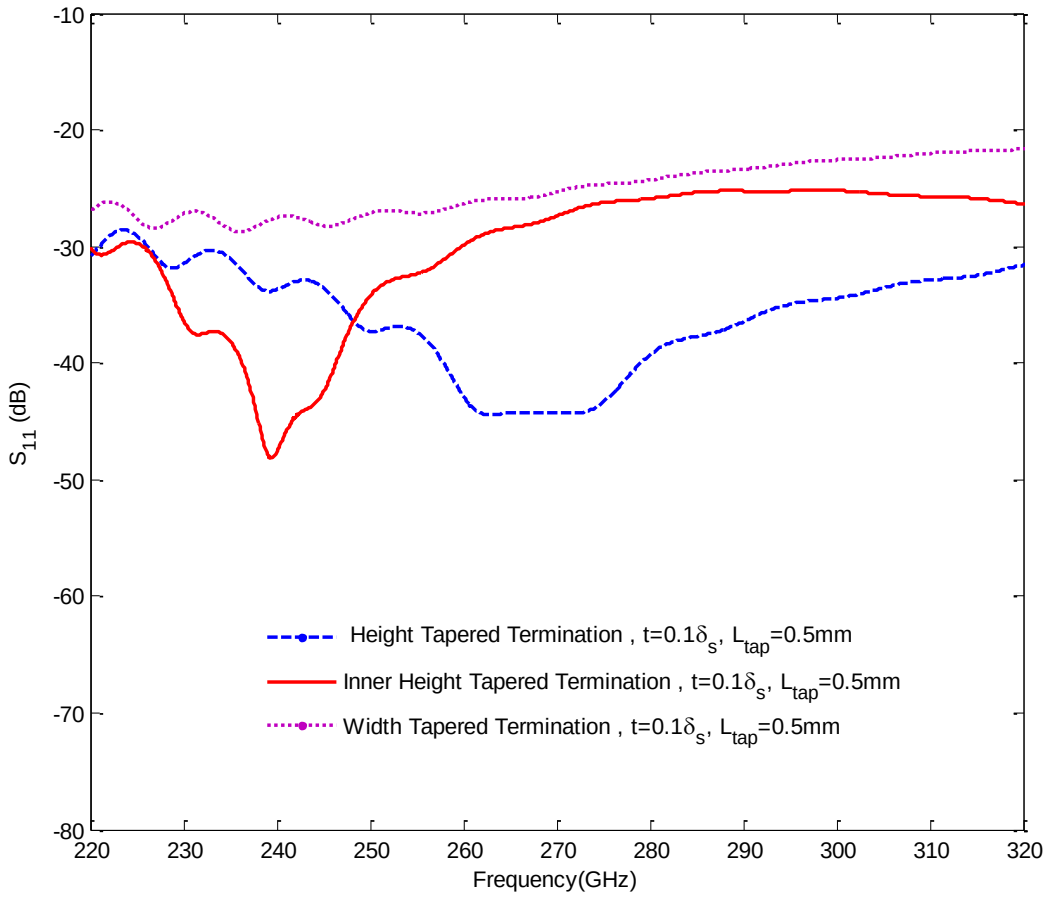

Fig. 5-14 Comparison of the S_{11} of a WR03 Platinum termination with different kinds of triangular tapering for $t = 0.1\delta_s$, L_{tap}=0.5 mm, L=*10* mm and d=*5* mm.

Fig. 5-14 shows the results after repeating the procedure above but Platinum is chosen as the material and the thickness of the conductor has been considered in CST simulation. The comparison of the three kinds of triangular tapering for Platinum has been carried out and they are compared in the similar manner, that means $t = 0.1\delta_s$. It can be concluded that between the three kinds of tapering, height tapering (dotted blue line) shows best result as in the frequency band, from 250 GHz to 320 GHz the S_{11} is better than -30 dB.

Beside the triangular shape for tapering, pyramid can be used for tapering too. Therefore section 5-2 will discuss about pyramidal tapering.

5-2 Pyramidal Tapering

Another kind of tapering is the pyramidal tapering. As shown in Fig. 5-15, in this kind of tapering, a pyramid with same cross section of waveguide is cut out inside the SU8 the depth of this pyramid is called length of tapering, L_{tap}.

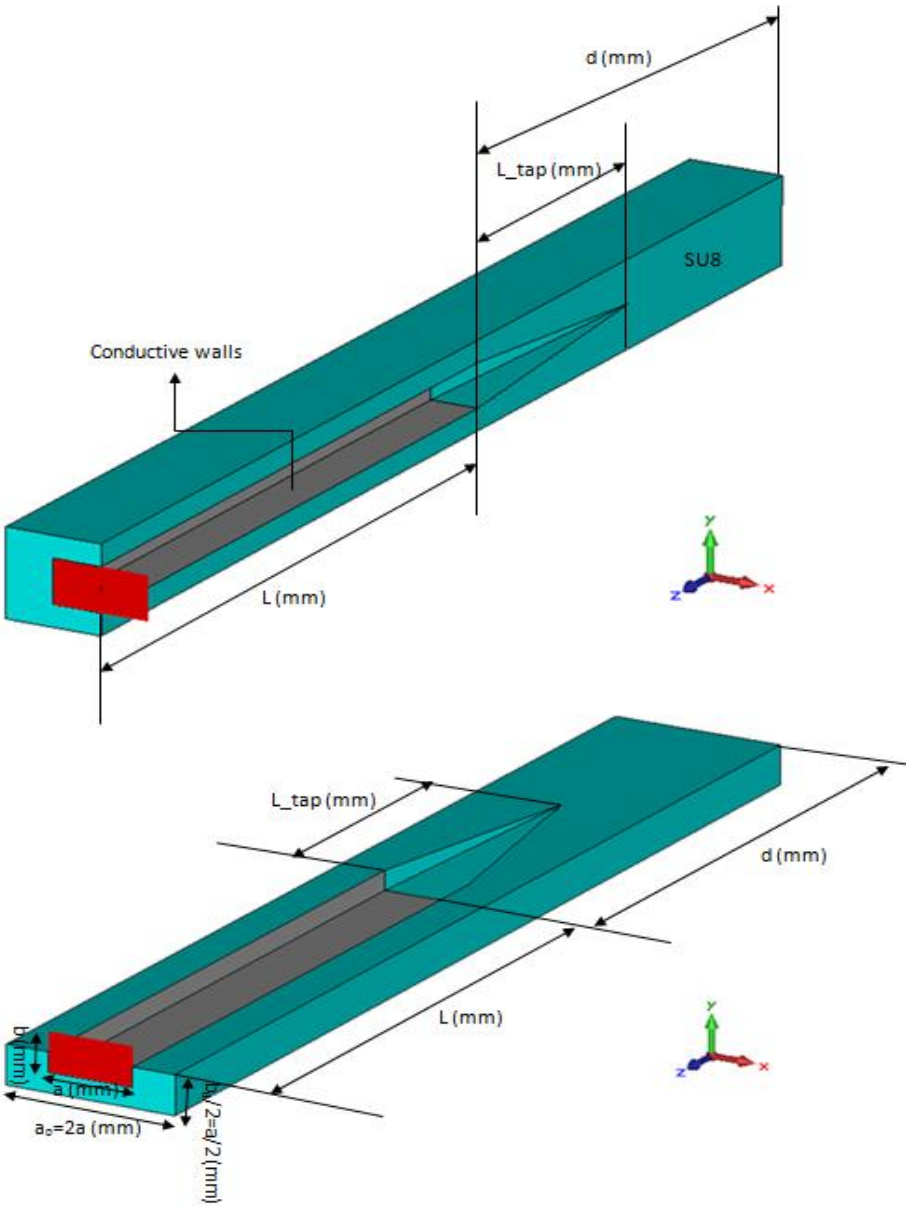

Fig. 5-15 General configuration of a waveguide termination with pyramidal tapering inside the SU8

(a)ZY sectioned view (b) XZ sectioned view

Fig. 5-16 displays the comparison of S_{11} of a WR03 termination with PEC for different values of L_{tap} with pyramidal tapering for L=10 mm and d=5 mm. Results show that L_{tap}=1 mm has optimal result but not as well as result of triangular tapering.

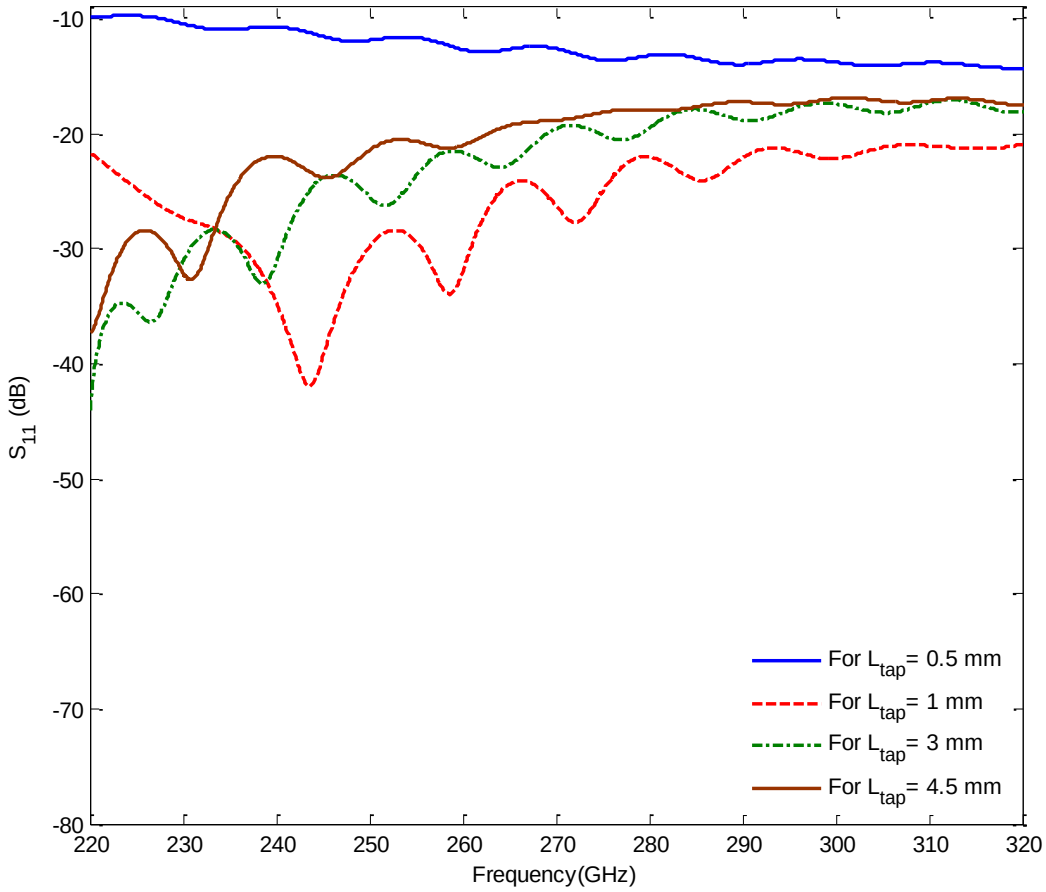

Fig. 5-16 Comparison of the S_{11} of a WR03 PEC termination for different values of L_{tap} with pyramidal tapering for *L=10mm* and *d=5mm*.

Fig. 5-17 shows the comparison between the S_{11} of a WR03 termination with Platinum conductor for different values of L_{tap} with pyramidal tapering for $t = 0.1\delta_S$, L=10 mm and d=5 mm. The results show that for L_{tap}=1 mm the S_{11} is lower than -27 dB at the whole frequency range. So L_{tap} = 1 mm is the best value for the length of the pyramid but is not as good as triangular tapered design.

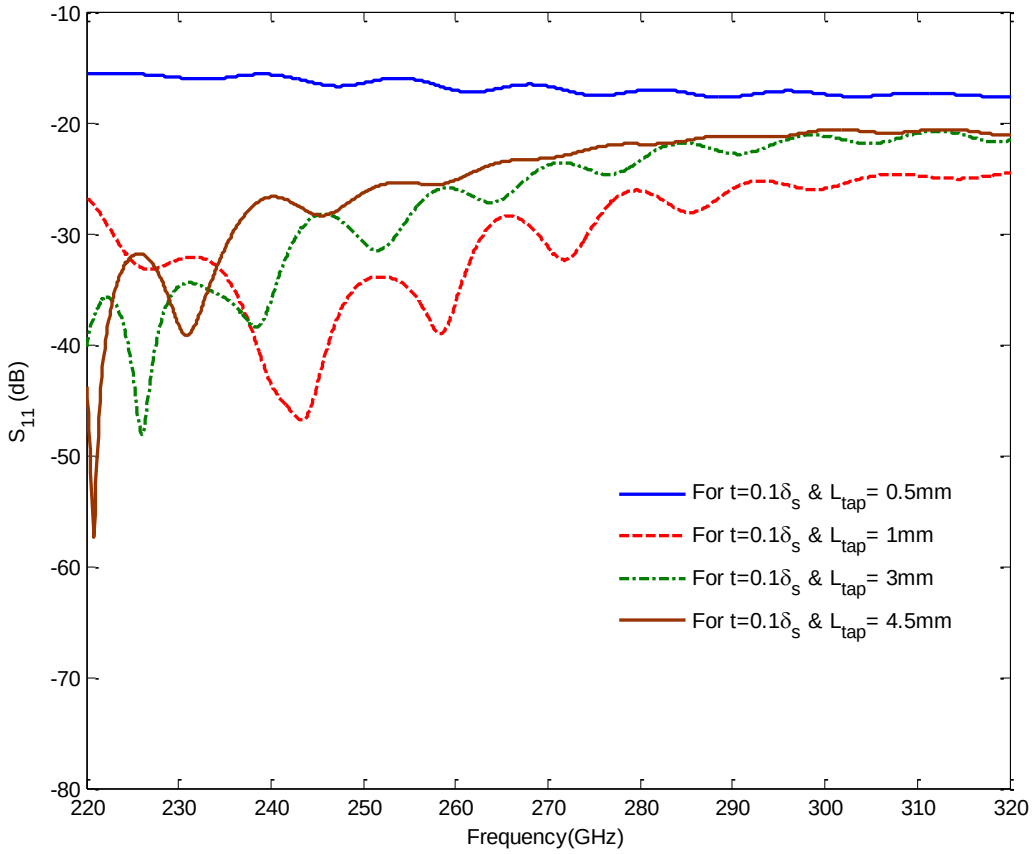

Fig. 5-17 Comparison of the S_{11} of a WR03 Platinum termination for different values of L_{tap} with pyramidal tapering for $t = 0.1\delta_S$, L=10 mm and d=5 mm.

5-2-2 Inner Pyramidal Tapering

For complete evaluation of pyramidal tapering, the inner pyramidal tapering is also simulated as shown in Fig. 5-18.

As discussed in previous section, pyramidal tapering, the L_{tap}= 1 mm has the best results between other lengths of tapering. So for inner pyramidal tapering the design has been done for L_{tap}= 1 mm.

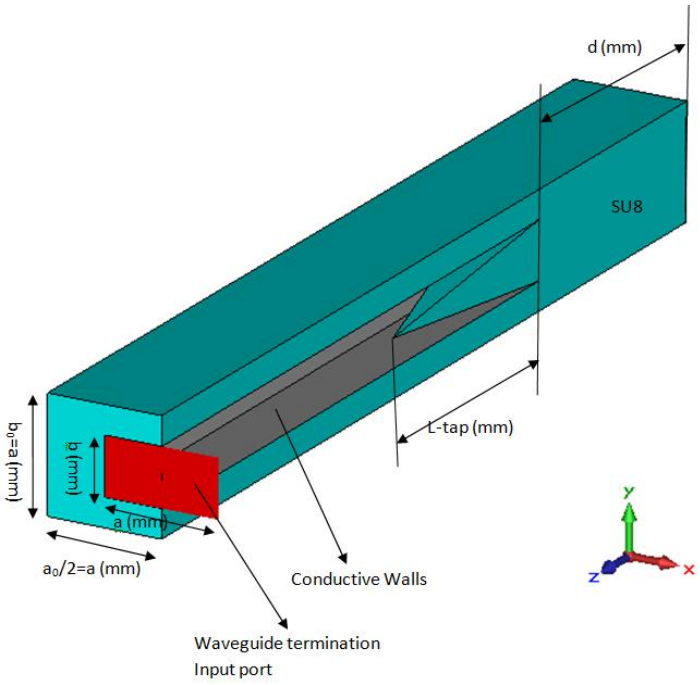

Fig. 5-18 General configuration of a waveguide termination with inner pyramidal tapering inside the Waveguide

The S_{11} results of the WR03 PEC termination, inner pyramidal tapering is shown in Fig. 5-19. It can be seen that the S_{11} changing between -12 dB to -25 dB for the frequency band of 220 GHz to 320 GHz.

Comparing Fig. 5-16 which is the S_{11} of the WR03 PEC pyramidal tapering termination and Fig. 5-19, it can be inferred that the pyramidal tapering is given the better result but for both pyramidal and inner pyramidal the physical implementation would be very hard.

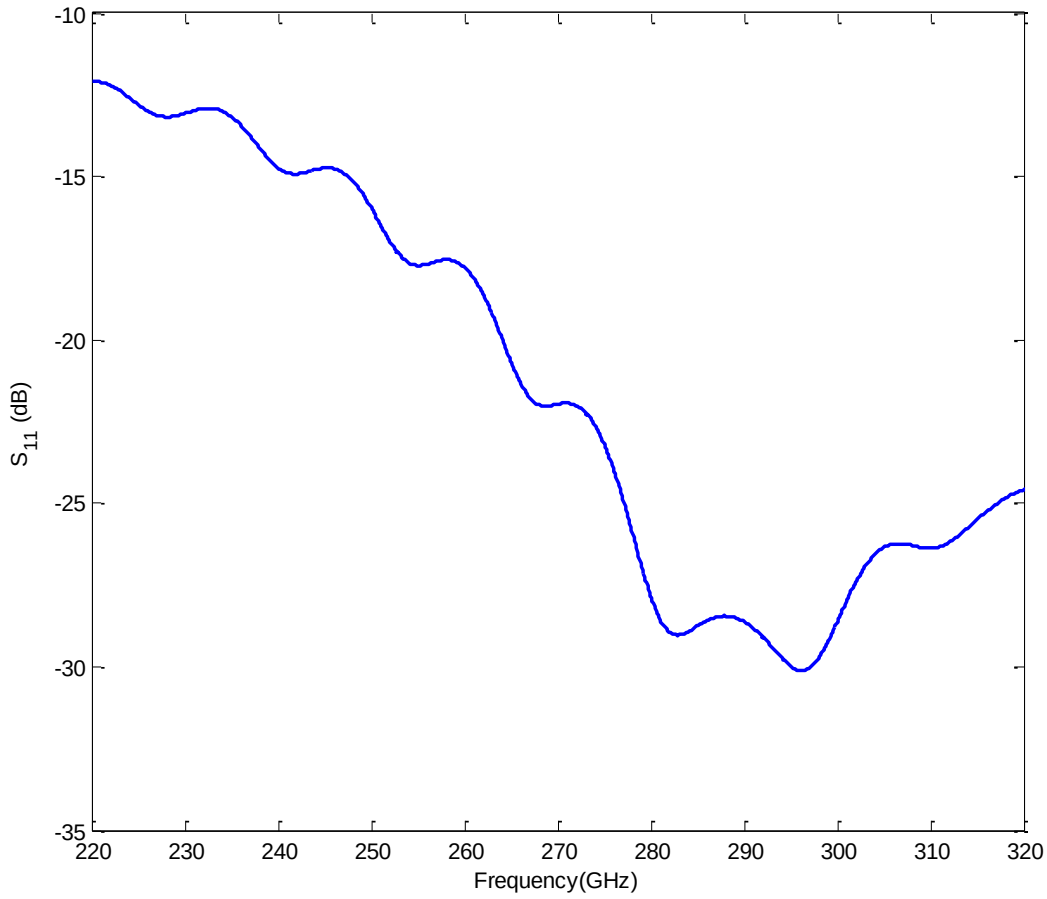

Fig. 5-19 The S_{11} of a WR03 PEC termination with inner pyramidal tapering for L_{tap}=1mm, L=10mm and d=5 mm.

Also the WR03 inner pyramidal termination has been designed with Platinum with thickness of $t = 0.1\delta_s$ = 29.7 mm, L=10 mm and d=5 mm.

Fig. 5-20 shows the S_{11} of a WR03 platinum termination with inner pyramidal tapering.

Comparison between Fig. 5-17 and Fig. 5-20 indicates that WR03 Platinum inner pyramidal is not as good as the WR03 Platinum pyramidal design.

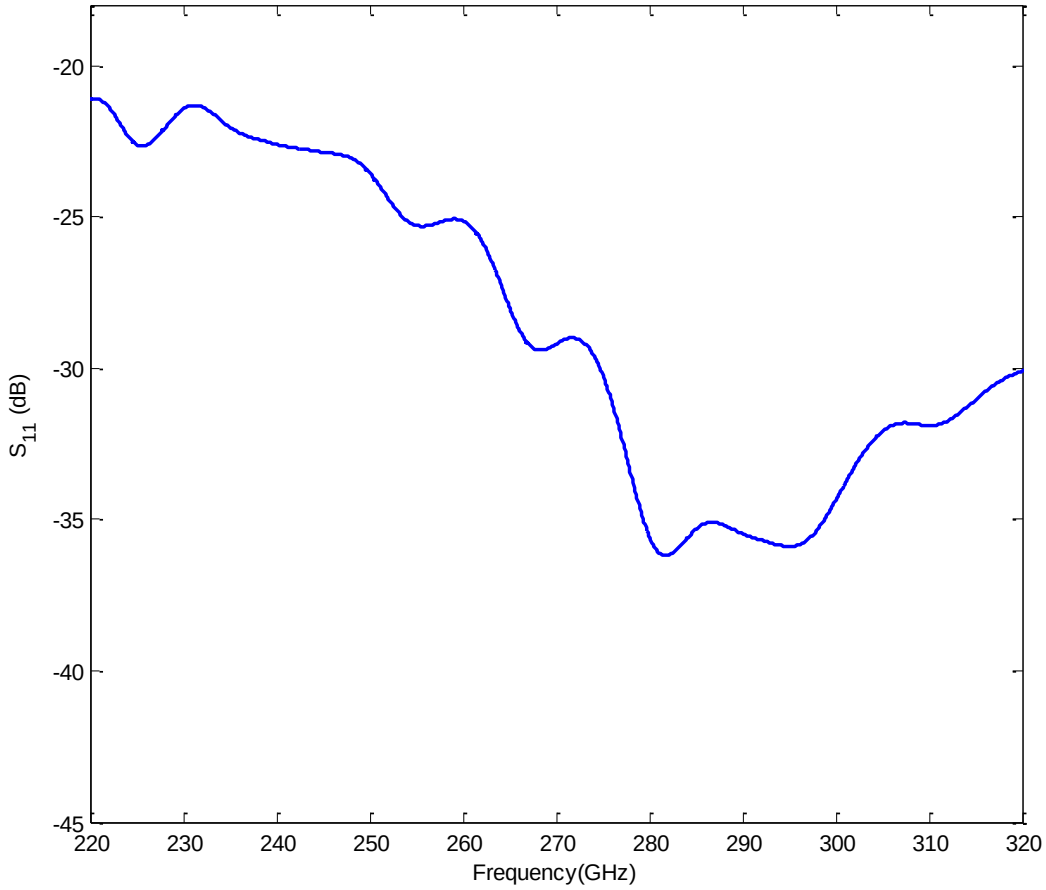

Fig. 5-20 The S_{11} of a WR03 Platinum termination with inner pyramidal tapering and metal thickness of $t = 0.1\delta_S$ for L_{tap}=1 mm, L=10 mm and d=5 mm.

Different values of L_{tap} has been tested in Microwave CST Simulation for WR03 inner pyramidal tapering with t=0.1δ_s, L=10 mm and d= 5 mm. It can be seen that the mean value of S_{11} for L_{tap} =1 mm is better than -28 dB.

Comparing the results of inner pyramidal tapering and pyramidal tapering, it can be seen that the first one is not a good approach for matched load for WR03 band waveguide.

5-3 Conclusion

In this chapter, different kinds of tapering for PEC, Silver and Platinum waveguide terminations have been analyzed and the optimum length of tapering has been discussed in all cases. Height, inner height and width tapering as well as the triangular tapers and also pyramidal tapering and inner pyramidal tapering are discussed in this chapter. It can be inferred that the triangular tapering shows better results in comparison to the pyramidal one. Additionally, for fabrication of the termination and physical realisation, the triangular tapering is easier than the pyramidal one, because it just needs tapering in two faces and not in all four ones. When the magnitude of S_{11} is high, this must mean that the impedance of the load is closely matched to the terminating rectangular waveguide. At the minima of the S_{11} there must be a resonance in termination.

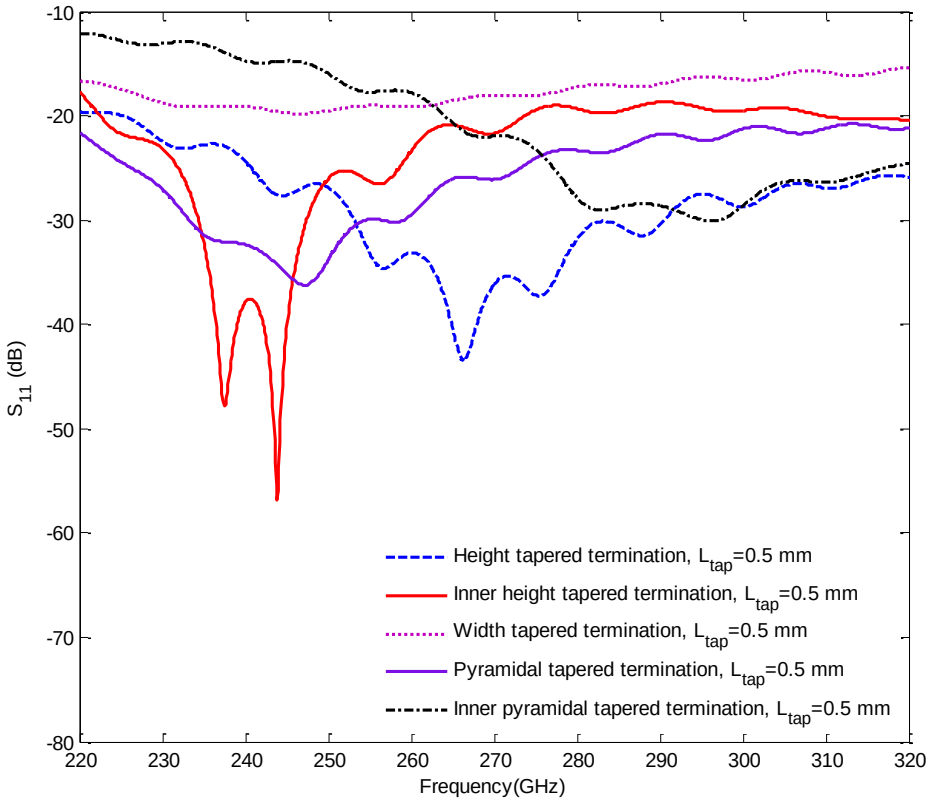

Fig. 5-21 Comparison of the S_{11} of a WR03 PEC termination with different kinds of tapering for, L=10 mm and d=5 mm.

As discussed above and according to Fig. 5-21 which is the comparison of the S_{11} versus frequency for all kinds of PEC tapered termination it can be concluded that among, the height tapering, inner height tapering, width tapering, pyramidal tapering and inner pyramidal tapering the height tapering approach has the best results for a matched load for WR03 waveguide.

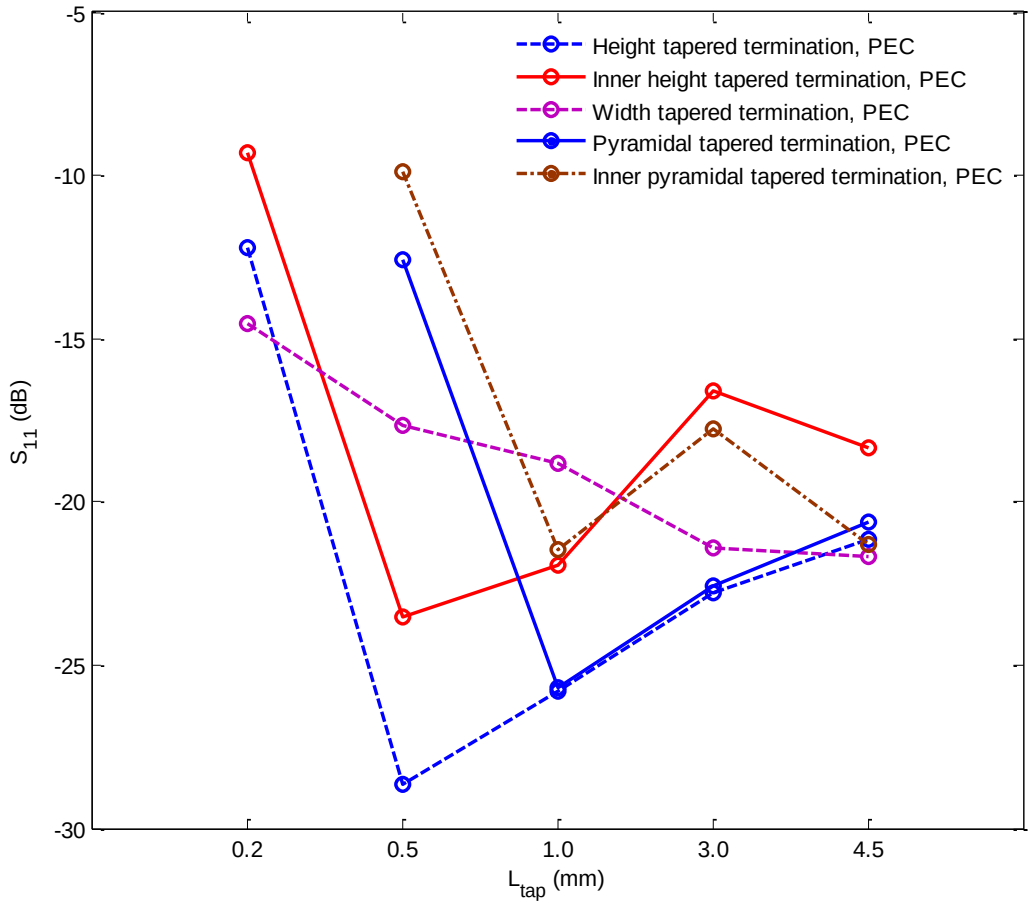

Fig. 5-22 Comparison of mean values of S_{11}(dB) versus L_{tap} (mm) for different tapering methods

Fig. 5-22 compared the mean values of S_{11} versus L_{tap} for all kinds of discussed tapering methods with PEC. It can be seen that the PEC height tapering termination with L_{tap} = 0.5 mm has the best result, less reflection, in comparison to other kinds of tapering where its magnitude of S_{11} is better than -29 dB.

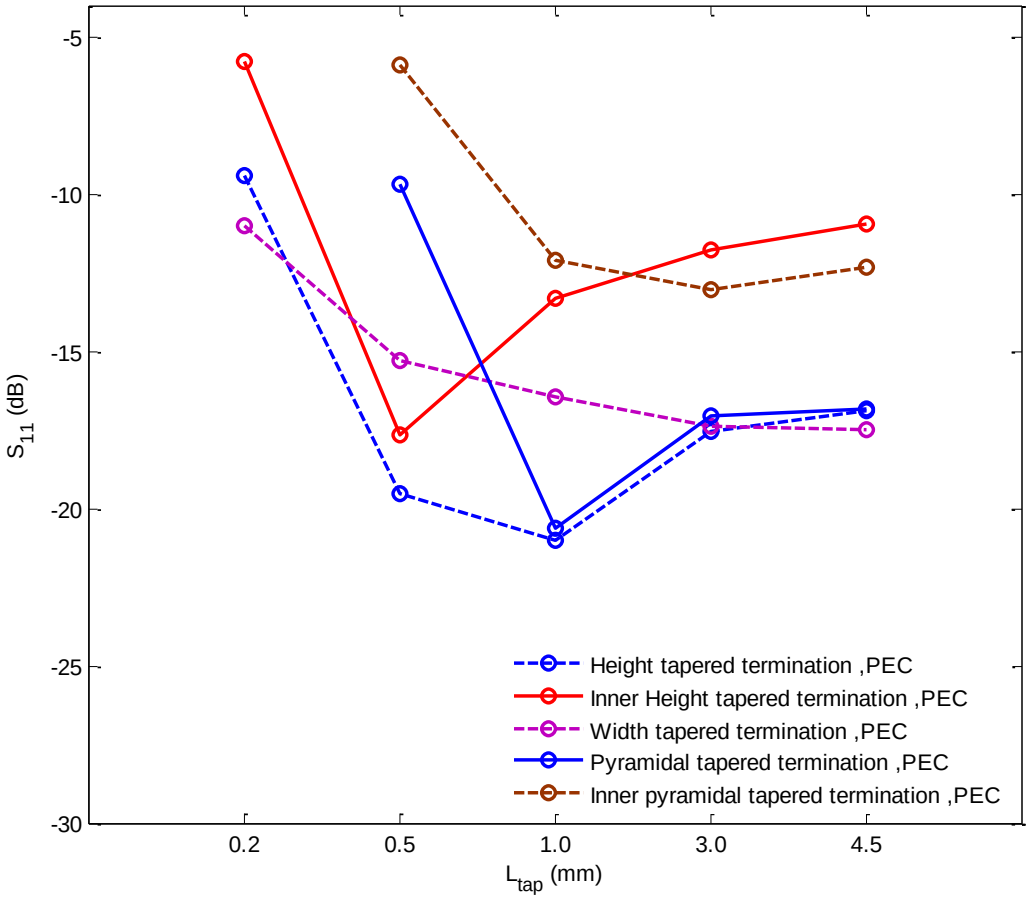

Fig. 5-23 Comparison of maximum values of S_{11}(dB) versus L_{tap} (mm) for different tapering methods

Also Fig. 5-23 compared the maximum values of S_{11} versus different values of L_{tap}, it can be seen that the maximum reflection will occur for inner height tapering design with L_{tap} =0.2 mm its S_{11} will be about 5 dB.

Chapter 6 HORN SHAPED WAVEGUIDE TERMINATION

6-1 Introduction

In Chapter 4 and Chapter 5 a WR03 termination, the use of simple rectangular waveguide with tapered SU8 has been investigated. To improve the value of reflection coefficient a conventional component is now considered i.e. a horn shaped waveguide. Chapter 6 will focus on the use of horn shaped waveguide terminations.

To decrease the reflection of a load one way is to flare out its ends into horn. Horns provide a low voltage standing wave ratio (VSWR) [27].

There are three basic types of horn shaping for rectangular waveguides as shown in Fig. 6-1.

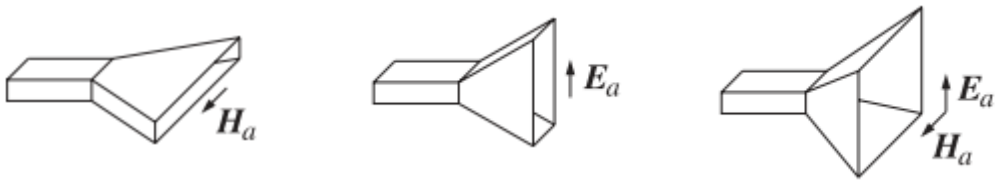

(*a*) (*b*) (*c*)

Fig. 6-1 (a) H-plane sectoral horn,(b) E-Plane sectoral horn,(c) Pyramidal horn

Horns can be flared exponentially, providing better matching over a broad frequency range but technically more difficult and more expensive to produce. Horns are suited for rectangular waveguide feeders as the horn acts as a gradual transition from waveguide mode

to a free space mode for the electromagnetic wave. Rectangular feed-horns are fed with the fundamental TE_{10} mode of the rectangular waveguide [27].

6-1-2 E-plane horn

The '*a*' dimension of the rectangular waveguide is constant and the waveguide is only flared out in '*b*' dimension (the direction of E-field). The complication in the analysis arises from the fact that arriving waves at the horn aperture are not in-phase due to the different path lengths from the horn apex (this is also called phase centre of horn) [28].

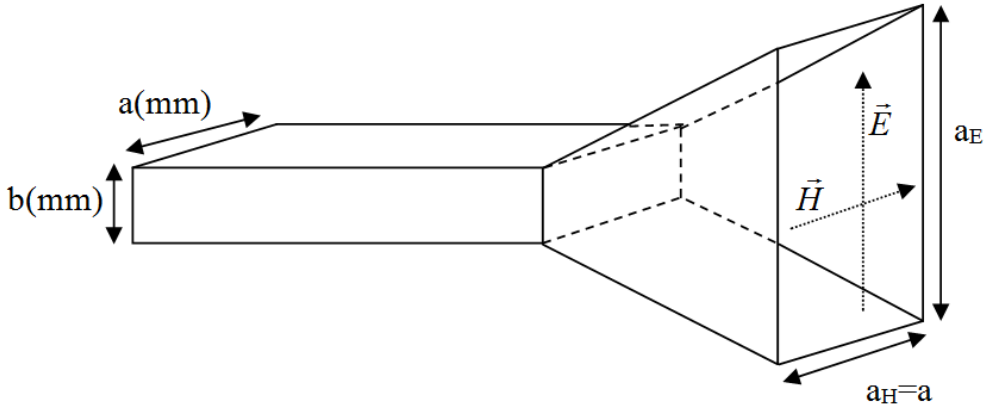

Fig. 6-2 E-plane horn waveguide

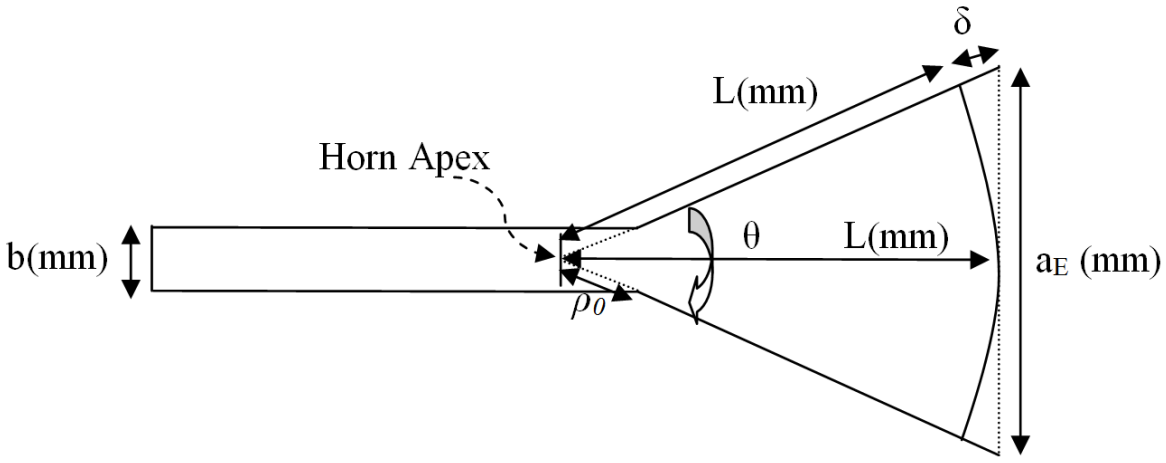

Fig. 6-3 Cross section of E-plane horn waveguide with dimensions used in analysis [28]

Fig. 6-2 and Fig. 6-3 present the E-plane horn dimensions where Θ is a flare angle and a_E known as aperture for E-plane in mm. The horn length which is an axial length of the horn from the throat to the aperture of the horn is called L and the path length is defined as δ [28].

As it can be seen from the Fig. 6-3 [28]:

$$\cos\ (\frac{\theta}{2}) = \frac{L}{L+\delta} \tag{6-1}$$

$$\sin\ (\frac{\theta}{2}) = \frac{a_E}{2(L+\delta)} \tag{6-2}$$

$$\tan\ (\frac{\theta}{2}) = \frac{a_E}{2L} \tag{6-3}$$

From the geometry of Fig. 6-3 [28]:

$$\theta = 2\tan^{-1}\left(\frac{a_E}{2L}\right) = 2\cos^{-1}\left(\frac{L}{L+\delta}\right) \tag{6-4}$$

Usually δ consider as 0.25λ or even less in the E-plane of the horn. The reason is if δ is sufficiently small then the field would have uniform phase over the whole aperture. Additionally to have uniform horn aperture distribution, the long horn length is required but this would make the process of fabrication hard. To make the device more practical the horn length should be as small as possible [28].

An optimum horn length (optimal in directivity) should be in the middle of the extreme values. For constant value of L, an increase of the aperture a_E and the flare angle θ, leads to improvement of the directivity of the horn and decrement of the beam width [28].

For extremely large values of flare angle the ratio of $L/L+\delta$ would be nearly one that leads the effect of δ on the distribution of the field magnitude is negligible. However when δ

becomes 180 degrees, at the edges of the aperture, the phase reversal will reduce the directivity[28].

Consequently the maximum directivity happens at the largest flare angle for which the δ does not exceed a certain value which in this project called δ_0. Hence, the optimum horn length can be calculated by the following equations [28]:

$$L_{opt} = \frac{\delta_0 \cos(\frac{\theta}{2})}{1-\cos(\frac{\theta}{2})} \tag{6-5}$$

Fig. 6-4 confirms accuracy of the above theory based experimental results measured by Donald Rhodes [28], and determines optimum dimensions (optimum relation between the flare angle and the length) for rectangular horn antennas to achieve most directivity.

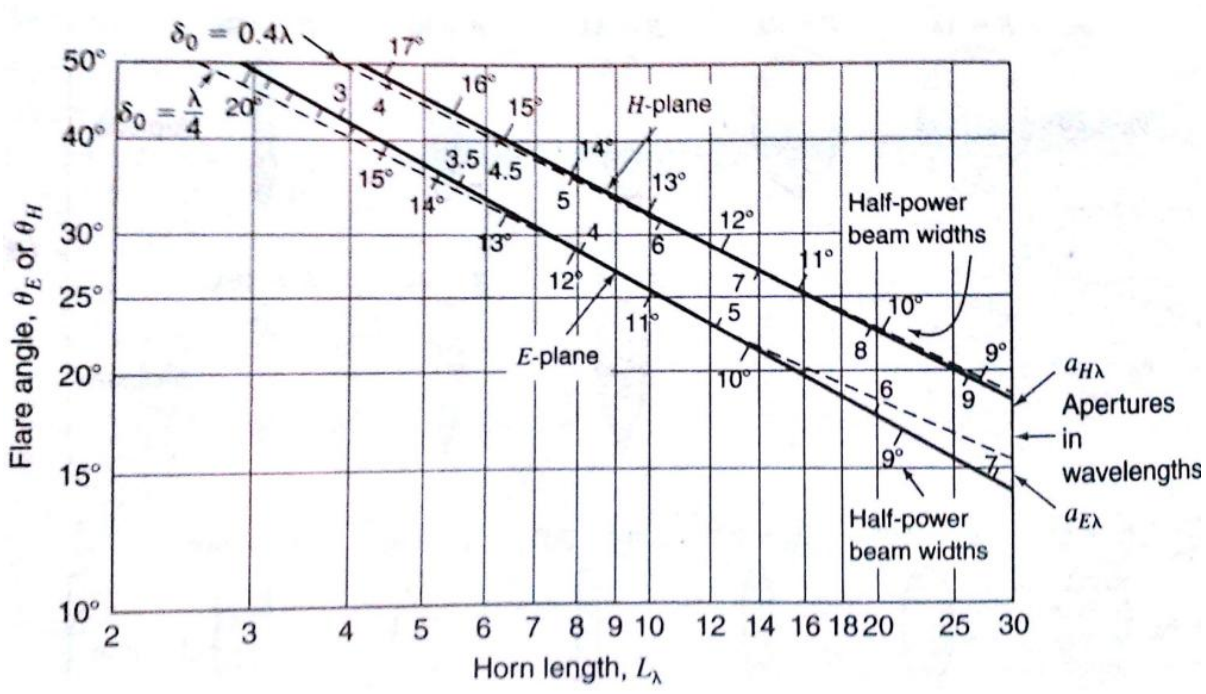

Fig. 6-4 Relation of flare angle for both E-plane and H-plane to horn length. Solid lines shows experimentally determined optimum dimensions for rectangular horn antennas. Dashed lines show calculated dimensions for δ_0=0.25 and 0.4λ-Taken from [28].

There are only a few papers in the literature which discuss the reflection coefficient of a horn shaped waveguide [29]-[32]. According to [31], the reflection coefficient of a sectoral E-plane long horn can be calculated by:

$$\Gamma = \Gamma_1 + \Gamma_2 \tag{6-6}$$

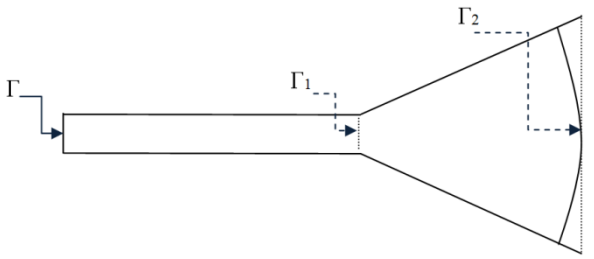

Fig. 6-5 Different definition for the reflection coefficients in a horn structure

As shown in Fig. 6-5, Γ_1 is the reflection coefficient due to junction, and is given by [31]:

$$\Gamma_1 = \frac{H_1^{(2)}(\beta\rho_0) - jH_0^{(2)}(\beta\rho_0)}{H_1^{(2)}(\beta\rho_0) + jH_0^{(2)}(\beta\rho_0)} \tag{6-7}$$

Where ρ_0 is depicted in Fig. 6-3 and $H_0^{(2)}$ and $H_1^{(2)}$ are respectively zero and first order of second kind of Hankel function. And Γ_2 is the reflection coefficient due to aperture [31].

$$\begin{aligned}\Gamma_2 = &-\exp\{-j2[\beta l - \phi(\beta\rho_0)] - jl(\sec\left(\frac{\theta}{2}\right) - 1)\}\times \\ &\{\frac{1}{4\phi_0\beta l} + \frac{1}{2\beta a}(\frac{k}{\beta} - 1)\exp\{\frac{1}{\beta}\sqrt{\frac{2k}{\pi a}}\exp[j(ka + \frac{\pi}{4})]\}\}\end{aligned} \tag{6-8}$$

Where $\phi(\beta\rho_0)$ is the phase angle of first order of first kind of Hankel function, $H_1^{(1)}(\beta\rho_0)$, and ϕ_0 is equal to θ/2 and θ is illustrated in Fig. 6-3.

6-2 Simulations

Here CST is used for simulation of the horn shaped structures. According to design purpose, which is the minimizing of the amount of reflection, accurate simulation may lead to optimal values of horn dimensions.

6-2-1 E-Plane or H-Plane

First, between E-plane and H-plane, one has to be chosen with respect to their advantages. It is noticeable that the pyramidal horn shaping is not feasible for fabrication and therefore one of the E-plane or H-plane sectoral horns should be chosen. To achieve this purpose a comparison between the amount of reflection coefficient in both cases of the E-plane and the H-plane with a simple open-ended waveguide in case of free space environment and PEC waveguide has been done.

6-2-1-1 *E-Plane Sectoral Horn*

Fig. 6-6 and Fig. 6-7 show the E-plane sectoral horn waveguide and the considered dimensions.

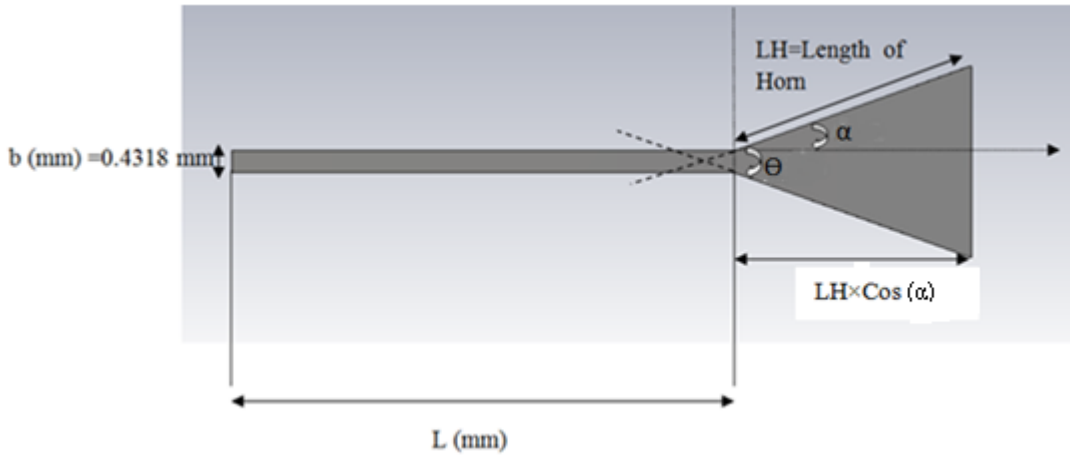

Fig. 6-6 E-plane horn shaped WR03 waveguide

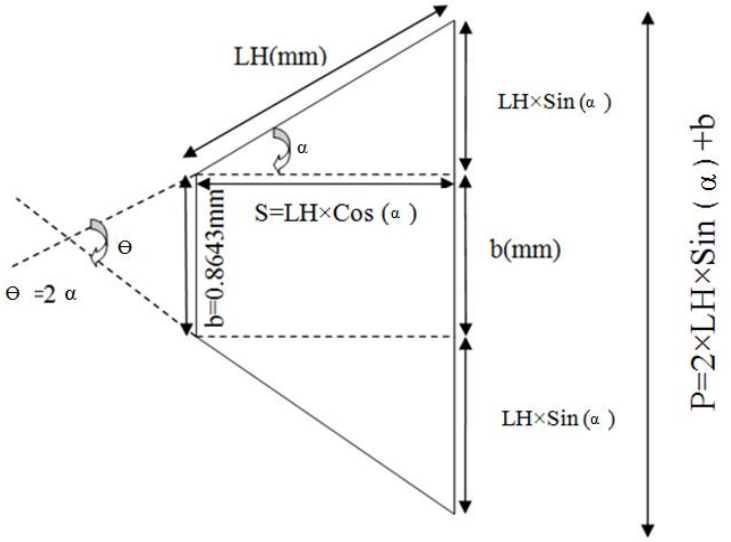

Fig. 6-7 Side view of E-plane horn shaped and considered dimensions

An E-plane horn shape WR03 rectangular waveguide with $\theta=20^{o}$ $=\alpha/2$ has been designed as shown in Fig. 6-8. The length of the waveguide is 10 mm and constant. As it is expected, changing the length of the waveguide does not significantly affect the result as the material is PEC. The length of the horn wall changes, *LH* = 0.5, 1, 2, 3 mm, to see its effect on S_{11}. It can be seen in Fig. 6-9 that for this case, the values of S_{11} are better than -11 dB.

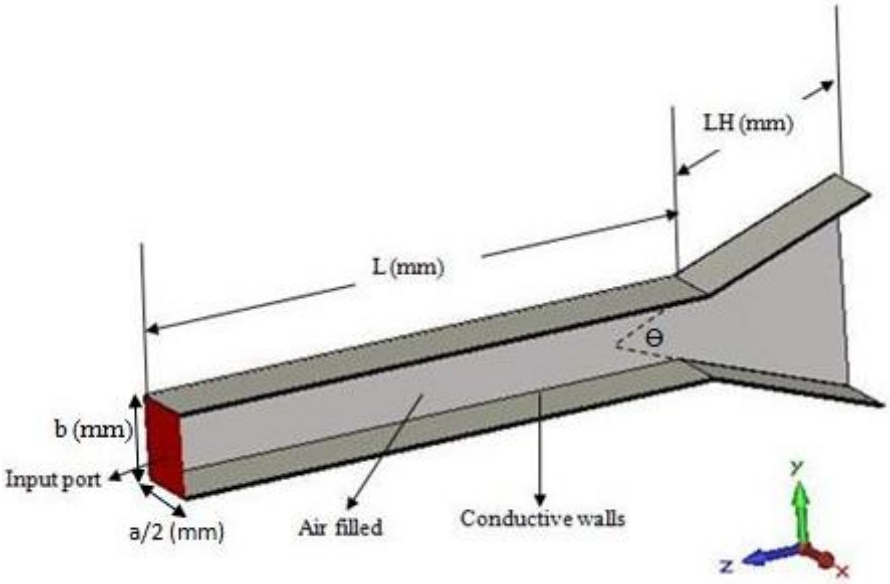

Fig. 6-8 PEC E-plane horn shaped WR03 rectangular waveguide

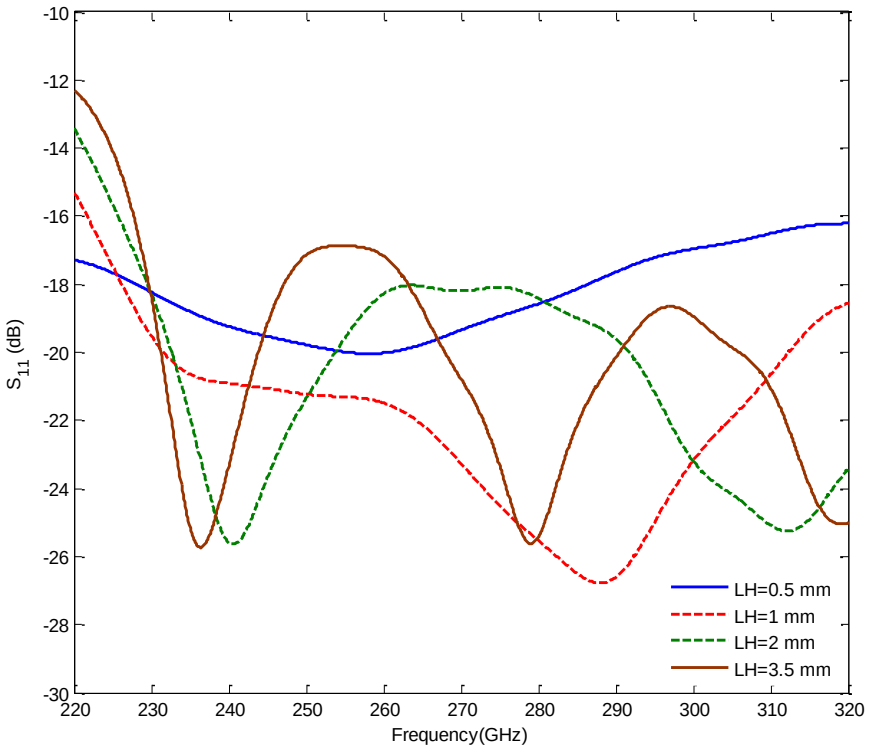

Fig. 6-9 S_{11} versus frequency for L=10mm and θ=20, LH =0.5, 1, 2, 3 mm. Time domain simulation, open add space boundary condition.

It can be seen that for length of horn equal to 1 mm, the average of S_{11} is about -23 dB which is very small amount of reflection.

6-2-1-2 *H-Plane Sectoral Horn*

Here the design of WR03 PEC rectangular waveguide H-plane horn with $\theta=20^{o}=\alpha/2$ is reported as shown in Fig. 6-10. The length of the waveguide is 10 mm and constant. The length of the horn changes, LH = 0.5, 1, 2, 3 mm, to see the effect of it on S_{11}.

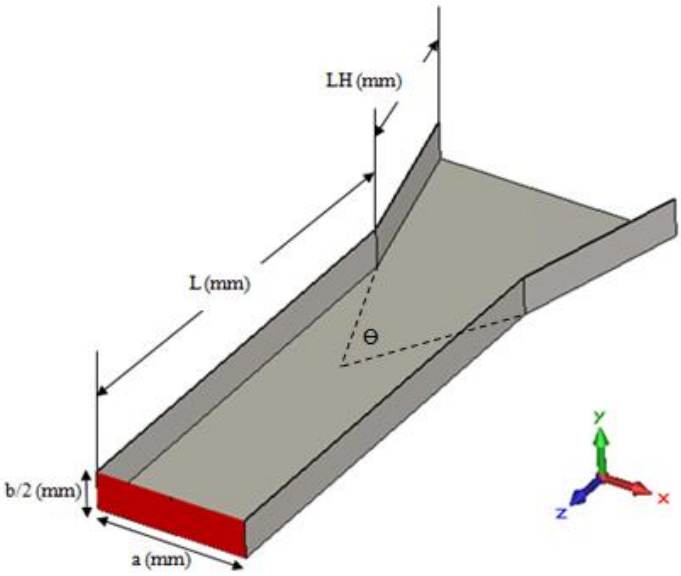

Fig. 6-10 H-plane horn shaped PEC WR03 rectangular waveguide

The reflection has been displayed in Fig. 6-11. It can be seen that, the values of S_{11} are varying between -7dB and -14 dB.

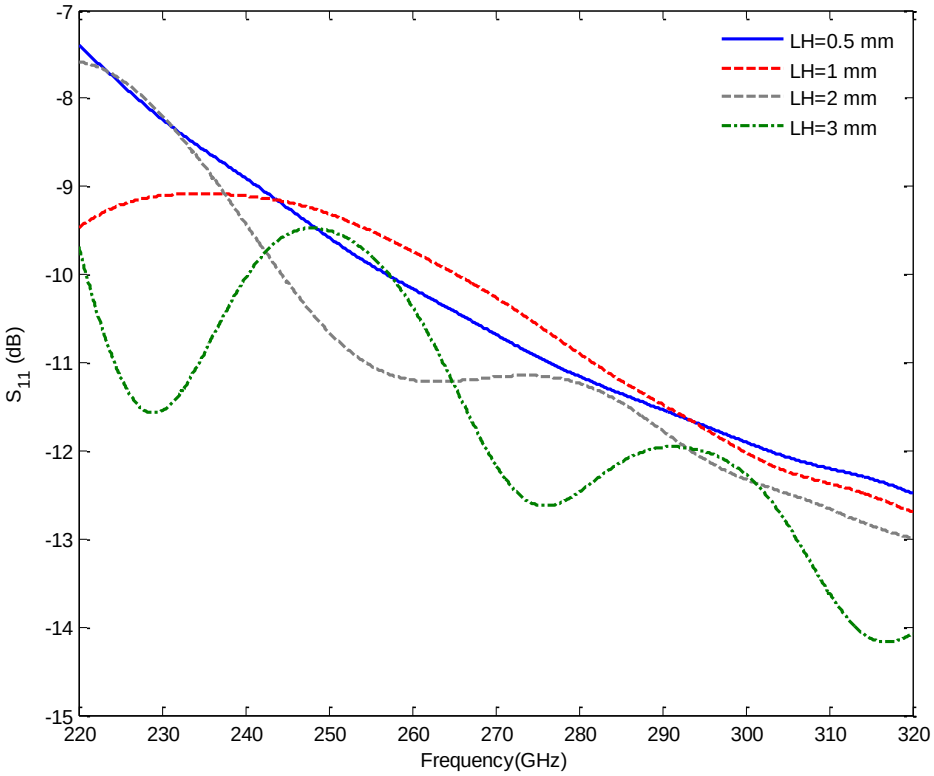

Fig. 6-11 S_{11} versus frequency for L=10mm and θ=20, LH =0.5,1,2,3 mm. Time domain simulation, open add space boundary condition

Comparing E-plane horn shape, Fig. 6-9, and H-plane horn shape, Fig. 6-11, shows that PEC WR03 rectangular waveguide E-plane Horn shape has better results and therefore must present a better impedance match. Note the different scales. Therefore E-Plane horn shaping has been chosen.

6-2-2 Optimum Length and angle

The length of the horn walls and the flared angle are two important factors in this design. To choose the optimum *LH*, length of the horn walls, θ must be assumed to be constant and *LH* has been evaluated for *LH* = 0.5, 1, 2, 3 mm. The following three figures show S_{11} versus frequency, PEC WR03 rectangular waveguide E-Plane Horn shaped for different values of angles, θ = 10, 15, 20 degree, has been chosen.

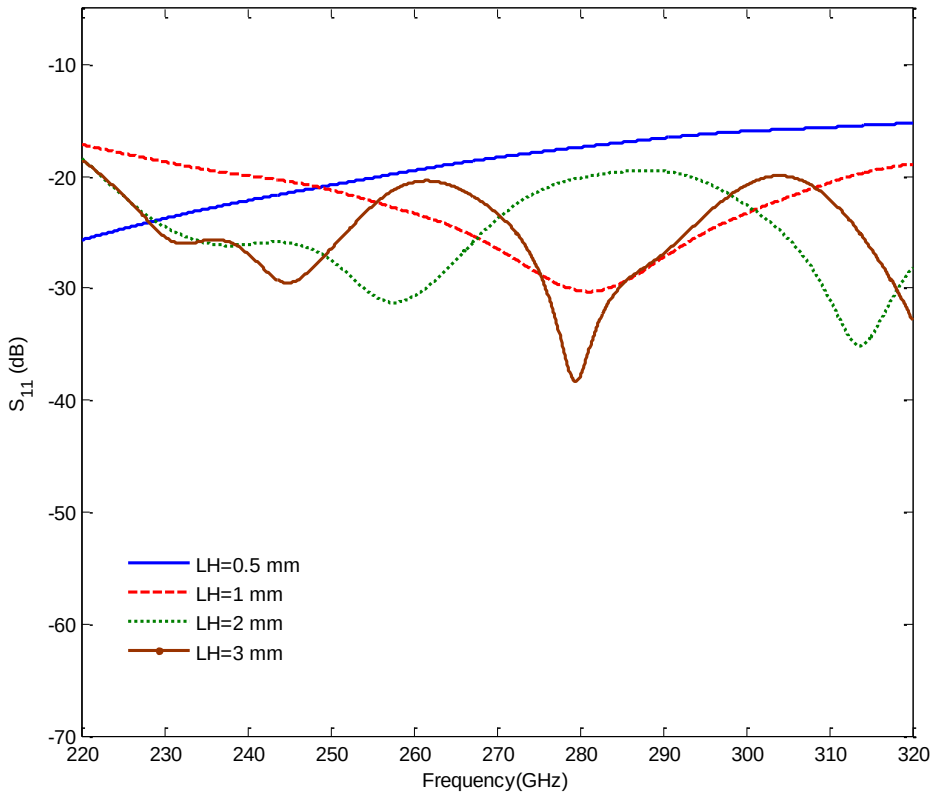

Fig. 6-12 S_{11} versus frequency, PEC WR03 rectangular waveguide E-Plane Horn shape for constant θ=10 degree and different length of horn part.

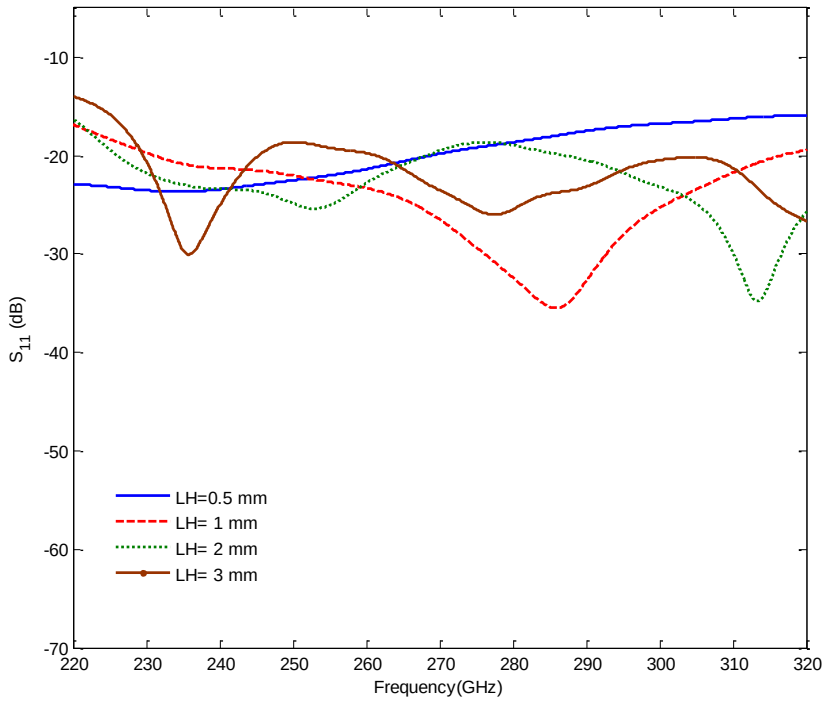

Fig. 6-13 S_{11} versus frequency, PEC WR03 rectangular waveguide E-Plane Horn shape for constant θ=15 degree and different length of horn part.

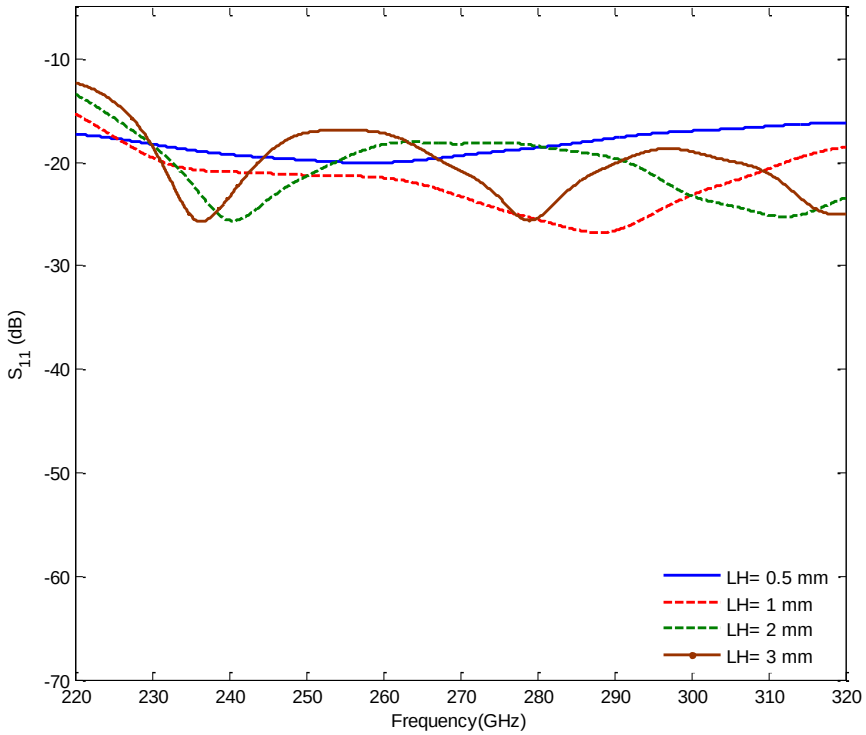

Fig. 6-14 S_{11} versus frequency, PEC WR03 rectangular waveguide E-Plane Horn shape for constant θ=20 degree and different length of horn part.

Moreover for E-Plane horn shape with LH = 1 mm and different values of θ the S_{11} is displayed in Fig. 6-15. θ=15 degree is the optimum result where its S_{11} is better than -15 dB.

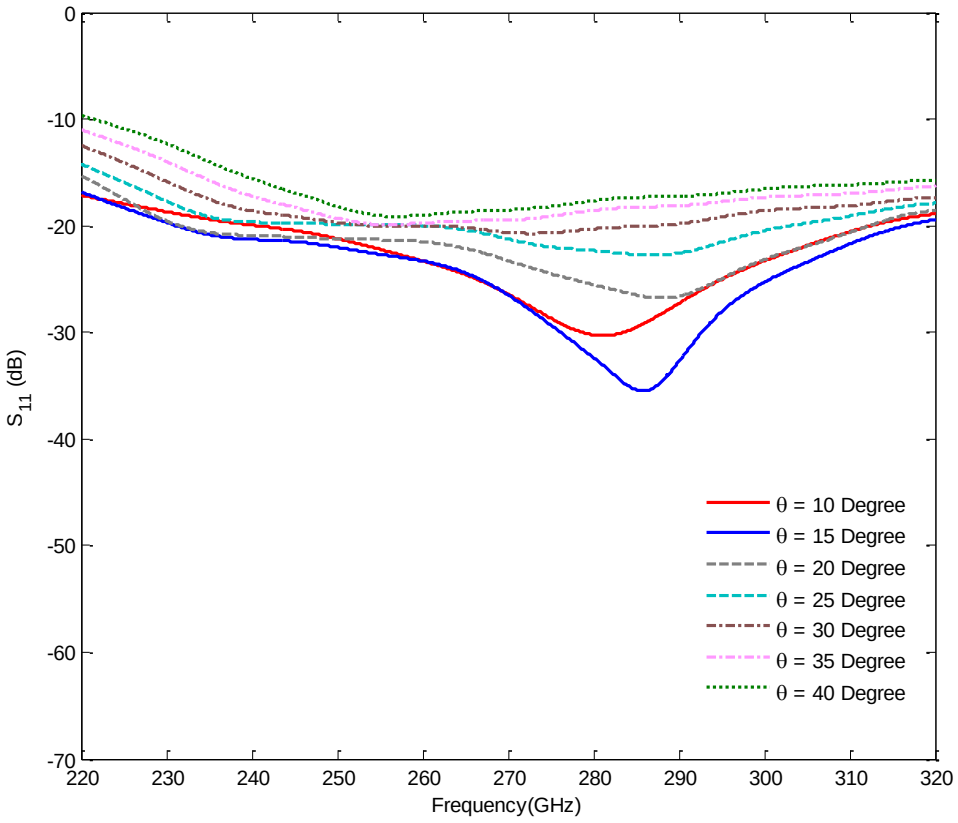

Fig. 6-15 S11 versus frequency, PEC WR03 rectangular waveguide E-Plane Horn shape for constant *LH*=1mm and different values of flare angle of horn part.

It can be deduced from the obtained results that *LH* = 1mm and θ =15 degree are optimal values (for goal of the minimum reflection) for WR03 horn shaped structure in case of free space environment and PEC waveguide.

6-2-3 In SU8 Medium

The very important difference between this case and routine case of horn shaped waveguides is the presence of SU8 as a dielectric environment. The considerable note is that the waveguide is air filled, but the environment is filled by SU8 which has a dielectric constant of 4.1 and loss tangent of 0.08 at 100GHz. This issue makes our case more difficult,

because the presence of SU8 in the environment decreases the inherent impedance of environment (η) from 377 ohm (η_0, for free space) to $377/\sqrt{4.1}=186$ ohm (for SU8 medium). This decrement of inherent impedance increases mismatch between an air-filled waveguide with impedance of $Z_{TE}=\left(k/\beta\right)\eta_0$ (which is greater than η_0) and SU8 medium. In other words, the reflection coefficient at the open end depends on the impedance outside the waveguide which has changed ($\eta=\eta_0/\sqrt{\varepsilon_r}$) so the reflection increases. In section 3-3 it has clearly shown the effect of SU8 in increasing of mismatch.

Previously in Chapter 5, Fig. 5-1 shows the air-filled open ended WR03 PEC waveguide in the SU8 medium which used outside wedge tapering (with tapering the length of L_{tap}) for improvement of mismatch and it has been shown that tapering of SU8 improves the reflection coefficient. Fig. 6-16 displays its reflection coefficient.

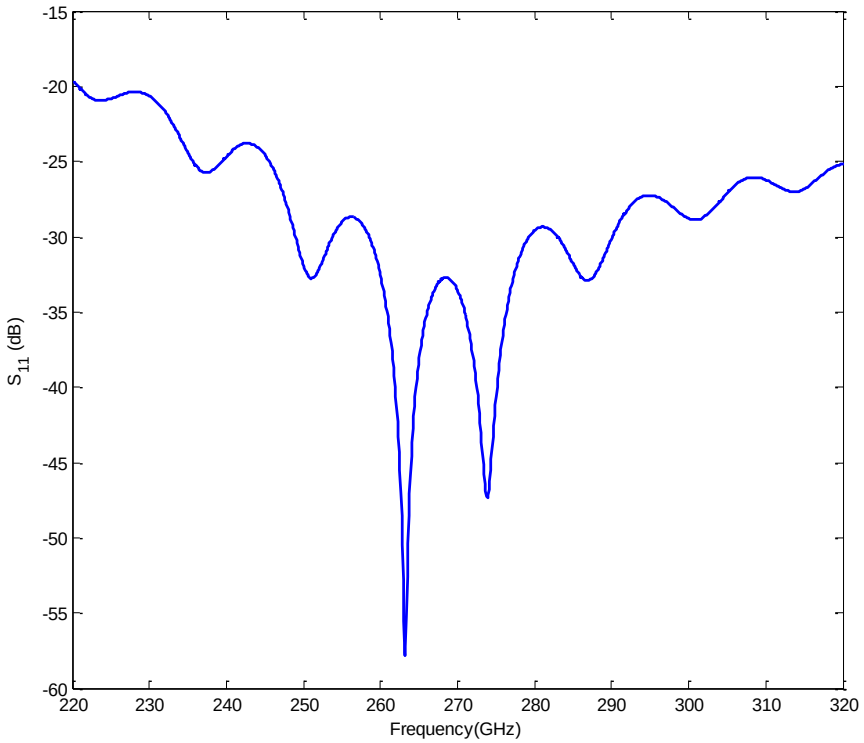

Fig. 6-16 S_{11} versus frequency for PEC WR03 open ended rectangular waveguide, triangular tapered, supported by SU8

It can be concluded from Fig. 6-16 that tapering of SU8 improves the reflection coefficient very well and its S_{11} is better than -20 dB in whole frequency band.

Now to make further improvement of the reflection coefficient of the open ended air-filled waveguide in the SU8 medium horn shaped WR03 waveguide used. It has been shown that E-plane horn shaping has more advantages; therefore E-plane sectoral horn shaping has been chosen to analyze.

Fig. 6-17 displays the open ended E-plane horn shaped WR03 PEC rectangular waveguide supported by SU8 which its reflection is shown in Fig. 6-18. It can be seen that horn shaping without tapering the SU8 cannot improve the reflection coefficient in comparison with simple case (without tapering). This issue comes from the fact that although horn shaping decreases the impedance of antenna and makes it closer to free space wave impedance, η_0, however it increases the open end aperture, which it is the boundary of air and SU8, and it increases the mismatch.

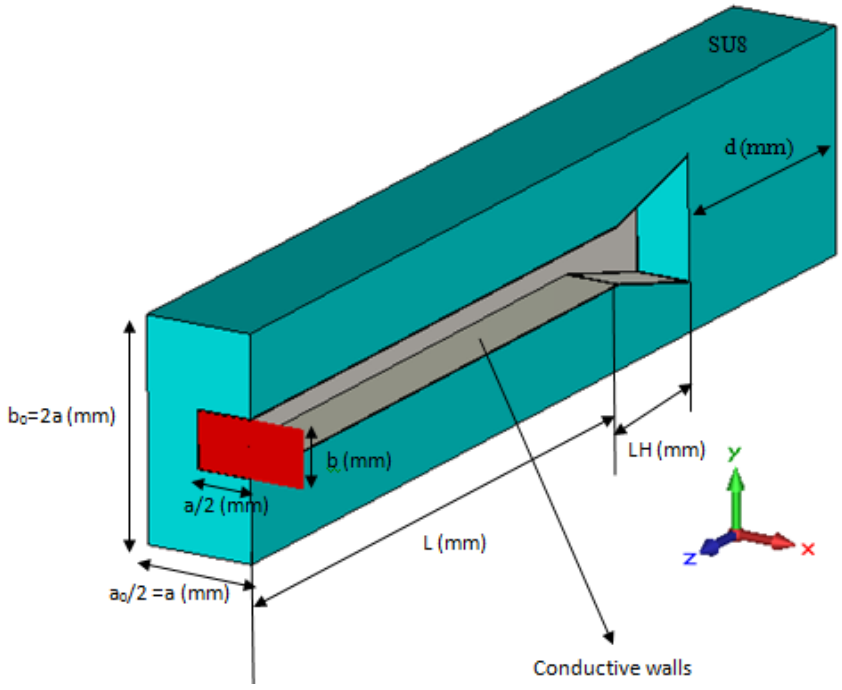

Fig. 6-17 Open ended E-plane horn shaped WR03 PEC rectangular waveguide supported by SU8 (green areas) for *LH*=1mm and θ=15 degree.

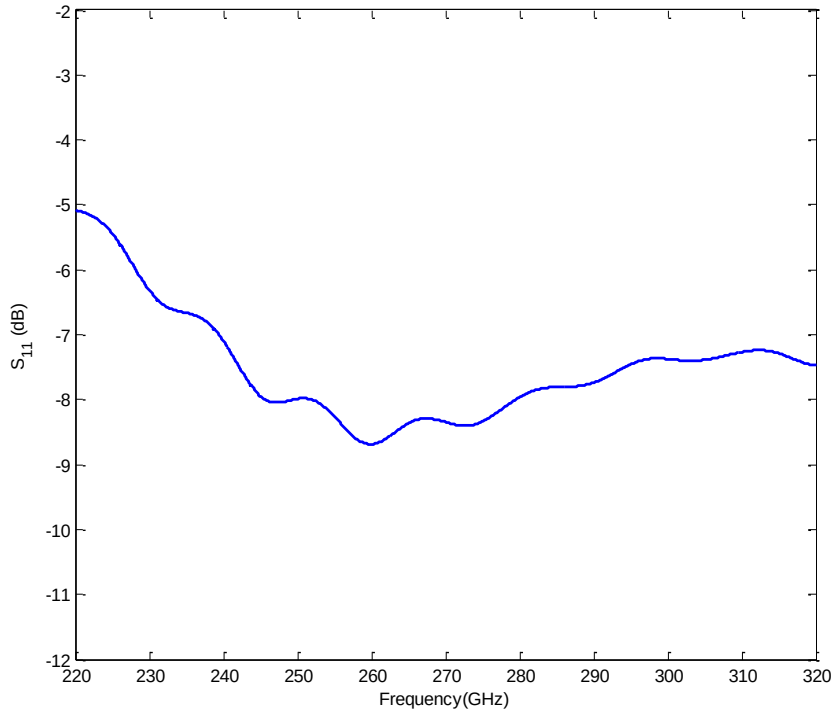

Fig. 6-18 S_{11} versus frequency for open ended E-plane horn shape WR03 rectangular waveguide supported by SU8 shown in Fig. 6-17.

As shown in Fig. 6-19, wedge tapering (with tapering length of L_{tap}) has been used for SU8 in case of E-plane horn shaped WR03 PEC waveguide to improve its reflection coefficient. Fig. 6-20 displays the S_{11} of the mentioned structure.

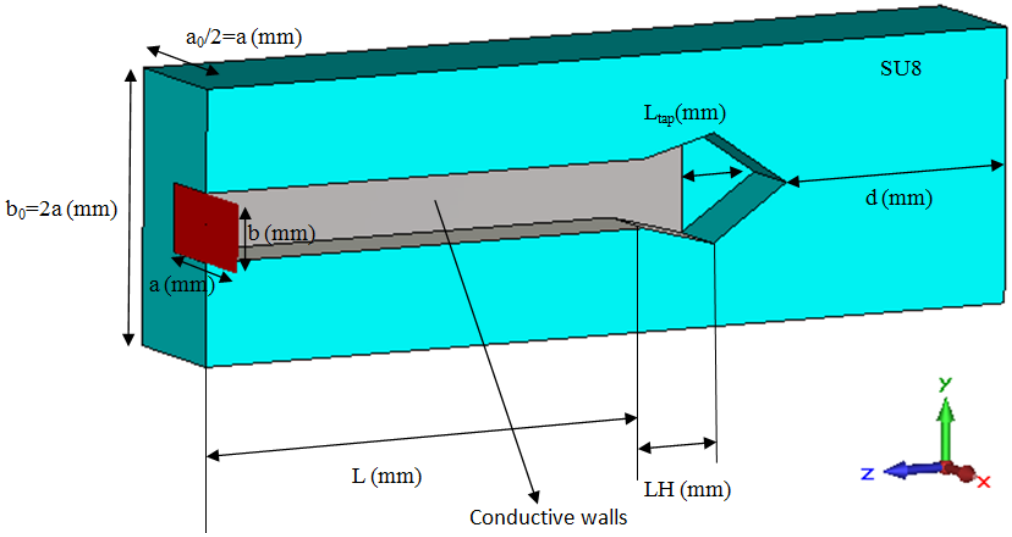

Fig. 6-19 WR03 PEC open ended E-plane horn shaped rectangular waveguide supported by SU8 by using outside wedge tapered. Gray sections show metal and green ones display SU8.

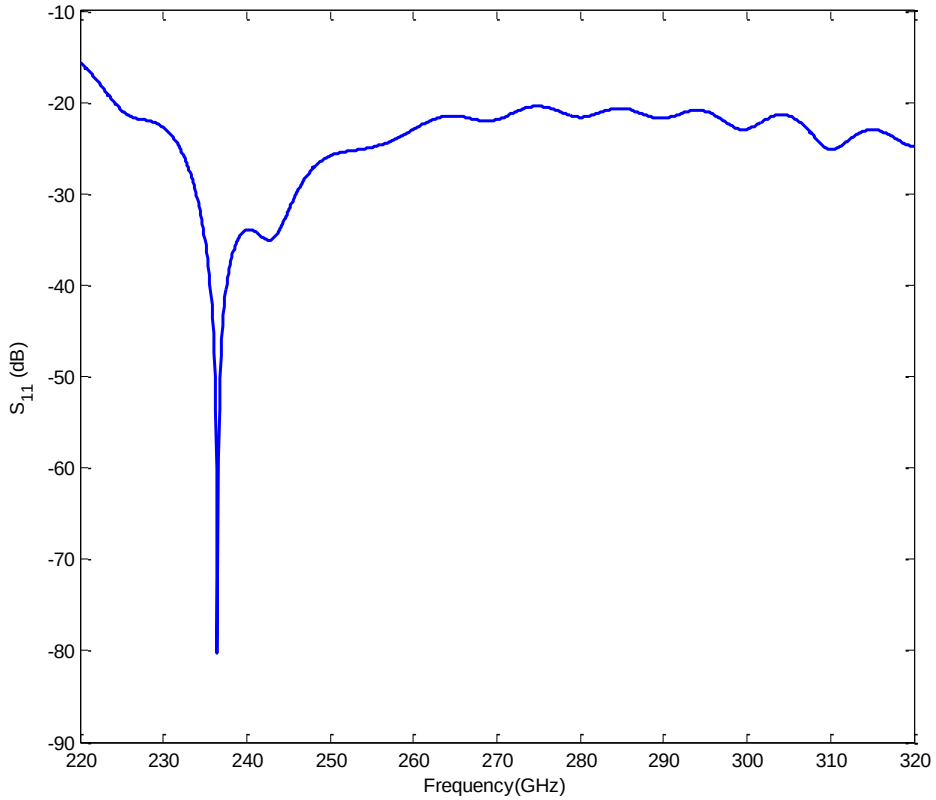

Fig. 6-20 S_{11} versus frequency for WR03 PEC open ended E-plane horn shaped rectangular waveguide supported by SU8 by using outside wedge tapered for L_{tap}=2 mm, LH=1mm and θ=15 degree.

The resonance may be the result of a mismatch between horn aperture and tapered edge in SU8 which make a standing wave there. Additionally the inside tapering, as shown in Fig. 6-21, is also analysed and the result acquired, as shown in Fig. 6-22, is not good.

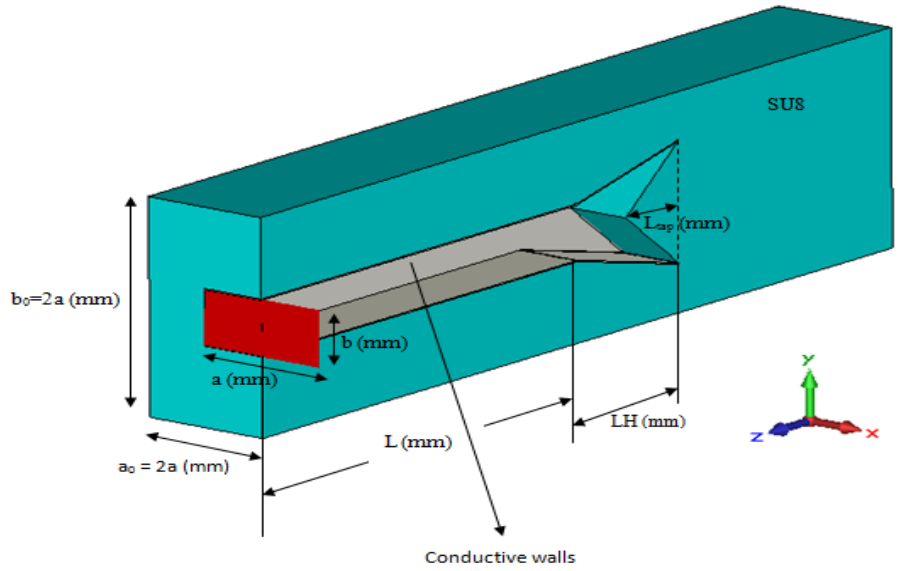

Fig. 6-21 WR03 PEC open ended E-plane horn shaped rectangular waveguide supported by SU8 by using inside wedge tapered. Gray sections show metal and green ones display SU8.

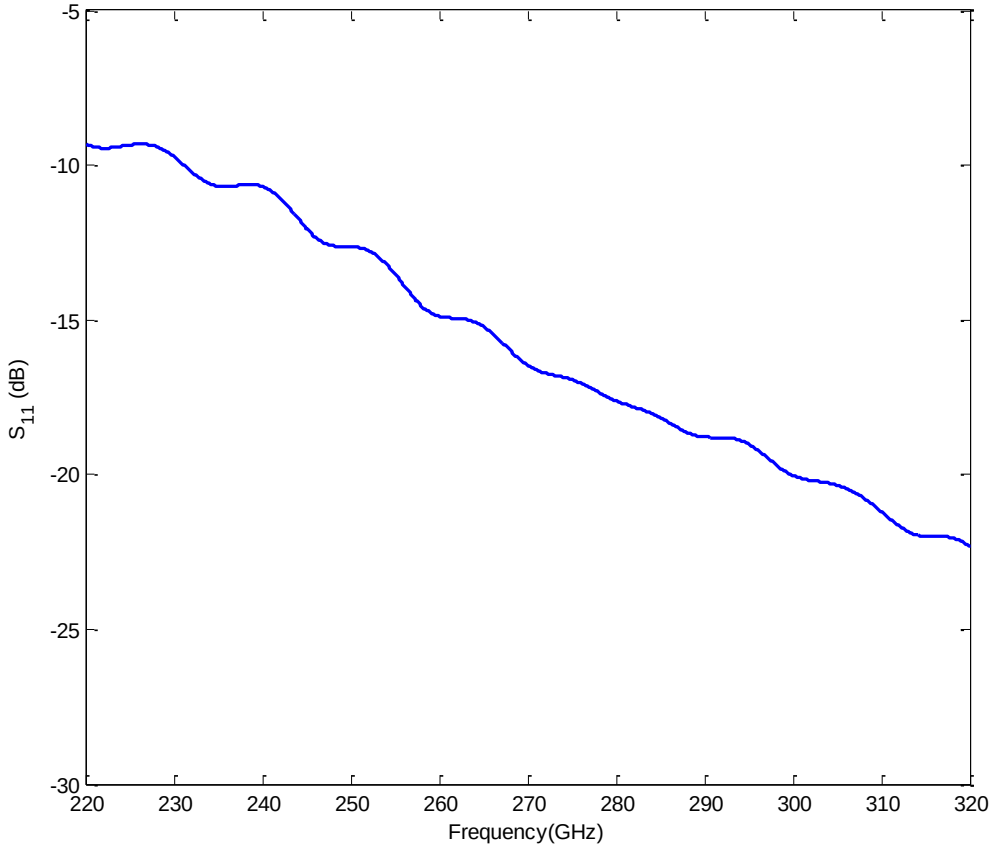

Fig. 6-22 S_{11} versus frequency for WR03 PEC open ended E-plane horn shaped rectangular waveguide supported by SU8 by using inside wedge tapered for L_{tap}=0.5mm, LH=1mm and θ=15 degree.

6-2-4 Adjusting of the SU8 boundary

The obtained results show that horn shaping of the open ended E-plane in the SU8 medium cannot improve the reflection coefficient. As mentioned before, it seems that this phenomenon came from the considerable mismatch between the waveguide and the large area of SU8 boundary at open ended section, even in tapered cases. Therefore the boundary of SU8 at open ended E-plane horn shape of the WR03 rectangular waveguide needs to be changed and optimised.

The parameter of '*Adj*' has been defined to show relative position of SU8 boundary as displayed in Fig. 6-23. *Adj=1* will be equal to Fig. 6-17 and *Adj=0* is corresponded to SU8 boundary exactly end of waveguide and before horn section. The conducting coating on the waveguide walls extends right to the end of the termination (Where *Adj* = 0).

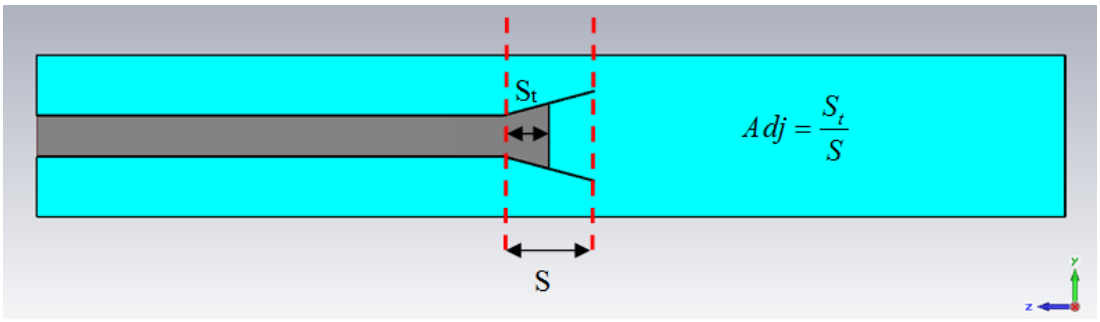

Fig. 6-23 Definition of '*Adj*' parameter, which shows the SU8 boundary relative position.

Fig. 6-24 shows Open-ended E-plane horn shaped WR03 PEC rectangular waveguide supported by SU8 with adjustable boundary.

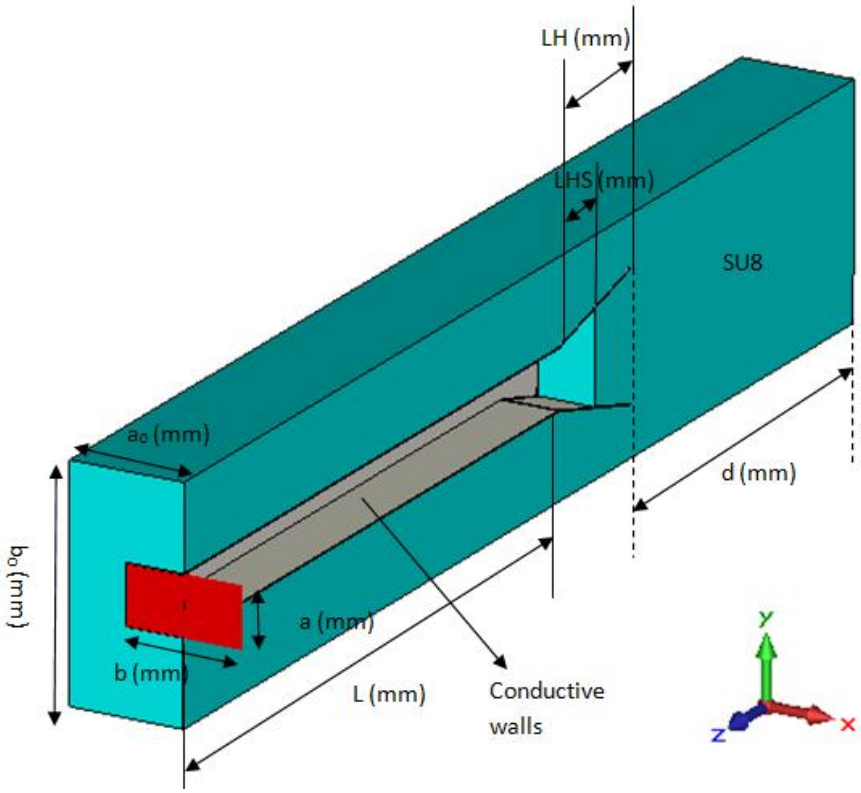

Fig. 6-24 Open ended E-plane horn shaped WR03 PEC rectangular waveguide supported by SU8 with adjustable boundary (*Adj*=0.5). Gray sections show metal and green ones display SU8.

Then the proposed open ended E-plane horn shaped WR03 PEC rectangular waveguide supported by SU8 has been simulated for different values of *Adj* parameter, as shown in Fig. 6-25.

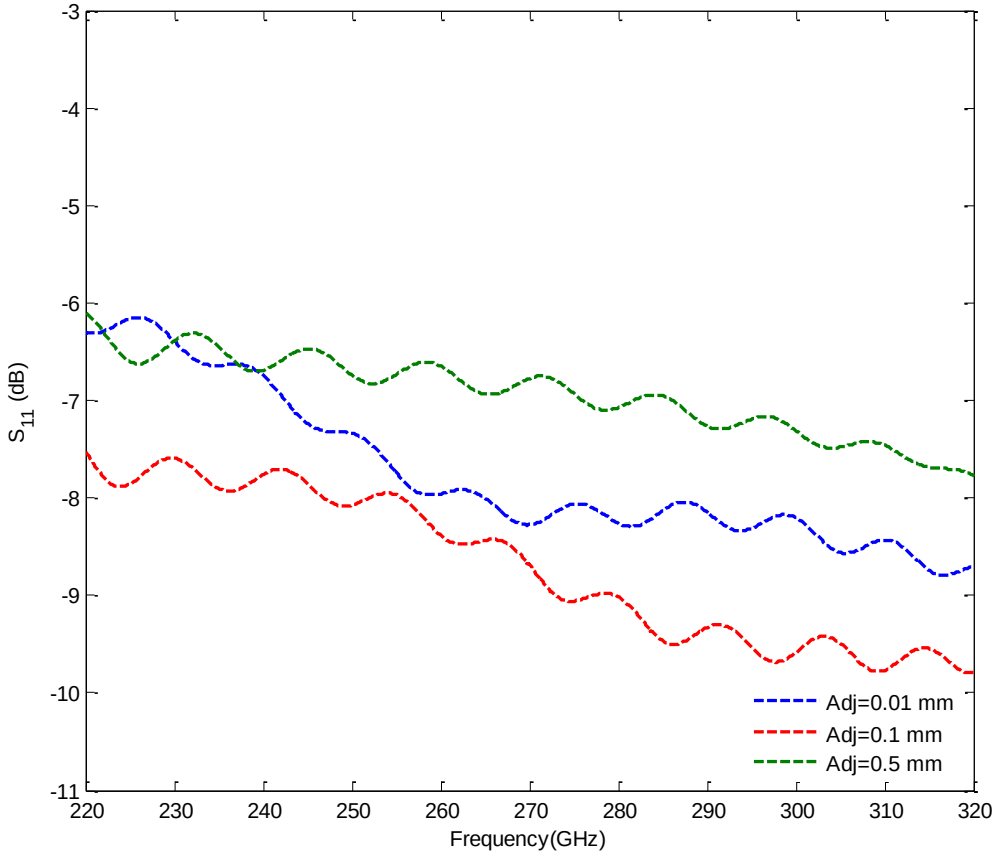

Fig. 6-25 S_{11} versus frequency for open ended E-plane horn shaped WR03 rectangular waveguide supported by SU8 for different amounts of *Adj* with *LH*=1mm and θ=15 degree shown in Fig. 6-24.

It can be seen that by adjusting the SU8 boundary, the reflection can be only slightly improved compared with Fig. 6-18 where *Adj*=0 structure.

6-2-4-2 *Adjusted tapered horn-shaped PEC structure*

It is better that all three ideas of horn shaping, adjusting and tapering are employed simultaneously to achieve best results. Fig. 6-26 shows an example of tapering which used all the three mentioned ideas. Note that waveguide walls extend right to the end of the termination.

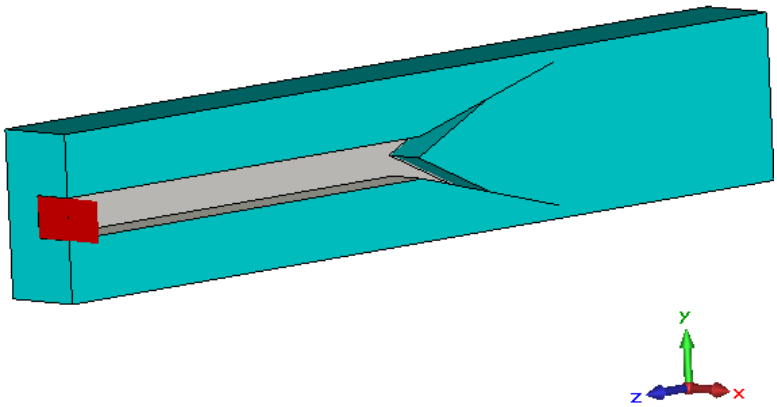

Fig. 6-26 Open ended E-plane horn shaped WR03 PEC rectangular waveguide supported by SU8 with inside wedge tapering and adjustable boundary

The magnitude of S_{11} of an open ended E-plane horn shaped WR03 PEC rectangular waveguide supported by SU8 with inside wedge tapering and adjustable boundary with *Adj*=0.01, *LH* = 2 mm and θ =15 degree for different values of L_{tap} is displayed in Fig. 6-27.

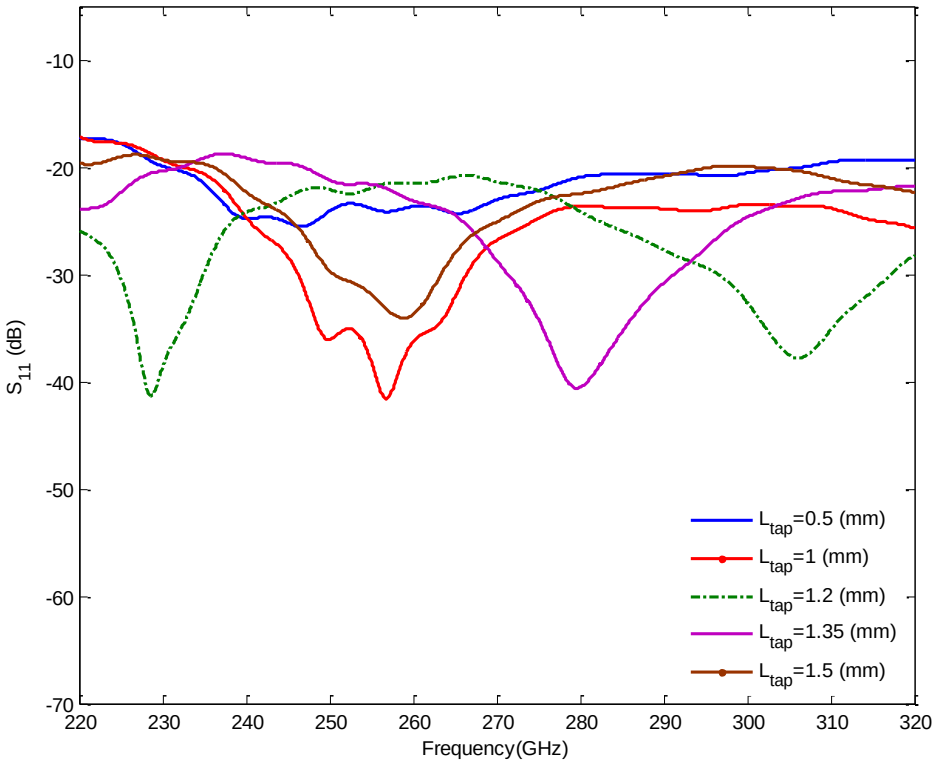

Fig. 6-27 The magnitude of $S_{11}$of an open ended E-plane horn shaped WR03 PEC rectangular waveguide supported by SU8 with inside wedge tapering and adjustable boundary with *Adj* = 0.01, LH=2 mm and θ=15 degree for different values of *Ltap*.

As can be seen from Fig. 6-27 the comparison between different L_{tap} values shows that for L_{tap} = 1.2 mm, the S_{11} is below the -21 dB and also for 300 GHz the S_{11} reaches -30 dB and it means the reflection is very low at this point.

So it can be inferred that the best result is obtained for L_{tap} = 1.2 mm, and its reflection is shown in Fig. 6-28.

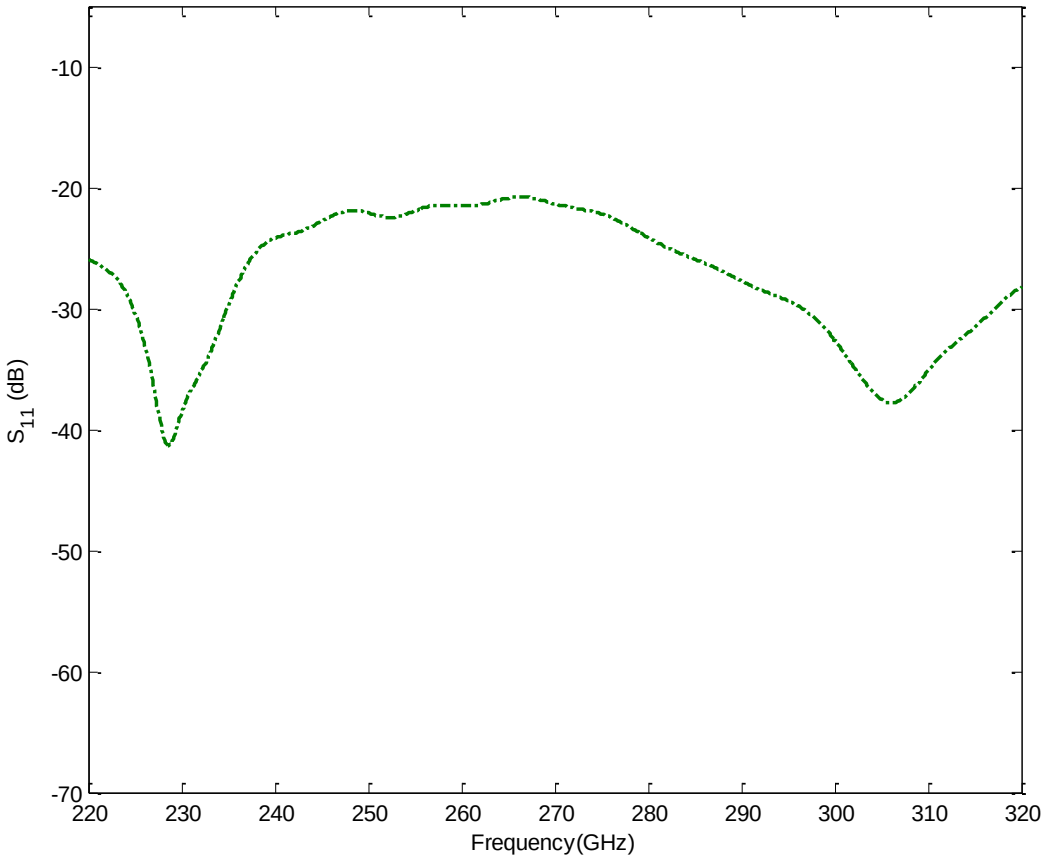

Fig. 6-28 The magnitude of $S_{11}$of an open ended E-plane horn shaped WR03 PEC rectangular waveguide supported by SU8 with inside wedge tapering and adjustable boundary for *Adj*=0.01, L_{tap}=1.2mm, *LH*=2mm and θ=15 degree

6-3 Conclusion

A WR03 termination with fairly good reflection coefficient (less than -35dB) proposed in Chapter 5. In this chapter it has been tried to improve the obtained reflection coefficient by using horn shaped structures.

Horn shaping is a good idea to improve matching between an open ended waveguide and environment space. In fact increasing the aperture of waveguide decreases the impedance of waveguide and slightly matches with environment.

But this case has a fundamental difference with typical applications of horn shaped waveguides. This difference is that the environment is filled by SU8 but waveguide is air filled. Therefore the inherent impedance of environment space decreases from 377 ohm to 186 ohm, in spite of that the impedance of waveguide has the previous value of an air-filled waveguide and with horn shaping it will be matched to inherence impedance of free space (377 ohm).

Chapter 7 COMPLETE MATCHED LOAD DESIGN IN SU8

7-1 Introduction

Different structures for WR03 termination have been discussed and simulated in chapters 4, 5 and 6. From the simulations it has been inferred that for simple termination and all kind of tapered terminations d = 5 mm can be a proper value. The waveguide length of L=10 mm has been shown that can produce enough loss to achieve the return loss better than 35 dB.

Between different kinds of tapering which has been analysed previously it can be concluded that triangular height with tapering length of L_{tap}= 0.5 mm is the best kind of tapering. Additionally, between silver and platinum it has been shown that platinum results in more losses and hence better reflection coefficient.

This chapter will discuss about the complete design of a WR03 matched load in SU8. As it has been shown, decreasing the metal thickness leads to lower reflection but this needs to be practical for physical realization. For example 10 nm thickness appears to be appropriate. Therefore section 7-2 contains a design of a WR03 platinum termination with height tapering and 10 nm conductor thickness. Additionally to have an applicable module in this section it has been discussed embedding the termination into a metal box.

Section 7-3 contains the fabrication process and physical realizations of the SU8 based 300 GHz waveguides. Additionally it will discuss about an H-plane 90-degree WR03 bend and the necessity of it due to the measurement.

7-2 WR03 matched load in SU8

Fig. 7-1 displays the S_{11} of a WR03 platinum termination with height tapering and metal thickness of t = 10 nm for L_{tap} = 0.5 mm, L=10 mm and d=5 mm.

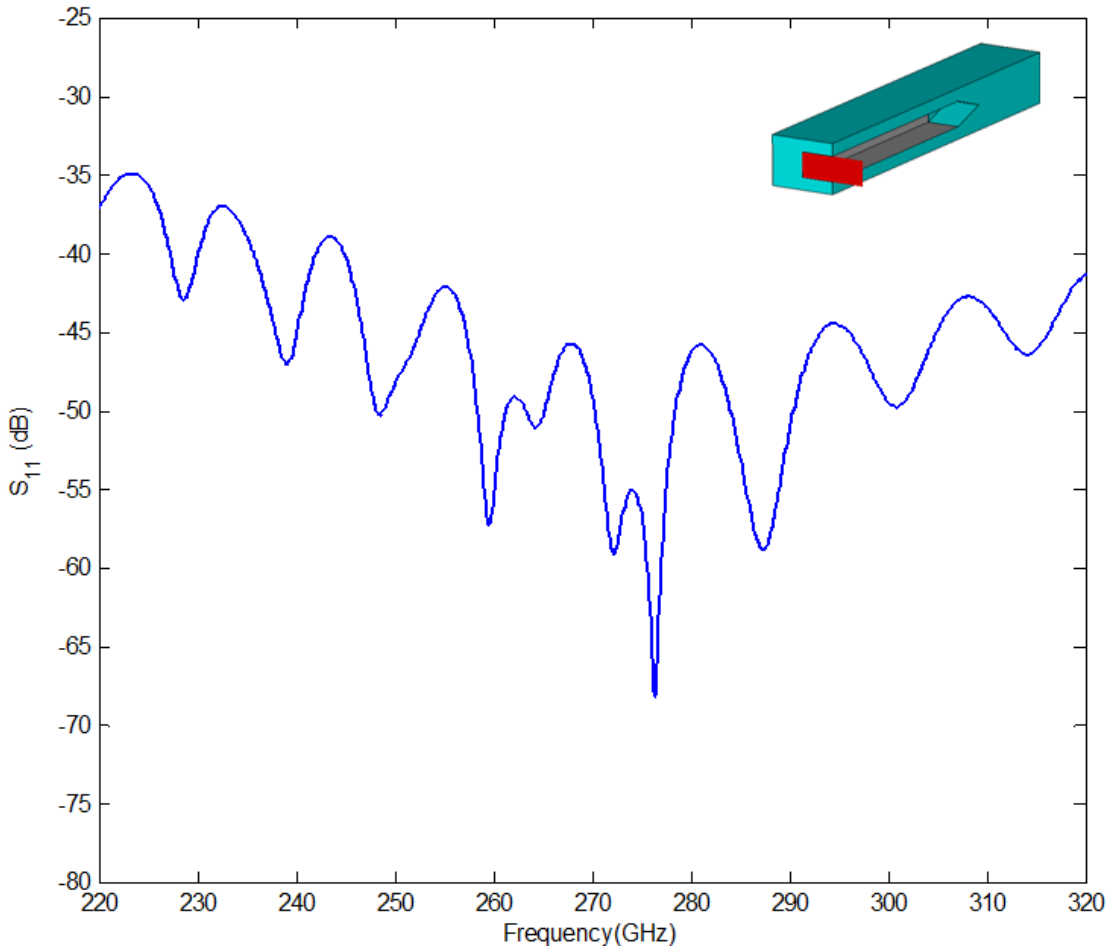

Fig. 7-1 The S_{11} of a WR03 platinum termination with height tapering and metal thickness of t=10 nm for L_{tap} = 0.5 mm, L = 10 mm and d = 5 mm.

It can be seen that the average return loss is better than 35 dB over the frequency range of 220 GHz to 320 GHz.

In a real application the termination will be embedded into metal box. Fig. 7-2 displays the simulation result of above-mentioned termination (WR03 platinum termination with height tapering and metal thickness of 10 nm) with and without box.

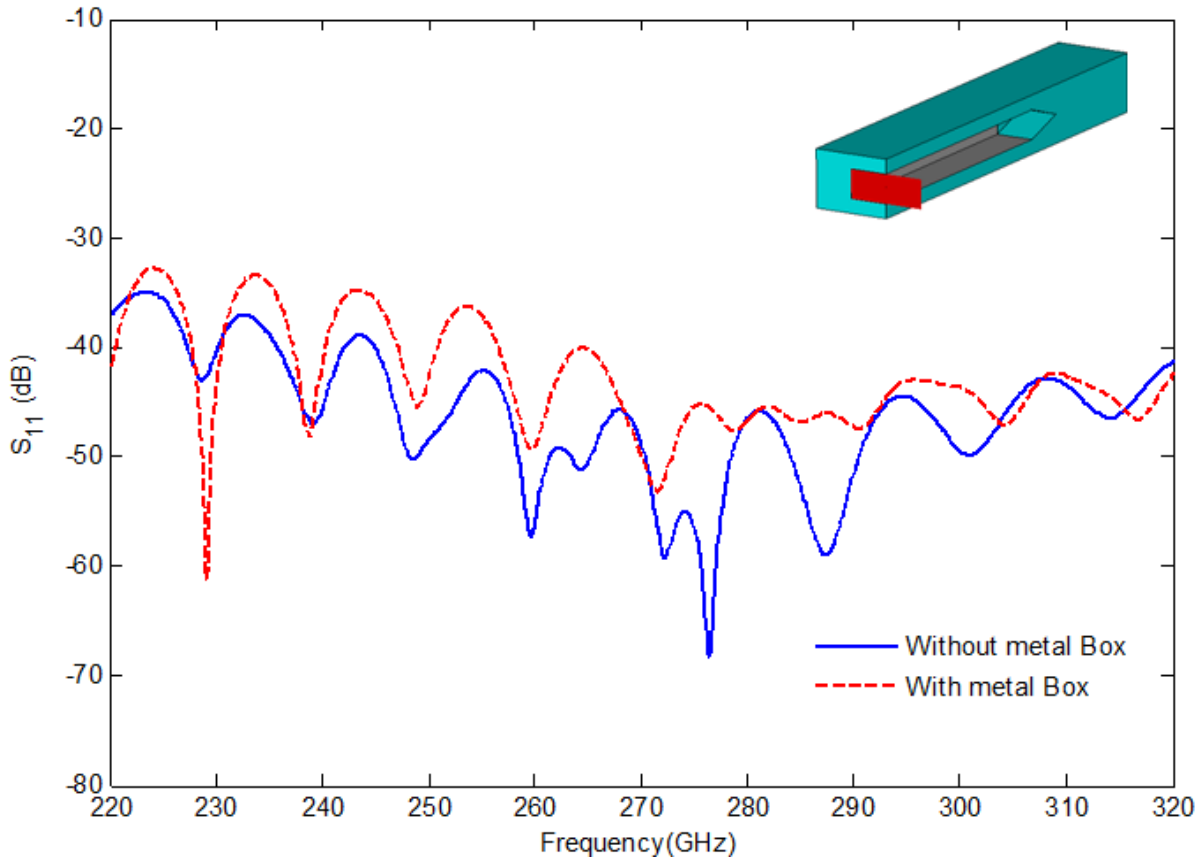

Fig. 7-2 Comparison of the S_{11} of a WR03 platinum termination with height tapering and metal thickness of t=10nm with and without metal box for L_{tap}= 0.5 mm, L=10 mm and d=5 mm.

Fig. 7-2 shows that using the metal box degrades the performance of the termination. To compensate this effect, the waveguide length of termination can be increased. Fig. 7-3 displays the termination with length of L=15 mm with metal box in compare with L=10 mm with and without box.

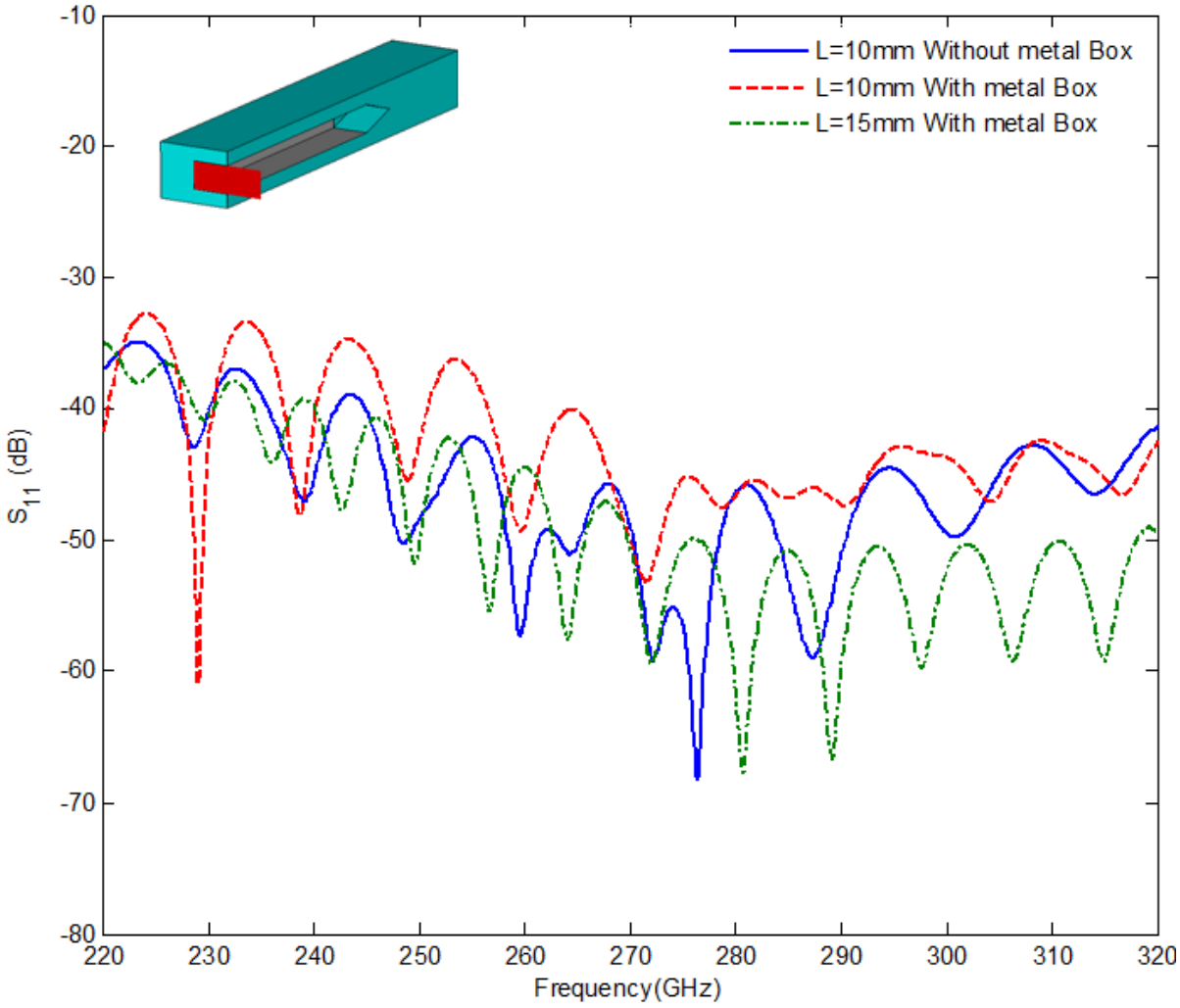

Fig. 7-3 Comparison of the S_{11} of a WR03 platinum termination with height tapering and metal thickness of t=10 nm for L_{tap}=0.5 mm and d=5 mm for L=10 mm with and without metal box and for L=15 mm with metal box.

Therefore the final suggestion for a good termination is a WR03 platinum termination with height tapering and metal thickness of t = 10 nm for L_{tap} = 0.5 mm, L = 15 mm and d=5 mm as shown in Fig. 7-4. Total dimensions of this termination will be 20 mm×2 mm×1 mm.

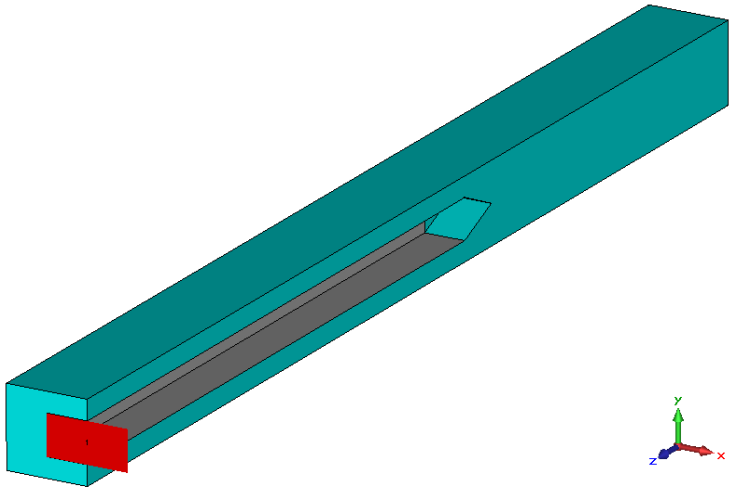

Fig. 7-4 The final suggestion, a WR03 Platinum termination with height tapering and metal thickness of t=10nm for L_{tap}=0.5 mm, L=15 mm and d = 5 mm. Total length of this termination will be 2 cm.

Fig. 7-5 displays the S_{11} of the final proposed structure for WR03 termination which shows a return loss of better than 35 dB in total frequency band of 220 GHz 320 GHz and better than 50 dB around 300 GHz.

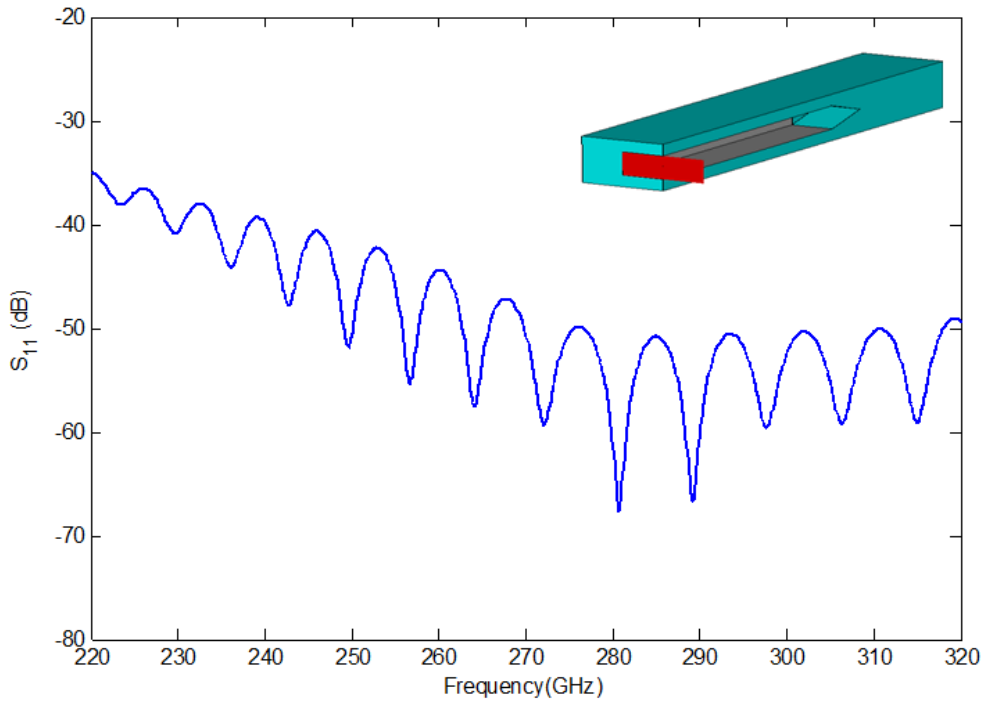

Fig. 7-5 The S_{11} of the final suggestion, a WR03 Platinum termination with height tapering and metal thickness of t=10nm for L_{tap}=0.5mm, *L=15mm* and *d=5mm* with metal box.

7-3 Fabrication Prerequisites

Physical realizations of the SU8 based 300 GHz waveguides are usually based on multi-layered micromachining technology [37]. The measurement of these devices is difficult and it needs special interconnection with standard waveguide flanges. For this purpose an H-plane 90-degree WR03 bend has to be designed. Because an H-plane 90-degree WR03 bend enables the accurate and direct connection between the micro-machined WR03 matched load termination and standard waveguide flanges [8]. Also necessity of this kind of bend comes from the measurement set-up. A typical measurement setup is shown in Fig. 7-6 with a VNA extension module for WR03, H-Band, 220-325 GHz, manufactured by OML [26] .

(a) (b)

Fig. 7-6 a) The V03VNA2 Series from OML [26], b) Flange as port of extension module for connection to device under test [19]

These frequency extension modules connect to the existing VNA test port(s) and leverage the inherent microwave network analyzer's performance and features to measure two-port S-parameters at higher frequencies [26].

7-4 H-plane bend

As it mentioned earlier about the necessity of designing of the H-plane bend, the initial step has been taken to design the H-Plane bend in CST Microwave Studio. The optimization of the design has been done in the same software package. Fig. 7-7 shows the schematic of the H-plane bend which is used as the model in CST and its accurate dimensions of the total bend structure with the layers of the designed WR03 bend. The quoted values are obtained after optimization of the model.

The blue parts are presenting vacuum which has been surrounded by PEC in the CST simulation the bend can be designed in two layers, four layers, six layers or much more. As the numbers of the layers increase the layers get thin and the S_{11} versus frequency would be better than 30 dB but the fabrication process would be more difficult. In this project the bend have been designed in 4 layers. The thickness of each layer is $a/4$= 0.21 mm.

The mentioned WR03 H-plane bend has to be designed based on 90 degree, multi-stepped and multi-mitered corners to provide a reliable interconnection between the SU8 based waveguide and the standard flange Fig. 7-6 (b).

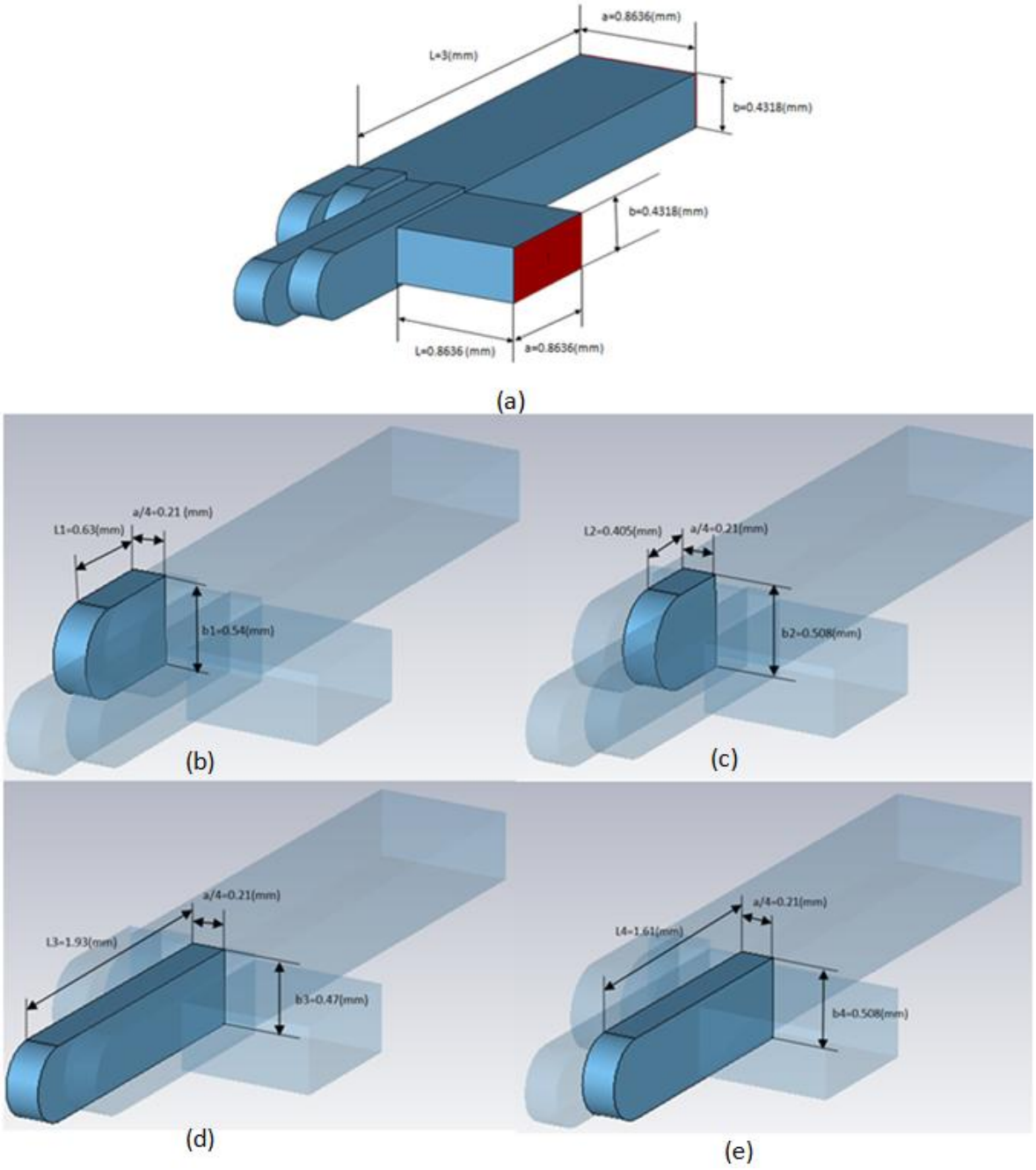

Fig. 7-7 Configuration of the designed H-plane multi-layered 90-degree WR03 bend, a) Schematic of total structure, b) first layer, c) Second layer, d) Third layer, and e) Fourth layer.

Fig. 7-9 shows the whole structure of the designed bend and its dimensions and its simulation result has been shown in Fig. 7-9. The magnitude of S_{11} versus frequency for the

designed WR03 bends which is better than 31 dB across the whole frequency band (220 GHz- 320 GHz).

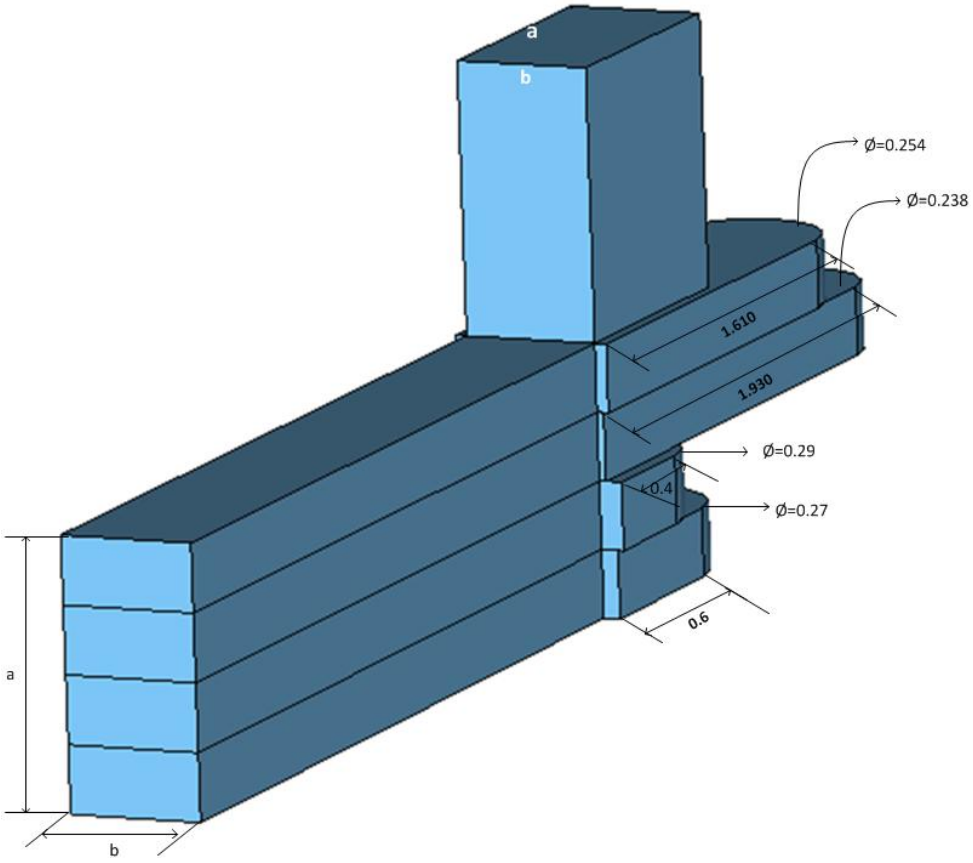

Fig. 7-8 H-plane 90 degree four layers bend dimensions

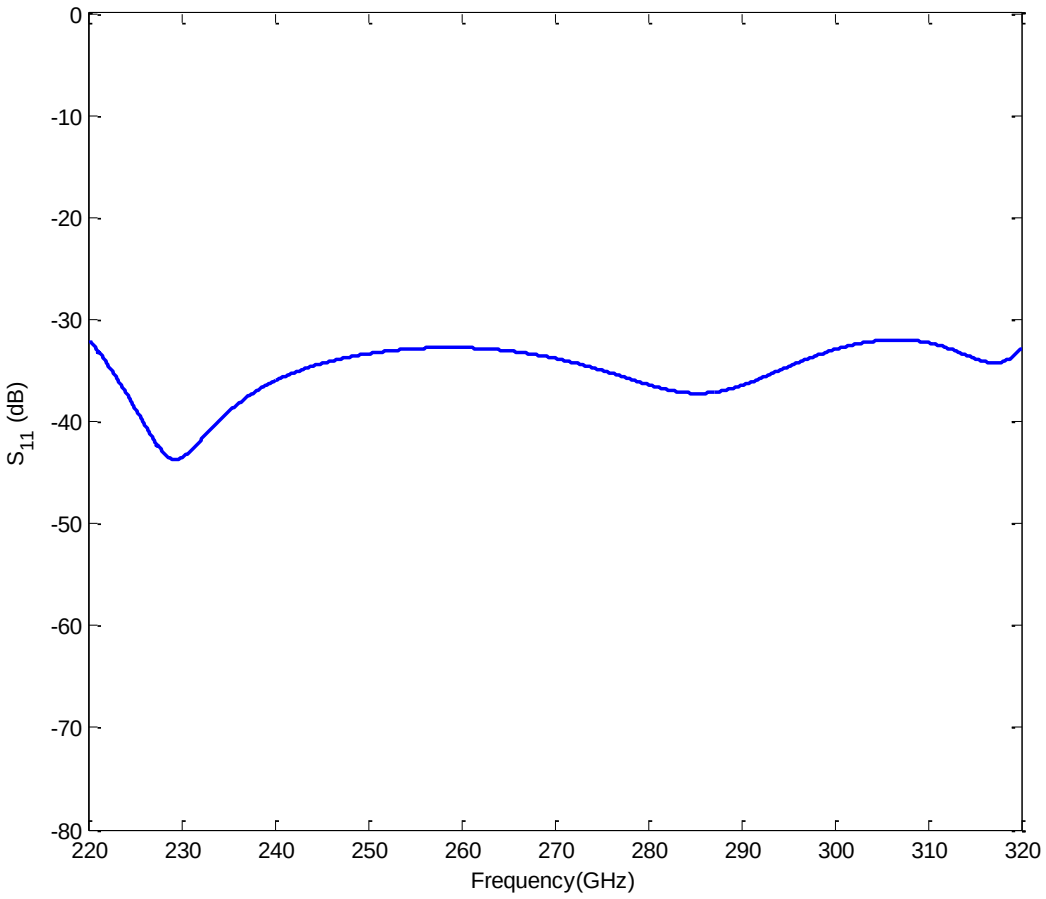

Fig. 7-9 S11 versus frequency for WR03 bend

The final step is to add the H-plane bend to the WR03 matched load. Fig. 7-10 illustrates the schematic of the WR03 matched load including the H-plane bend which has been designed by CST Microwave Studio. The blue part shown in the figure is vacuum which is surrounded by PEC in CST simulation apart from the tapered end and input port which are open boundaries.

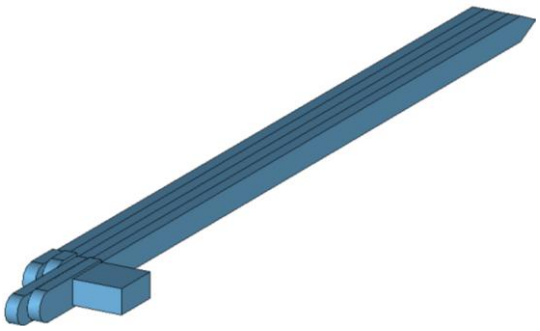

Fig. 7-10 Schematic view of WR03 matched load waveguide termination including H-plane bend

The total length of the WR3 matched load including the designed bend is 24.93 mm. Fig. 7-11 presents the S_{11} versus frequency for the whole designed matched load with bends. This design is ready for fabrication. The return loss is better than 30 dB over the whole frequency band.

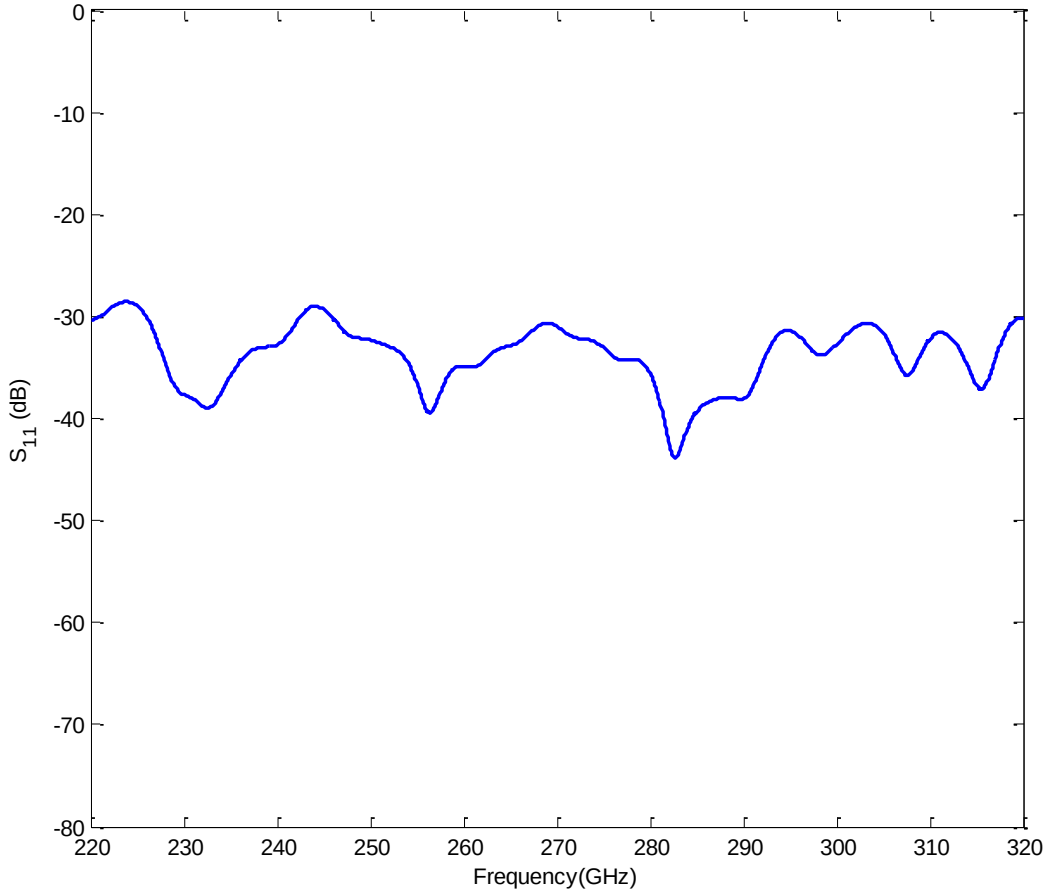

Fig. 7-11 S11 versus frequency for WR03 matched load attached to the WR03 bend

Fig. 7-12 shows the standard flange for WR03 waveguide is UG387 Flange, which will be used for measurement process.

Fig. 7-12 UG387 Flange, the standard flange for WR03 waveguide.

Finally for the fabrication of the whole structure of WR03 termination a 6-layer structure is used. Four layers are considered for the bend section and two thicker layers are dedicated for two sides of the bending. Accurate dimension features of UG387,Fig. 7-12, flange is considered for the implementation on all layers. The six SU8 layers with total thickness of 3×*a* (‘*a*’ is the width of waveguide which is equal to 863.4 μm for WR03) are shown in Fig. 7-13. First and sixth layers have thickness of ‘*a*’ and four middle layers have thickness of ‘*a/4*’. Each layer has length of 30 mm and width of 24 mm. The detailed dimensions of the holes are shown in Fig. 7-14.

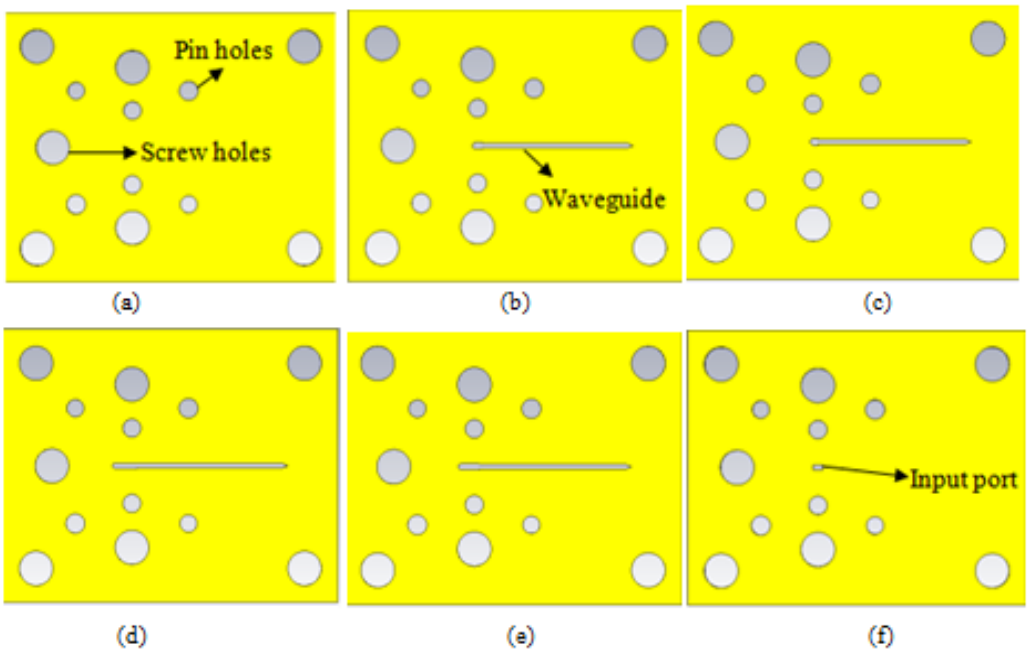

Fig. 7-13 6-layer structure for implementation of the proposed WR03 termination, a) First layer with thickness of *a*, b) Second layer with thickness of *a/4*, c) Third layer with thickness of *a/4*, d) Fourth layer with thickness of *a/4*, e) Fifth layer with thickness of *a/4*, and f) Sixth layer with thickness of *a*.

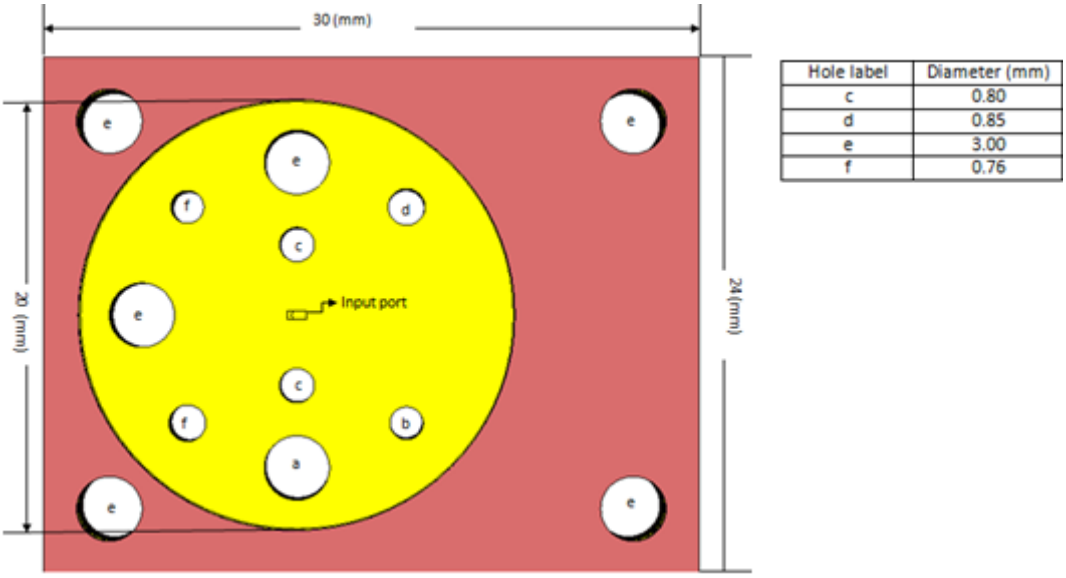

Fig. 7-14 Dimensions of the metal plates with thickness of 3 mm and the holes at both sides for supporting the SU8 structure.

The final 6-layer structure needs two 24 mm×30 mm metal plates with thickness of 3 mm at both sides for supporting the SU8 structure (they can be made from brass), Fig. 7-14

shows the dimensions of the metal plates with thickness of 3 mm and the holes at both sides to support the SU8 structure.

The whole structure is displayed in Fig. 7-15 from both front and back view.

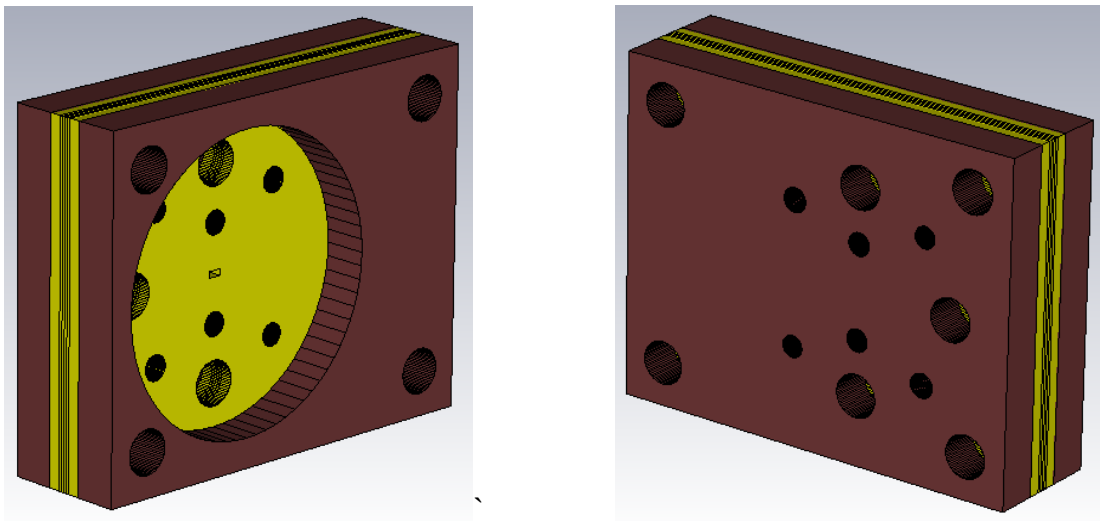

(a) (b)

Fig. 7-15 Two metal plates at both sides for supporting the SU8 structure, (a) Front view, (b) Back view.

Chapter 8 CONCLUSIONS AND FUTURE WORK

8-1 Conclusions

In this thesis a matched load and H-plane bend for WR03 waveguide has been designed and investigated. The design procedure started with the study of the reflection coefficient from an open ended WR03 waveguide into air and SU8. Different conductive materials and thickness values were examined using different SU8 tapering at the open ended terminal of the WR03 rectangular waveguide. To design the complete WR03 rectangular waveguide the H-Plane bend was designed and the whole structure simulated using CST.

In Chapter 3, the CST simulation results for a WR03 rectangular waveguide open ended into air were presented and analysed. As the final design was intended to be used within SU8 material, the effect of SU8 dielectric was considered in the study. The presence of SU8 increased the mismatch of open ended terminal of WR03 rectangular waveguide significantly, which was not desirable. To overcome this issue the possibility of increasing the amount of path loss was investigated by studying the effect of different conductor materials on conductor loss and leakage loss.

Six different common conductors were studied in Chapter 3. From the results obtained wasbeen concluded that the maximum attenuation is achieved using Titanium whilst Silver has been found to have the smallest attenuation. Other conductors were considered, Nickel and Platinum showed an attenuation level between those observed for Titanium and Silver conductors.

It has been found that the amount of the attenuation for a conductor with normal thickness ($t>>\delta_s$) is not sufficient. The study of thin film ($t<<\delta_s$) conductors was another

consideration of the present study It was observed that the thickness significantly influences the attenuation of the signal.

When the thickness of the metal material is much less than the skin depth ($t<<\delta_s$), leakage loss will appear in the waveguide walls. It has been shown that the amount of loss will exponentially increased if the conductor is made thin. Although the thinner conductor material gave more attenuation and less reflection, the implementation limitations of the device should also be taken into account.

In Chapter 4 a simple WR03 waveguide termination was designed and simulated with CST.As a signal reflection was found, numerous different techniques were explored in Chapters 5 and 6, for example Height tapering, Inner height tapering, Width tapering, Pyramidal tapering and Horn shaping.

Parameters such as the length of tapering and the distance from an open ended terminal to the end of the termination were tested. The length of the tapering was found to significantly influence the results. Based on the findings arising from the CST simulations, height-tapering stood out from the aforementioned tapering techniques, with S_{11} being better than 29 dB. This was achieved by using a tapering length equal to 0.5 mm.

After obtaining the optimum termination structure, in Chapter 7 the possible fabrication method of the matched load was discussed. To make an applicable module, it seems very plausible to embed the termination into a metal box. Putting the termination into the metal box degraded the result significantly. It was found that in order to compensate for the degradation of the performance of the matched load the length of the waveguide should be increased by 5 mm. The final proposed structure for the WR03 waveguide termination has a return loss better than 35 dB across the frequency band and better than 50 dB around 300 GHz. For the measurement of the WR03 waveguide termination and, interconnection the H-plane bend with a standard waveguide flange is needed.

The H-plane bend directs the connection between the WR03 matched load termination and the standard waveguide flange, and makes it accurate.

As it has been discussed in Chapter 7, the H-plane bend can be designed in two, four and six layers. The more layers the better the performance and less reflection. However, the fabrication process would be more difficult with increasing numbers of layers.

An H-plane bend was designed with performance of S_{11} better than 30 dB in the whole desired frequency band with four layers based on 90 degree, multi-stepped and multi-mitered corners.

The final step of this study was to design the whole structure of WR03 matched load combined with the H-plane bend. The total number of designed layers is six, with four layers designed for the main structure and two thick layers have been designed for the two sides of the bending. The total length of the final proposed design is 24.93 mm with S_{11} better than 32 dB in the frequency range of 220 GHz to 320 GHz.

8-2 Future Work

The main aim of this study has been to propose a good structure for a waveguide termination in WR03 band.

In this work analysis of thin film conductor layers for WR03 waveguide and also different kinds of tapering in open-ended side have been performed. Furthermore, the essential procedures for implementation of the proposed termination have been done.

In order to build further on the findings of the present investigation the final proposed structure could be manufactured and measured. At the moment there is no process available within the research group for this tapered termination. There also does not appear to be any suitable technology reported in the literature. Such structures have been made for X-band in styrophome [14] these structures prepared by cutting which is not convenient for 300 GHz. Imperial college London research groups has developed etching technology which might be adapted to make taper structure. Additionally, the realization of this termination can be analysed by using other conductors, including gold, Titanium, or etc.

Combination of this termination with other modules such as quadrature hybrid, 180-degree coupler or circulator could be worth investigations as an integrated structure.

Also an analytical expression (closed form expression) of loss calculation for thin film waveguide would be interesting.

REFERENCES

[1] Collin, Robert E. "Foundation for microwave engineering," 2nd edition. Electrical Engineering Series (1992).

[2] Wu, Ke. "Integration and interconnect techniques of planar and non-planar structures for microwave and millimeter-wave circuits-current status and future trend." In IEEE Asia-Pacific Microwave Conference, APMC 2001, vol. 2, pp. 411-416.

[3] "SU-8:Thick Photo-Resist for MEMS", Ed. F. Chollet, 19 Sep 2011,[Online] Available from : http: //memscyclopedia.org/su8.html [Accessed: 10 DEC 2012]

[4] http://www.microwaves101.com/encyclopedia/waveguidedimensions.cfm

[5] Talal Skaik, Yi Wang, Maolong Ke, Shilong Qian and Michael Lancaster. "A micromachined WR-3 waveguide with embedded bends for direct flange connections." In Microwave Conference (EuMC), 2010 European, pp. 1225-1228. IEEE, 2010.

[6] Yi Wang , Maolong Ke, Michael J. Lancaster, and Jian Chen. "Micromachined 300-GHz SU-8-based slotted waveguide antenna." Antennas and Wireless Propagation Letters, IEEE 10 (2011): 573-576.

[7] Xiaobang Shang, Maolong Ke, Yi Wang, and Michael J. Lancaster. "Micromachined WR-3 waveguide filter with embedded bends." Electronics Letters 47, no. 9 (2011): 545-547.

[8] Xiaobang Shang, Michael J. Lancaster, Maolong Ke, and Yi Wang. "Measurements of micromachined submillimeter waveguide circuits." In Microwave Measurement Symposium (ARFTG), 2010 76th ARFTG, pp. 1-4. IEEE, 2010.

[9] Talal Skaik, Yi Wang, Maolong Ke, Shilong Qian, and Michael Lancaster. "A micromachined WR-3 waveguide with embedded bends for direct flange connections." In Microwave Conference (EuMC), 2010 European, pp. 1225-1228. IEEE, 2010.

[10] A Ismail, and RSA Raja Abdullah. "Micromachined W-band rectangular waveguide utilising SU-8." International Journal of Engineering and Technology 4, no. 2 (2007): 245-252.

[11] Hsu Tai-Ran, "MEMS and Microsystems: Design, Manufacture", and Nanoscale Engineering(2nd edition, Wiley) (2008)

[12] David M Pozar, "Microwave engineering 3rd." Danvers, MA: Wiley (2005).

[13] pesona.mmu.edu.my/~wlkung/ADS/rf/lesson5.pdf

[14] T. Stander, van der Walt, P.W.; Meyer, P.; Steyn, W.; , "A comparison of simple low-power wedge-type X-band waveguide absorbing load implementations," AFRICON 2007 , vol., no., pp.1-4, 26-28 Sept. 2007.

[15] Mike J. Lancaster, Passive microwave device applications of high-temperature superconductors. Cambridge University Press, 2006.

[16] A. D.Yaghjian, "Approximate formulas for the far field and gain of open-ended rectangular waveguide," IEEE Trans. Antennas Propagat., Vol. 32, 378{384, 1984.

[17] K. T. Selvan, , "Studies on the classical gain approximations and the aperture-reflection coefficient of rectangular waveguide antennas," IEEE Trans. Electromag. Compat., Vol. 40, 343-347,1998.

[18] Kim Jong-Heon, Bayanmunkh Enkhbayar, Jae-Hoon Bang, Bierng-Chearl Ahn, and Eun-Jong Cha. "New formula for the reflection coefficient of an open-ended rectangular waveguide with or without an infinite flange." Progress In Electromagnetics Research M 12 (2010): 143-153.

[19] Yi Wang; M.J. Lancaster, Maolong Ke; Xiaobang Shang, "Measurements of micromachined waveguide devices at WR-3 band using a T/R-T module based network analyzer," Microwave Measurement Conference (ARFTG), 2011 77th ARFTG , vol., no., pp.1-4, 10-10 June 2011.

[20] Flann Microwave [Online] Available from: http://www.flann.com/Products_Home/Terminations/terminations.html [Accessed : 07 DEC 2013]

[21] Waveguide Terminations and Dummy Loads [Online] Available from ::http://www.atmmicrowave.com/wave-termination.html. [Accessed: DEC 2015]

[22] V.V. Komarov , "Matched loads on waveguides with capacitance gap," 3rd International Conference on Microwave and Millimeter Wave Technology, Proceedings. ICMMT 2002., vol., no., pp. 955- 958, 17-19 Aug. 2002.

[23] Amineh Khajehpour and Seyed Abdullah Mirtaheri. "Analysis of pyramid EM wave absorber by FDTD method and comparing with capacitance and homogenization methods." Progress In Electromagnetics Research Letters 3 (2008): 123-131.

[24] T. Schrader , K. Kuhlmann, R. Dickhoff, J. Dittmer, and M. Hiebel. "Verification of scattering parameter measurements in waveguides up to 325 GHz including highly-reflective devices." Advances in Radio Science 9 (2011): 9-17.

[25] S. Lucyszyn, , D. Budimir, Q. H. Wang, and I. D. Robertson. "Design of compact monolithic dielectric-filled metal-pipe rectangular waveguides for millimetre-wave applications." In Microwaves, Antennas and Propagation, IEE Proceedings, vol. 143, no. 5, pp. 451-453. IET, 1996.

[26] http://www.omlinc.com/images/pdf/VxxVNA2/OML-V03VNA2_Datasheet.pdf

[27] Constantine A Balanis, Antenna theory: analysis and design. John Wiley & Sons, 2012.

[28] John D. Kraus and Ronald J. Marhefka. "Antenna for all applications." Upper Saddle River, NJ: McGraw Hill (2002).

[29] M. Hamid, "Reflection coefficient at a horn-waveguide junction." Antennas and Propagation, IEEE Transactions on 15, no. 4 (1967): 564-565.

[30] Shockley, T., and C. Lewis. "Determination of the reflection coefficient at a horn-waveguide junction using the collocation method." Antennas and Propagation, IEEE Transactions on 18, no. 1 (1970): 104-105.

[31] Krishnasamy Selvan, Hanumantha Rao, and S. Geetha. "High-frequency reflection from the aperture of a long E-plane sectoral horn." Antennas and Propagation Magazine, IEEE 41, no. 3 (1999): 58-59.

[32] M. F. Iskander, and M. A. K. Hamid. "Scattering coefficients at a waveguide-horn junction." Electrical Engineers, Proceedings of the Institution of 123, no. 2 (1976): 123-127.

[33] Sheet resistance [Online] Available from : http://www.ece.gatech.edu/research/labs/vc/theory/sheetRes.html [Accessed: JAN 2014]

[34] https://www.cst.com/Support/Tickets/RenderTicket

[35] Sheet resistance [Online] Available from : http://en.wikipedia.org/wiki/File:Sheet_resistance.jpg [Accessed: FEB 2014] Public domain copy right

[36] J.C.Chaston,. "The Growing Industrial Use of the Platinum Metals." In Platinum Rev, 1982.

[37] M.J. Lancaster, J. Zhou, and Wang, Y., et al.: 'Design and high performance of a micromachined K-band rectangular coaxial cable', IEEE Trans. Microw. Theory Tech., 2007,55, (7), pp. 1548–1553.